JMeXFRI

Indexed in: EMBASE/Excerpta Medica, Scopus, BIBLAT, MIAR, DOAJ, ASCI-Database, Latindex
Preserved in: CLOCKSS

Journal of the Mexican Federation of Radiology and Imaging

J Mex Fed Radiol Imaging

Volume 4. Number 1, January-March 2025
ISSN: 2938-1215
eISSN: 2696-8444

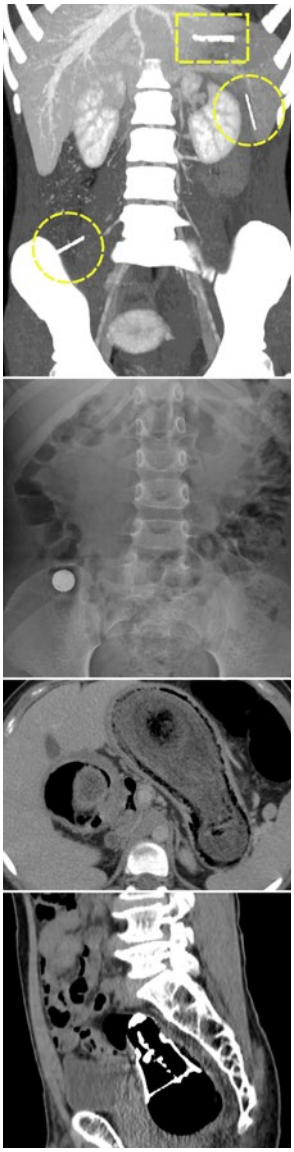

Official Journal of the

FEDERACIÓN MEXICANA DE RADIOLOGÍA E IMAGEN, A.C

PERMANYER
www.permanyer.com

WWW.JMeXFRI.COM

JMeXFRI

Journal of the Mexican Federation of Radiology and Imaging

J Mex Fed Radiol Imaging

Volume 4. Number 1, January-March 2025

ISSN: 2938-1215

eISSN: 2696-8444

The *Journal of the Mexican Federation of Radiology and Imaging* (JMeXFRI) is the official journal of the Federacion Mexicana de Radiologia e Imagen. The aim of the journal is to disseminate scientific knowledge and technological developments for innovation in diagnostic and therapeutic radiology with original articles on basic and clinical aspects of modern radiology in an international context with global impact. JMeXFRI is published in American English with 4 issues per year (print and online) and the first issue was published in the first quarter of 2022. Articles undergo a rigorous, double-blind peer-review process. Publication of articles in JMexFRI is free of charge and all published articles are open access.

The journal publishes the following types of manuscripts: *Full Research Article, Pictorial Essay, Brief Research Article, Technical Note, In-Depth Review, Case Report, Images in Radiology, and Editorial.*

EDITORIAL BOARD

Jorge Elias Jr. Ph.D.
Departamento de Imagenes Medicas, Oncologia e Hematologia, Faculdade de Medicina Ribeirao Preto, Universidade Sao Paulo Ribeirao Preto, Sao Paolo, Brazil

Valdair F. Muglia, M.D.
Faculdade de Medicina de Ribeirão Preto, Universidade de Saõ Paulo, Ribeirão Preto, Sao Paolo, Brazil

Carlo Catalano, M.D.
Department of Diagnostic Radiology La Sapienza University of Rome Rome, Italy

OBSTETRIC AND GYNECOLOGIC RADIOLOGY

Luciana Pardini Chamie, M.D., Ph.D.
Centro de Diagnostico Ultrasonografico Especializado en Imagen de la Mujer, Sao Paolo, Brazil

BREAST RADIOLOGY

Javier Romero-Enciso, M.D.
Department of Radiology, Fundacion Santa Fe, Bogota, Colombia

NUCLEAR AND MOLECULAR MEDICINE

Begoña Martinez-Sanchis, M.D.
Department of Nuclear Medicine, Hospital Universitario y Politecnico La Fe, Valencia, Spain

Cesar N. Cristancho-Rojas, M.D., M.Sc.
School of Public Health, Oregon Health & Science University, Portland, OR., USA

NEURORADIOLOGY

Roy F. Riascos-Castaneda, M.D.
Department of Radiology and Neurosurgery, Memorial Hermann Hospital System, Houston, TX., USA

Rafael Rojas-Jasso, M.D.
Department of Radiology, Beth Israel, Deaconess Medical Center, Boston, MA., USA

Henrique Carrete Jr., M.D., Ph.D.
Department of Diagnostic Imaging, Universidad de Sao Paulo, Sao Paulo, Brazil

Carlos Torres, M.D.
Department of Diagnostic Imaging, The Ottawa Hospital, Ottawa, Canada

MUSCULOSKELETAL RADIOLOGY

Javier Fernandez-Jara, M.D.
Department f Radiology, Hospital Universitario Sanitas La Zarzuela, Madrid, Spain

Jose Luis del Cura, M.D.
Radiodiagnosis Service, Hospital Universitario Donostia, San Sebastian-Donostia, Spain

Diego F. Lemos, M.D.
Department of Radiology, University of Vermont Medical Center, Burlington, VT, USA

PEDIATRIC RADIOLOGY

George Bisset, M.D.
Department of Radiology, Children's Hospital Pennsylvania, PA., USA

Sara Reis Teixeira, M.D., Ph.D.
Department of Radiology, Children's Hospital Pennsylvania, PA. USA

CHEST AND CARDIOVASCULAR RADIOLOGY

Fernando R. Gutierrez, M.D.
Department of Radiology and Cardiothoracic Imaging, The Mallickrodt Institute of Radiology, St. Louis, MO., USA

Jorge Carrillo-Bayona, M.D.
Department of Radiology, Hospital Universitario Mayor, Bogota, Colombia

Carlos S. Restrepo, M.D.
Department of Cardiothoracic Radiology, Texas University, San Antonio, TX., USA

Sebastian Rossini, M.D.
Department of Radiology, Instituto Radiologico Mater Dei, Buenos Aires, Argentina

Santiago Martinez-Jimenez, M.D.
Department of Radiology, Saint Luke's Hospital of Kansas City, Kansas City, KS., USA

L. Antonio Sosa-Lozano, M.D.
Department of Cardiothoracic Radiology, Medical College of Wisconsin, Milwaukee, WI., USA

GENITOURINARY RADIOLOGY

Daniela Stoisa, M.D.
Department of Radiology, Diagnostico Medico Oroño, Rosario, Santa Fe, Argentina

Valdair F. Muglia, M.D.
Faculdade de Medicina de Ribeirao Preto, Universidade de Sao Paulo Ribeirao Preto, Sao Paulo, Brazil

ULTRASOUND

Edward G. Grant, M.D.
Department of Radiology, USC Norris Cancer Center, Los Angeles, CA., USA

Juan P. Niedmann-Espinosa, M.D.
Department of Ecotomography, Clinica Alemana de Santiago, Santiago de Chile, Chile

VASCULAR AND INTERVENTIONAL RADIOLOGY

Manuel Cifrian-Perez, M.D., Ph.D.
Imaging Clinic Department, Hospital Universitario y Politecnico La Fe, Valencia, Spain

ARTIFICIAL INTELLIGENCE

Luis Martí-Bonmatí, M.D., Ph.D.
Grupo de Investigación Biomédica en Imagen (GIBI230) Instituto de Investigación Sanitaria La Fe Área Clínica de Imagen Médica, Hospital Universitario y Politécnico La Fe Valencia, Spain

Leonor Cerda-Alberich, Ph.D
Imaging Clinic Department, Hospital Universitario y Politecnico La Fe, Valencia, Spain

Felipe Campos Kitamura, M.D., Ph.D.
Dasalnova, Dasa, Sao Paulo, Brazil

GRAPHICAL ABSTRACTS COMMITTEE

Oscar A. Chavez-Barba, M.D.
Department of Radiology, Antiguo Hospital Civil de Guadalajara "Fray Antonio Alcalde", Guadalajara, Jal., Mexico

Adriana Parada-Gallardo, M.D.
Department of Radiology, Hospital General de Zapopan, Zapopan, Jal., Mexico

J.M. Ignacio Lopez-Mendez, M.D.
Department of Radiology and Imaging, Hospital de Especialidades, CMNO Instituto Mexicano del Seguro Social, Guadalajara, Jal., Mexico.

Juan Pablo Lopez-Gutierrez, M.D.
Department of Radiology and Imaging, Hospital General de Zona 3, Instituto Mexicano del Seguro Social Aguascalientes, Ags., Mexico

Gerardo Llamas-Linares, M.D.
Centro Universitario de Imagen Diagnostica, Hospital Universitario "Dr. Jose E. Gonzalez", Monterrey, N.L., Mexico

Alejandra I. Castillo-Cervantes, M.D.
Centro Universitario de Imagen Diagnostica, Hospital Universitario "Dr. Jose E. Gonzalez", Monterrey, N.L., Mexico

SOCIAL MEDIA COMMITTEE

Guillermo Elizondo-Riojas, M.D., Ph.D.
Centro Universitario de Imagen Diagnostica, Hospital Universitario "Dr. Jose E. Gonzalez", Monterrey, N.L., Mexico

Oscar A. Chavez-Barba, M.D.
Department of Radiology, Antiguo Hospital Civil de Guadalajara "Fray Antonio Alcalde", Guadalajara, Jal., Mexico

J. Mario Bernal-Ramirez, M.D.
Department of Medical Clinics, Centro Universitario de Ciencias de la Salud, Universidad de Guadalajara, Guadalajara, Jal., Mexico

Adriana Parada-Gallardo, M.D.
Department of Radiology, Hospital General de Zapopan, Zapopan, Jal., Mexico

A. Sofia Sanchez-Gomez, M.D.
Department of Radiology, Grupo RIO Centro Integral de Diagnostico Medico. Guadalajara, Jal., Mexico

RADIOLOGICAL AND CLINICAL CORRELATION BOARD

GASTROENTEROLOGY

Linda E. Muñoz-Espinosa, M.D., Ph.D.
Liver Unit, Hospital Universitario "Dr. Jose E. Gonzalez", Monterrey, N.L., Mexico

David Marti-Aguado, M.D., Ph.D.
Servicio Medicina Digestiva, Hospital Clinico Universitario, Valencia, Spain

GASTROINTESTINAL AND GENERAL SURGERY

Carlos Nuño-Guzman, M.D., M.Sc.
Department of Surgery, Antiguo Hospital Civil de Guadalajara "Fray Antonio Alcalde", Guadalajara, Jal., Mexico

OBSTETRICS AND GINECOLOGY

Sergio Fajardo-Dueñas, M.D., M.Sc.
Division of Obstetrics and Ginecology, Nuevo Hospital Civil de Guadalajara, Guadalajara, Jal., Mexico

NEUROLOGY

Jose L. Ruiz-Sandoval, M.D., M.Sc.
Department of Neurology, Antiguo Hospital Civil de Guadalajara "Fray Antonio Alcalde", Guadalajara, Jal., Mexico

Follow us

https://linkedin.com/company/jmexfri

https://instagram.com/jmexfri

https://facebook.com/jmexfri

https://youtube.com/@jmexfri

https://x.com/jmexfri

Original papers should be deposited in their electronic version through the following URL:

https://publisher.jmexfri.permanyer.com

PERMANYER
www.permanyer.com

Permanyer Mexico
Temistocles, 315
Col. Polanco, Del. Miguel Hidalgo
11560 Ciudad de Mexico
mexico@permanyer.com

Permanyer
Mallorca, 310 – Barcelona (Cataluña), España
permanyer@permanyer.com

www.permanyer.com

ISSN: 2696-8444
Ref.: 10990AMEX251

JMeXFRI

Journal of the Mexican Federation of Radiology and Imaging

Check for updates

EDITORIAL

Training Mexican research radiologists: how can this be achieved?

Ana M. Contreras-Navarro

Scientific Writing Editor, Journal of the Mexican Federation of Radiology and Imaging (JMeXFRI), Zapopan, Jalisco, Mexico

"Radiologists who research, write and publish… teach well and interpret better".

Ana M. Contreras-Navarro

Radiology has been a primarily clinical specialty that has not attracted research-oriented radiologists[1]. The differences between a clinical radiologist and a research radiologist lie in their professional focus and goals. The clinical radiologist participates in patient care using diagnostic imaging and performing interventional therapy in medical units and hospitals. In contrast, the research radiologist focuses on basic or clinical research (experimental clinical, epidemiological, and behavioral studies, or outcomes and health services research). The development of radiology research in Mexico has evolved with different profiles described below:

- *Clinical radiologists* often participate as professors and, in some cases, have an interest in conducting clinical research for theses in residency programs that conclude with a conference presentation and, eventually, the publication of an original scientific article.
- *Clinical radiologists with a Master of Science (MSc) and/or a Doctor of Philosophy (PhD) degree* often participate as professors and conduct clinical research for theses in residency programs, culminating in a conference presentation and eventually publication of an original scientific article.
- *Research radiologists with an MSc and/or PhD* usually work in laboratories or research centers and conduct laboratory research involving experiments that advance the general knowledge of radiology and/or uni-or multicenter studies on diagnostic imaging and image-guided treatment.

The roles of clinical and research radiologists are fundamental and complementary. Ideally, they should have a foundation that combines both approaches and enables them to innovate clinical practice.

Specialty, subspecialty, and high-specialty radiology academic programs in Mexico have significantly advanced the training of nationally and internationally recognized clinical radiologists. The research they do as a thesis to obtain a radiologist degree is usually a curricular requirement. Professors who mentor radiologists are a heterogeneous group with different educational backgrounds and levels of experience. Approximately 600 residents per year are granted a radiologist degree in Mexico, meaning the same number of research studies were presented as theses. However, very few of these theses are published as original scientific articles[2].

In 2022, the Federacion Mexicana de Radiologia e Imagen (FMRI) [Mexican Federation of Radiology and Imaging] launched the *Journal of the Mexican Federation of Radiology and Imaging* (JMeXFRI) to disseminate scientific knowledge and technological developments in diagnostic and therapeutic imaging innovations with

Corresponding author:
Ana M. Contreras-Navarro
E-mail: acontreras530@gmail.com

Received for publication: 13-12-2024
Accepted for publication: 23-12-2024
DOI: 10.24875/JMEXFRI.M25000099

Available online: 24-04-2025
J Mex Fed Radiol Imaging. 2025;4(1):1-3
www.JMeXFRI.com

a global impact[2,3]. In addition, since 2023, the FMRI has published the annual call for "Best Radiology Theses for Publication in the JMeXFRI" and recognized the need for web-based training, creating the Scientific Writing Workshop (SWW) to address the need for optimal writing and publication of these theses as original scientific articles[2]. The SWW is fully customizable. It develops radiologists' and residents' skills in scientific writing and publishing. The theses published in JMeXFRI are based on procedural data collected from patients rather than a research question, meaning they are descriptive rather than hypothesis-based[1]. Even so, much can be done to publish this data in the JMeXFRI.

The majority (80-90%) of radiologists and residents in Mexico prefer to develop as clinicians, focusing on patient care and pursuing a career that promises professional and economic success in the short and medium term, so although some of them are interested in research, they do not focus on this area. As a result, few clinical radiologists or residents pursue an MSc or PhD degree. In addition, many clinical radiologists and residents do not feel comfortable doing research because they lack formal training, but they have great ideas that could improve the quality of patient care[4]. Research is a complex process that requires talented, academically oriented radiologists and residents. Clinical radiologists who are not trained in research methodology may therefore underestimate the amount of work involved in research studies or not understand the intricacies of research processes, writing and publishing scientific articles.

Residents who participate in research during their training are more likely to hold an academic position in their field of interest than those who do not. In my more than three decades of experience as a clinical researcher, and more recently as co-editor of JMeXFRI, I have seen residents enjoy doing research. About 10 to 20% of radiologists and residents are research-oriented and are passionate about reading and writing. They should be given the opportunity to do research[5]. This opportunity was given to me by Dr. Gerardo Gamba-Ayala, who was my mentor and discovered my passion for research during my residency in Internal Medicine at the Instituto Nacional de Ciencias Medicas y Nutricion Salvador Zubiran [National Institute of Medical Sciences and Nutrition Salvador Zubiran]. As a resident, I participated in several research studies and published scientific papers. A modular program that integrates research training with topics such as methodology, research protocol development, and writing and publishing scientific articles should be developed. Individualized, competency-based, research-oriented training for some residents can be developed in hospitals and medical units with the appropriate infrastructure and serve as "centers of excellence" in imaging research programs[1]. These organizations can captivate, nurture, and maintain a cadre of well-trained multi and interdisciplinary radiology research teams and provide protected research time during residency training by reducing the clinical burden of radiologists and residents involved in research studies, allowing them to devote more time to research[1]. This requires the involvement of residents in the protocol development process from the earliest stages of their residency training and faculty mentoring to encourage learners to achieve research accomplishments, such as writing and publishing original research. Research training raises the national profile and reputation of the residency program[4].

Artificial intelligence (AI) can support research training. The multidisciplinary nature of AI requires collaboration between academia and industry, as well as between clinicians and researchers, who share their specific expertise[6]. Radiologists with knowledge of AI/AI practitioners will help identify opportunities and provide the clinical context where AI can be best applied for research.

For little more than four decades, public and private universities in Mexico have offered master's and doctoral programs for clinicians. Likewise, the Consejo Nacional de Ciencia y Tecnologia (CONACYT) [National Council of Science and Technology] was created to financially support researchers in all fields of science. Some hospitals and clinical research units of public institutions, such as the Instituto Mexicano del Seguro Social [Mexican Social Security Institute], have hired clinical researchers as full-time employees, and some have granted scholarships abroad for research stays. I was one of the beneficiaries of this program, thanks to Dr. Onofre Muñoz-Hernandez, a visionary research leader who selected research-oriented clinicians and gave them the opportunity to conduct full-time clinical research at IMSS. These clinical researchers return to the hospitals to conduct clinical research in collaboration with clinicians and residents, integrating internationally competitive research teams. Due to recent changes in institutional policies or retirements, the number of clinical researchers has decreased without integrating new researchers. On the other hand, the Programa Nacional de Posgrados de Calidad para Especialidades Medicas [National Quality Postgraduate Program for Medical Specialties], sponsored by the

CONACYT, was developed to provide economic support to residents and professors to promote research and the publication of original scientific articles. The Secretaria de Ciencia, Humanidades, Tecnología e Innovación (SECIHTI) [Secretariat of Science, Humanities, Technology and Innovation] recently replaced the CONACYT. The SECIHTI began operations on January 1, 2025. It provides government funding and offers research scholarships for postgraduate studies at national and foreign universities and hospitals. Research-oriented radiologists and residents from public and private healthcare institutions can apply for research grants. The FMRI organizes national meetings and congresses to share scientific advances and promote private participation in research funding, including industry partners.

One of the main characteristics of countries with scientific and technological development is their high public and private investment in the research training of human resources. In contrast, in Mexico, investment in research infrastructure and human resources is insufficient. Therefore, despite the importance of research training, e.g. through master's degree programs, many clinical radiologists and residents find themselves limited by the lack of grants and funding. Research radiologists can provide a unique perspective on performing research. High quality scientific publications produced during research training are a mark of excellence and one of the most widely accepted currencies in research. Radiologists need to assume a key role in establishing multidisciplinary research communities and use their expertise in imaging to lead these research efforts rather than assuming a secondary, "technical support" role in these groups[1]. The visible radiologist embodies the educator, researcher and innovator in radiology[7]. In addition, a research radiologist can maximize the value of their clinical work and provide the highest level of clinical care through translational radiology, which integrates basic, clinical, and social research through the transfer and application of scientific knowledge for innovation in patient care and technological development of products, processes, and services.

In conclusion, we must train research radiologists to promote and conduct research in Mexico to ensure the future of radiology as an independent, innovative branch of medicine. The training of Mexican research radiologists requires a paradigm shift through residency reform, including a training system that focuses on talented, research-oriented radiologists and residents. The FMRI supports a new generation of research radiologists capable of conducting high-impact research, improving the quality of medical care, and positioning Mexico as an innovation leader in radiology.

Acknowledgments

The author thanks to Dr. J.M. Ignacio Lopez-Mendez for his suggestions for this scientific article.

Funding

Not applicable.

Conflicts of interest

The author discloses no potential conflicts of interest.

REFERENCES

1. Petrou M, Foerster BR, Reich DS. Translational research in radiology: challenges and role in a patient-based practice. Acad Radiol. 2009;16(5): 593-596. doi: 10.1016/j.acra.2009.01.017.
2. Contreras-Navarro AM. What I talk about when I talk about writing scientific articles. J Mex Fed Radiol Imaging. 2023;2(3):149-151. doi: 10.24875/JMEXFRI.M23000057.
3. Figueroa-Sanchez M, Ornelas-Cortinas GE, Contreras-Navarro AM. Celebrating the 50th anniversary of the Federación Mexicana de Radiología e Imagen (FMRI). J Mex Fed Radiol Imaging. 2024; 3(3):135-137. doi:10.24875/JMEXFRI.M24000081.
4. Jewell CM, Kraut AS, Miller DT, Ray KA, Werley EB, Schnapp BH. Metrics of Resident Achievement for Defining Program Aims. West J Emerg Med. 2022;23(1):1-8. doi: 10.5811/westjem.2021.12.53554.
5. Ramon y Cajal S. Advice for a young investigator. Cambridge MA. USA. The MIT Press. 1999. p. 150.
6. Elizondo-Riojas G, Negreros-Osuna AA, Bernal-Ramirez JM, Conde-Castro B. Artificial intelligence in radiology. J Mex Fed Radiol Imaging. 2024;3(2):72-81. doi:10.24875/JMEXFRI.M24000073.
7. Casale-Menier DR. The visible radiologist: balancing clinical expertise and technological Advances. J Mex Fed Radiol Imaging. 2023;2(4): 223-225 doi:10.24875/JMEXFRI.M23000059.

JMeXFRI

Journal of the Mexican Federation of Radiology and Imaging

Check for updates

IN-DEPTH REVIEW

Update on the PI-RADS-ACR scoring system

*Gabriel de Lion-Gouvea, Arthur Senna-Ogata, Thalyne A. Leite-de Lima, and Valdair F. Muglia**

Department of Medical Images, Oncology and Hematology, Ribeirao Preto School of Medicine, University of Sao Paulo; Sao Paulo, Brazil

ABSTRACT

The incorporation of magnetic resonance imaging (MRI) in the assessment of prostate cancer (PCa) is a key example of how imaging can impact patient management. The MRI diagnostic pathway is now endorsed by major clinical guidelines, and the acquisition, interpretation and reporting of MRI findings are standardized by the Prostate Imaging Reporting and Data System (PI-RADS) from the American College of Radiology. PI-RADS has evolved significantly since its first version and is now available in version 2.1. However, there is still room for improvement. This article aims to review the inception of PI-RADS, its application and the future perspectives for this important scoring system.

Keywords: *Prostate cancer. Magnetic resonance imaging. PI-RADS. Oncology.*

INTRODUCTION

Prostate imaging is a remarkable example of how imaging technology can significantly impact specific fields of medicine. Although researchers were attempting to obtain high-quality images of the prostate as early as the 1980s[1], it was not until the 1990s and early 2000s—when diffusion-weighted imaging (DWI) was added to the prostate magnetic resonance imaging (MRI) toolkit—that rapid and impressive advances were made in this field[2,3].

From a technical perspective, several challenges needed to be addressed. The first was to improve the signal-to-noise ratio. Initially, this was achieved by using high magnetic fields and endorectal coils, which were effective but quite uncomfortable for patients[4]. With advances in MRI hardware and software, image quality further improved, allowing diagnostic images to be obtained with either 1.5T or 3.0T systems and only external pelvic coils (preferably with multiple channels)[5].

In the late 2000s, numerous studies in the medical literature reported reasonable accuracy of MRI in the diagnosis of prostate cancer (PCa)[6-8]. Based on these solid premises, in 2012, the European Society of Urogenital Radiology (ESUR) published the first version[9] of what is now known as the Prostate Imaging Reporting and Data System (PI-RADS). PI-RADS not only introduced a scoring system for risk stratification for PCa, but also provided recommendations for image acquisition, interpretation and reporting. Like other RADS systems, PI-RADS uses a five-point scale to indicate the likelihood of clinically significant PCa, with a score of 1 indicating a very low probability and a score of 5 indicating a very high probability. Individual scores are routinely assigned for each sequence, with an overall score summarizing the likelihood of PCa[10].

***Corresponding author:**
Valdair F. Muglia
E-mail: fmuglia@fmrp.usp.br

Received for publication: 01-02-2025
Accepted for publication: 07-02-2025
DOI: 10.24875/JMEXFRI.M25000095

Available online: 24-04-2025
J Mex Fed Radiol Imaging. 2025;4(1):4-15
www.JMeXFRI.com

Table 1. Descriptive findings of PI-RADS scores 1 to 5, for MRI T2W and DWI sequences for the peripheral zone (PZ) and transition zone (TZ)

Score	T2W		DWI
	PZ	TZ	PZ or TZ
1	Uniform hyperintense signal intensity (normal)	Normal appearing TZ (rare) or a round, fully encapsulated nodule ("typical nodule")	No abnormality (i.e., normal) on ADC and DWI with high b-value
2	Linear or wedge-shaped hypointensity or diffuse mild hypointensity, usually indistinct margin	A mostly encapsulated nodule OR a homogeneously circumscribed nodule without encapsulation. ("atypical nodule") or a homogeneous, mildly hypointense area between the nodules	Linear/wedge-shaped hypointensity on ADC and/or linear/wedge-shaped hyperintensity on DWI with high b-value
3	Heterogeneous signal intensity or non-circumscribed, round, moderate hypointensity Includes others that do not qualify as 2, 4 or 5	Heterogeneous signal intensity with obscured margin Includes others that do not qualify as 2, 4 or 5	Focal (discrete and different from background) hypointensity in ADC and/ or focal hyperintensity in DWI with high b-value; may be markedly hypointense in ADC or markedly hyperintense in DWI with high b-value, but not both.
4	Circumscribed, homogeneous, moderately hypointense focus/mass, confined to the prostate and < 1.5 cm in greatest dimension	Lenticular or non-circumscribed, homogeneous, moderately hypointense, and < 1.5 cm in greatest dimension	Focal markedly hypointense on ADC and markedly hyperintense on DWI with high b-value; < 1.5 cm in greatest dimension
5	As 4, but ≥ 1.5 cm in greatest dimension or definitive extraprostatic extension/ invasive behavior	As 4, but ≥ 1.5 cm in greatest dimension or definitive extraprostatic extension/invasive behavior	As 4, but ≥ 1.5 cm in greatest dimension or definitive extraprostatic extension/ invasive behavior

ADC: apparent diffusion coefficient; DWI: diffusion-weighted imaging; MRI: magnetic resonance imaging; PI-RADS: Prostate Imaging Reporting and Data System; PZ: peripheral zone; TZ: transition zone; T2W: T2-weighted.
Adapted from the American College of Radiology® Committee on PI-RADS®[16].

In 2015, the second version of PI-RADS was released, marking a collaborative effort between the ESUR, the American College of Radiology (ACR), and AdMeTech[11]. This version was more user-friendly and simplified and facilitated wider adoption in the radiology community. A subsequent update, PI-RADS version 2.1, was released in 2019[12]. This update introduced minor changes, particularly in the assessment of transition zone (TZ) lesions, as well as further refinements to the classification system.

Today, prostate MRI and PI-RADS are recognized as the gold standard for the evaluation of patients with suspected PCa. They are supported by international guidelines, including those of the European Association of Urology (EAU)[13], the American Urological Association (AUA)[14], and the National Comprehensive Cancer Network (NCCN)[15].

PI-RADS CATEGORY ASSIGNMENT

Scoring system is based on a multiparametric (mp) MRI assessment of the prostate combining T2-weighted (T2W), DWI and dynamic contrast-enhanced (DCE) imaging sequences. It is a 5-point scale, with 1 indicating a very low probability and 5 a very high probability of clinically significant PCa[16].

T2W imaging is essential for differentiating the zonal anatomy of the prostate, identifying abnormalities within the gland, and detecting invasion of the seminal vesicle, extraprostatic extension (EPE) and lymph node involvement[17]. Based on T2W imaging, clinically significant PCa in the peripheral zone (PZ) typically appear as round or poorly defined hypointense focal lesions. However, this pattern is not exclusive to malignancies and can also be observed in various other conditions such as prostatitis, hemorrhage, glandular atrophy, benign prostatic hyperplasia (BPH), biopsy-related scarring, and post-treatment changes (e.g., hormone therapy or ablation)[16].

On the other hand, tumors in the TZ on T2W imaging are characterized by ill-defined, homogeneous and moderately hypointense lesions with a "smudgy fingerprint" or "erased charcoal" appearance. Other features include spiculated margins, a lenticular shape, the absence of a complete hypointense capsule, and possible invasion of the urethral sphincter or anterior fibromuscular stroma. The presence of one or more of these features usually increases the likelihood of clinically significant TZ cancer. Table 1 summarizes the T2 and DWI findings for PZ and TZ, according to each PI-RADS score[16]. As mentioned above, knowledge of zonal anatomy is essential, as the criteria for categorizing lesions

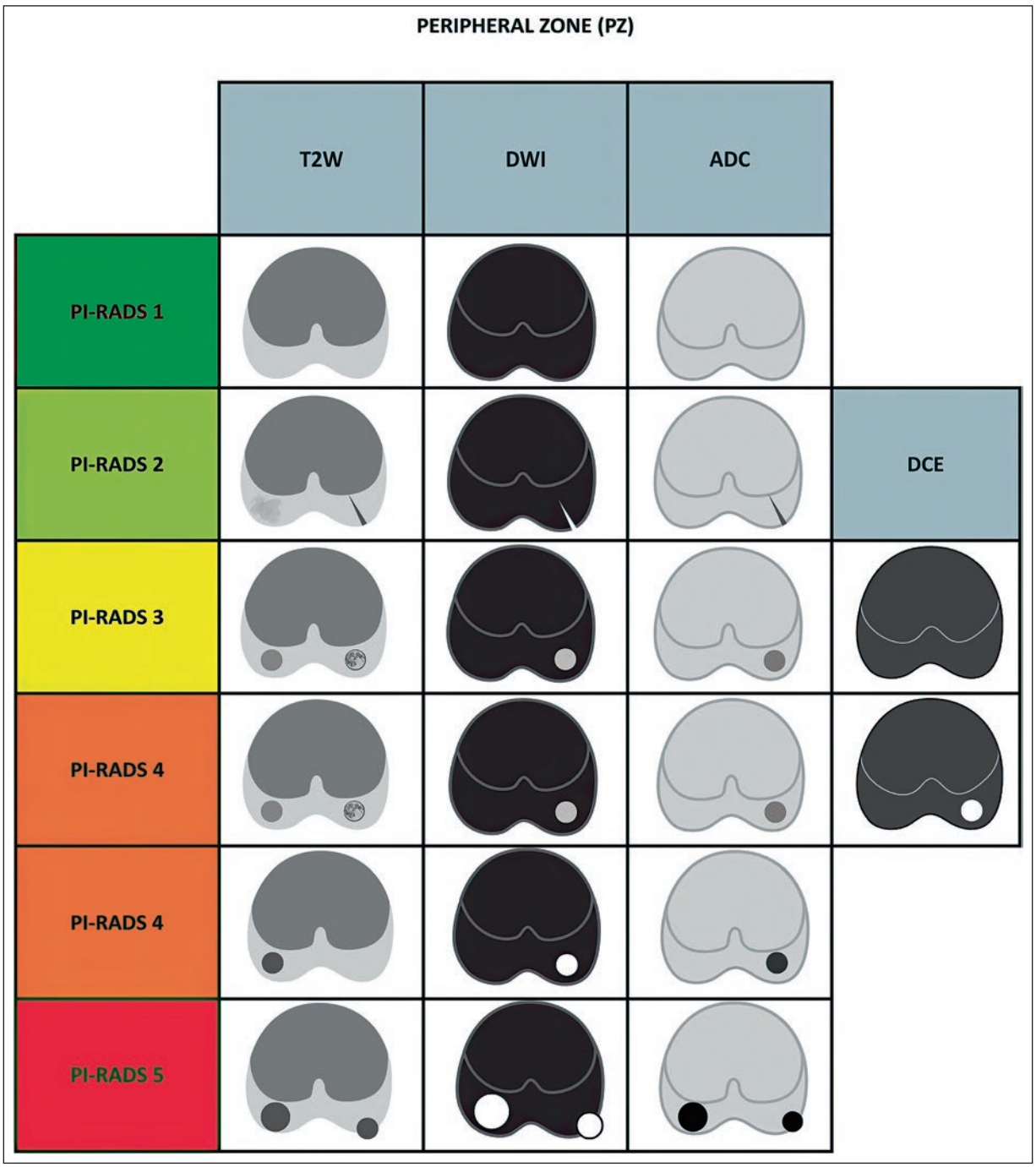

Figure 1. Schematic drawing showing how to score prostate MRI of the PZ lesions in PCa. DWI is the dominant sequence and can upgrade or downgrade any lesion. Early asymmetric enhancement on DCE can upgrade a PI-RADS 3 lesion.

ADC: apparent diffusion coefficient; DCE: dynamic contrast-enhanced; DWI: diffusion-weighted imaging; MRI: magnetic resonance imaging; PCa: prostate cancer; PI-RADS: Prostate Imaging Reporting and Data System; PZ: peripheral zone; T2W:T2-weighted.

change accordingly[18]. Some key points for scoring of PZ and TZ are listed below:

- *PZ:* the DWI sequence is dominant. Lesions scored 3 on DWI remain PI-RADS 3 if DCE is negative but are upgraded to PI-RADS 4 if there is positive focal enhancement on DCE. Figure 1 summarizes all categories in PZ.
- *TZ*: the T2W sequence is dominant. Round, encapsulated nodules are categorized as PI-RADS 1.

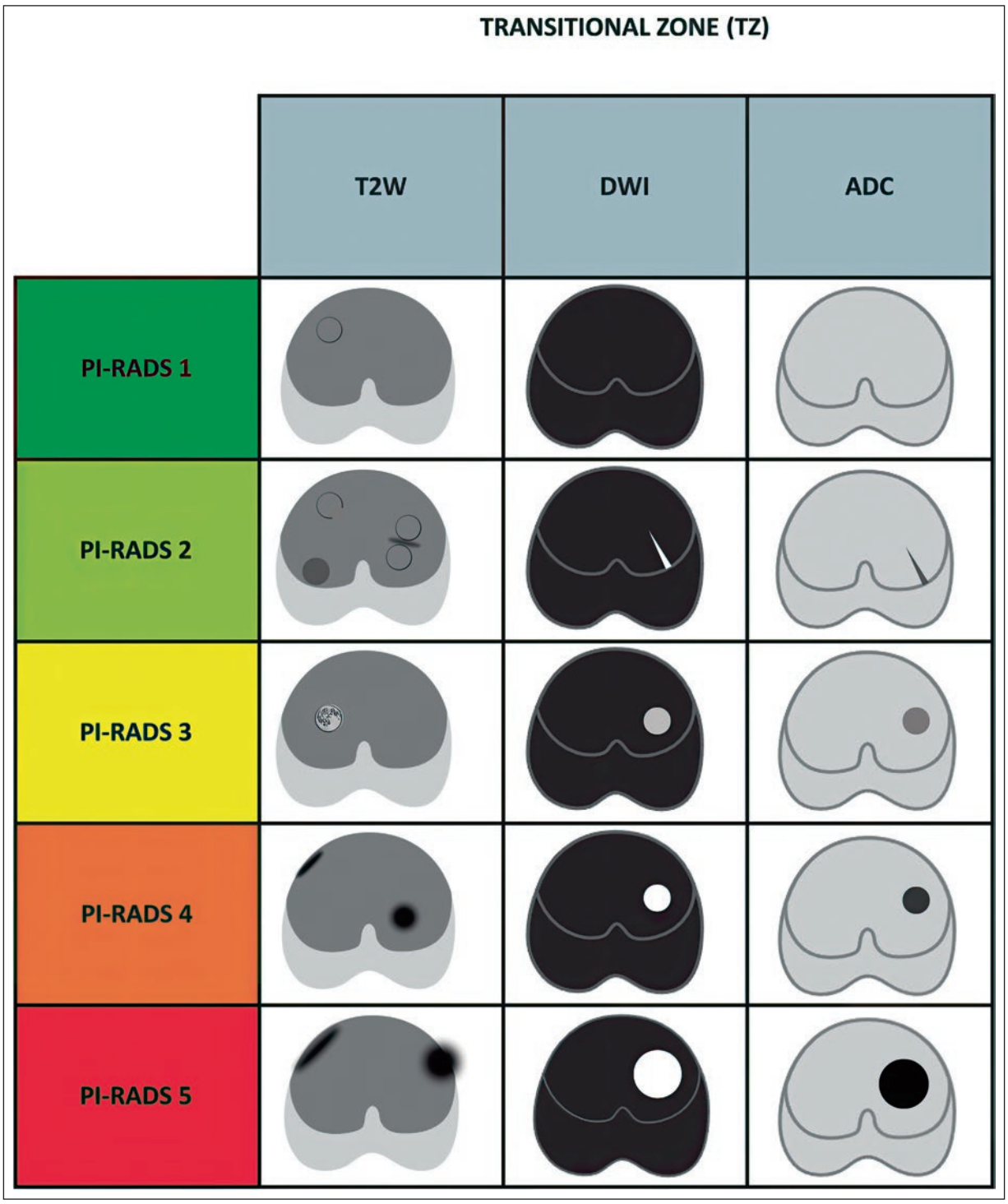

Figure 2. Schematic drawing showing how to score prostate MRI of the TZ lesions in PCa. T2W is the dominant sequence in TZ, and can upgrade or downgrade any lesion. A PI-RADS 4 on DWI can upgrade a PI-RADS 2 lesion on T2W for a final PI-RADS 3 category. Similarly, a PI-RADS 5 on DWI can upgrade a PI-RADS 3 lesion to T2W for a final PI-RADS 4 category.

ADC: apparent diffusion coefficient; DWI: diffusion-weighted imaging; MRI: magnetic resonance imaging; PCa: prostate cancer; PI-RADS: Prostate Imaging Reporting and Data System; T2W:T2-weighted; TZ: transition zone.

Lesions scored 2 at T2W remain PI-RADS 2 if DWI is ≤ 3, but are upgraded to PI-RADS 3 if DWI is ≥ 4. Figure 2 summarizes all categories in TZ.

The use of dominant sequences to upgrade or downgrade lesions is particularly important for those scored 2 to 4 in the T2W sequence, regardless of

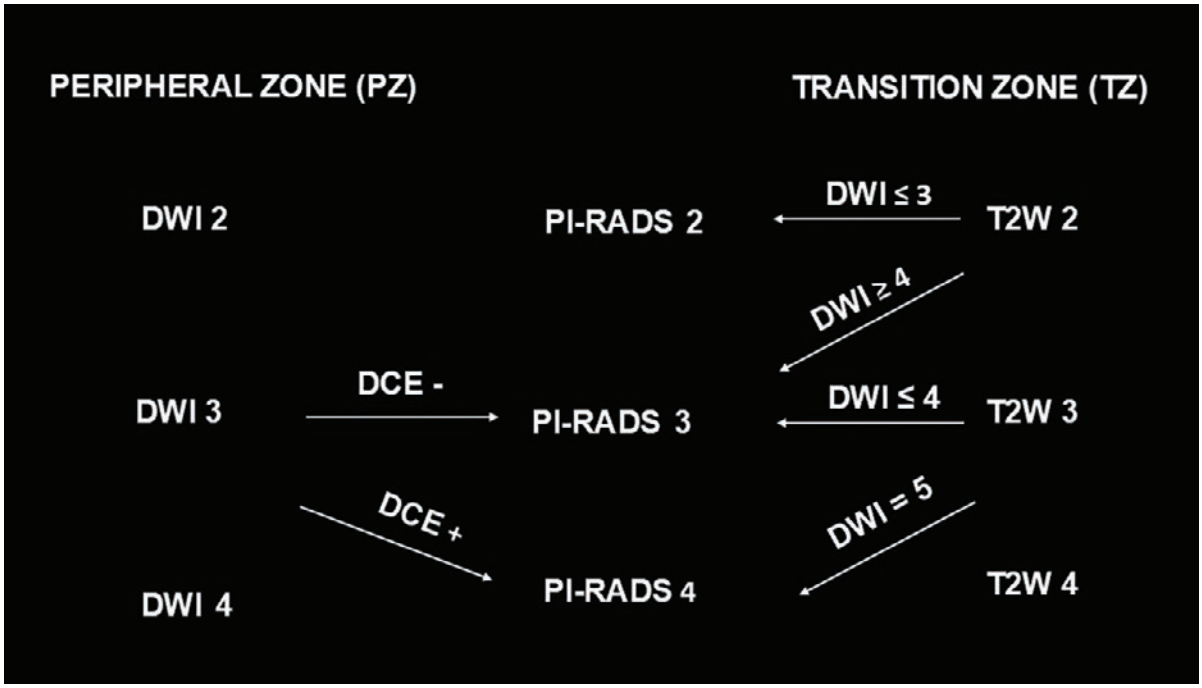

Figure 3. How to use dominant prostate MRI sequences in PZ and TZ for scored 2 to 4 lesions.

DCE: dynamic contrast-enhanced; DWI: diffusion-weighted imaging; MRI: magnetic resonance imaging; PI-RADS: Prostate Imaging Reporting and Data System; PZ: peripheral zone; T2W: T2-weighted; TZ: transition zone.

whether they are in PZ or TZ. Figure 3 illustrates these concepts. The refinement of lesion descriptions in the peripheral and transition zones improves diagnostic accuracy, especially for small-volume or atypically located cancers[19]. In addition, studies have highlighted the importance of standardizing radiological reports to improve reproducibility and diagnostic accuracy[20,21]. Figures 4 to 9 illustrate the application of the above criteria and show pathologically proven cases.

PI-RADS CATEGORY ASSIGNMENT IN BIPARAMETRIC MRI (bpMRI)

The bpMRI is an alternative to the traditional mpMRI approach using only T2W and DWI sequences without intravenous contrast administration[16,22]. Despite its simplicity, bpMRI can be used effectively in the context of PI-RADS, provided certain adjustments and considerations are made[23].

Advantages of bpMRI

- Cost reduction, as no contrast agent is required.
- Shorter examination time, which increases patient acceptance.
- Lower risk of adverse reactions or complications associated with the use of gadolinium.
- Easier implementation in centers with limited infrastructure without significantly compromising diagnostic performance in selected cases.

Disadvantages of bpMRI

- Potential limitations in detecting small lesions or in cases where contrast enhancement is critical for diagnosis.
- Reduced accuracy in specific populations, including: patients with low prostate cancer volume (< 0.5 cm^3); cases of prostatitis or very large prostates (> 80 ml); post-treatment changes (e.g. fibrosis after biopsy or radiotherapy); lesions in difficult locations (e.g. anterior fibromuscular stroma or central zone) and aggressive neoplasms with an infiltrative pattern[23].

Recent studies have shown that bpMRI has good diagnostic accuracy in selected cases. For example, a review by Junker et al.[22] found bpMRI to have comparable sensitivity to mpMRI in detecting clinically significant prostate cancer in intermediate-risk populations[24]. In addition, researchers such as Cuocolo et al.[25] have

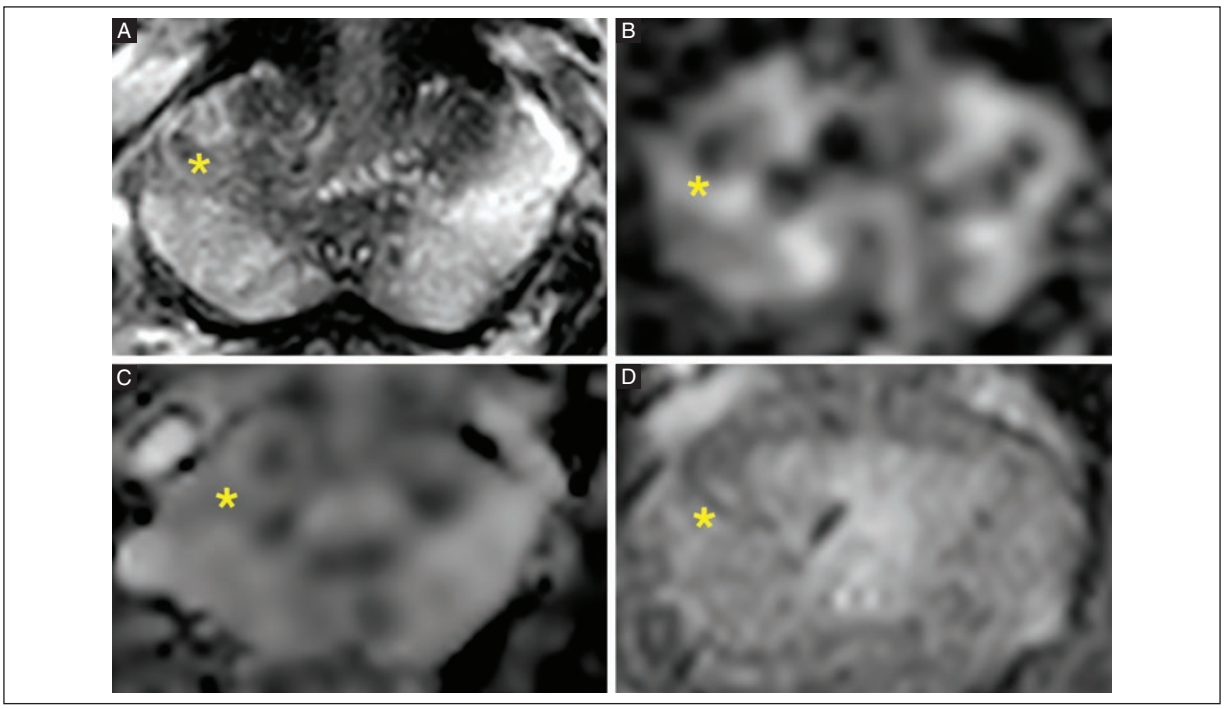

Figure 4. Prostate MRI with a PI-RADS 2 PZ score. **A:** axial T2W, a linear hypointensity area is seen (asterisk). **B:** axial T1 DWI, b = 1400 mm/s^2 (asterisk). **C:** ADC map (asterisk). **D:** axial T1W post-contrast with discrete enhancement (asterisk), not different from the remaining PZ. Follow-up showed stability for more than 2 years, presumably with chronic prostatitis.

ADC: apparent diffusion coefficient; DWI: diffusion-weighted imaging; MRI: magnetic resonance imaging; PCa: prostate cancer; PI-RADS: Prostate Imaging Reporting and Data System; PZ: peripheral zone; T1W: T1-weighted; T2W: T2-weighted.

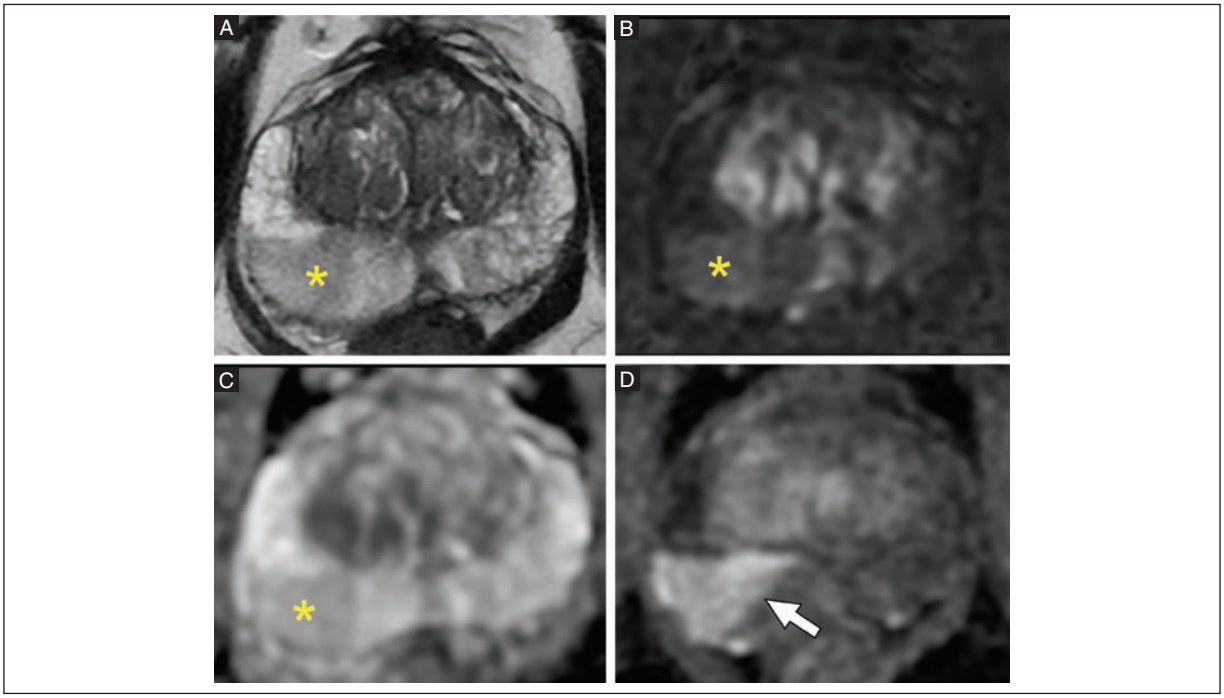

Figure 5. Prostate MRI with a PI-RADS score of 3+1 in the PZ. **A:** a hypointense area is seen on T2W (asterisk). **B:** with a subtle high signal in DWI (b = 1400 mm/s^2) (asterisk). **C:** low signal in the ADC map (asterisk). **D:** marked enhancement on the DCE, delimiting an area with a longest axis of 2.4 cm (arrow). It is important to remember that all PI-RADS 3+1 will be the final score 4, regardless of size. The follow-up showed stability for more than 2 years, presumably a chronic prostatitis.

ADC: apparent diffusion coefficient; DCE: dynamic contrast-enhanced; DWI: diffusion-weighted imaging; MRI: magnetic resonance imaging; PCa: prostate cancer; PI-RADS: Prostate Imaging Reporting and Data System; PZ: peripheral zone; T2W: T2-weighted.

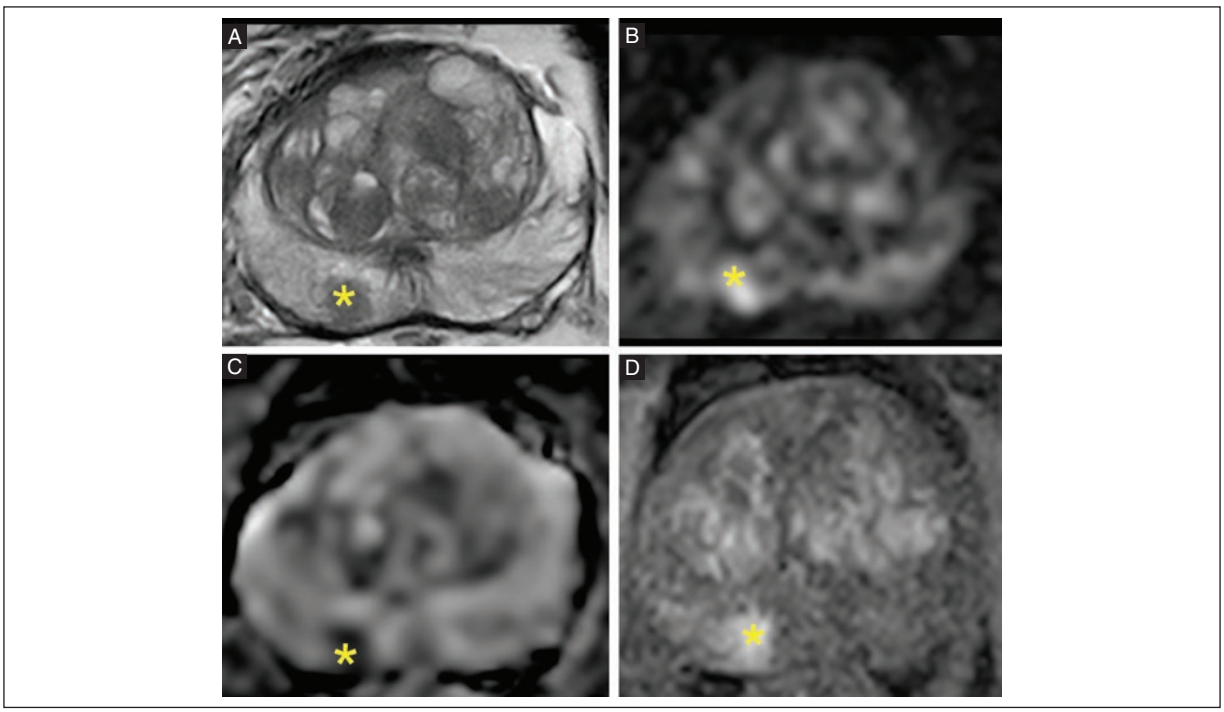

Figure 6. Prostate MRI with a PI-RADS score of 4 in the PZ. **A:** a well-defined nodule with hypointensity on the T2W axial (asterisk). **B:** marked focal hyperintensity in the DWI (asterisk). **C:** marked focal hypointensity on the ADC map (asterisk). **D:** on the DCE, the enhancement is earlier and stronger than in a normal PZ (asterisk). The subsequent fusion biopsy confirmed an ISUP 2 prostate adenocarcinoma.

ADC: apparent diffusion coefficient; DCE: dynamic contrast-enhanced; DWI: diffusion-weighted imaging; ISUP: International Society of Urological Pathology; MRI: magnetic resonance imaging; PI-RADS: Prostate Imaging Reporting and Data System; PZ: peripheral zone; T2W: T2-weighted.

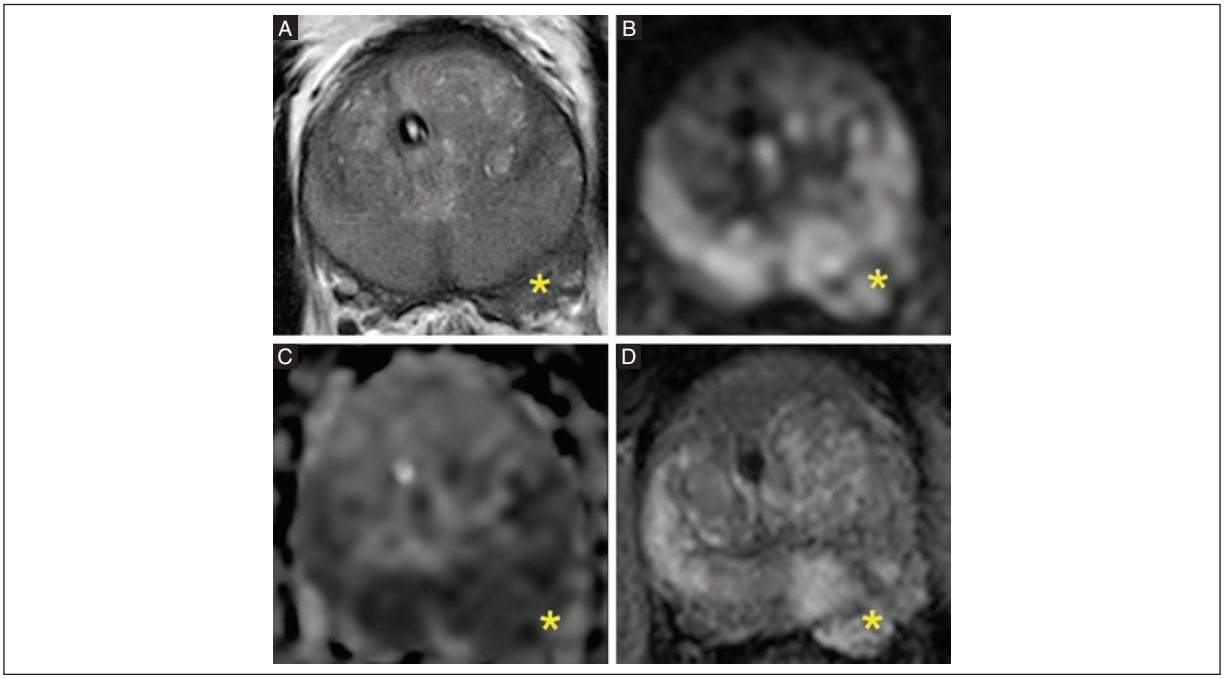

Figure 7. Prostate MRI with a PI-RADS score of 5 in the PZ. **A:** an extensive lesion in the mid-portion of the prostate, with diffuse hypointensity in the axial T2W in the PZ of both lobes with gross extraprostatic extension (asterisk), involving the left neurovascular bundle. **B:** marked high signal in the DWI (asterisk). **C:** low signal on the ADC map (asterisk). **D:** DCE image shows early enhancement of the lesion (asterisk). The subsequent biopsy confirmed an ISUP 4 prostate adenocarcinoma.

ADC: apparent diffusion coefficient; DCE: dynamic contrast-enhanced; DWI: diffusion-weighted imaging; ISUP: International Society of Urological Pathology; MRI: magnetic resonance imaging; PI-RADS: Prostate Imaging Reporting and Data System; PZ: peripheral zone; T2W: T2-weighted.

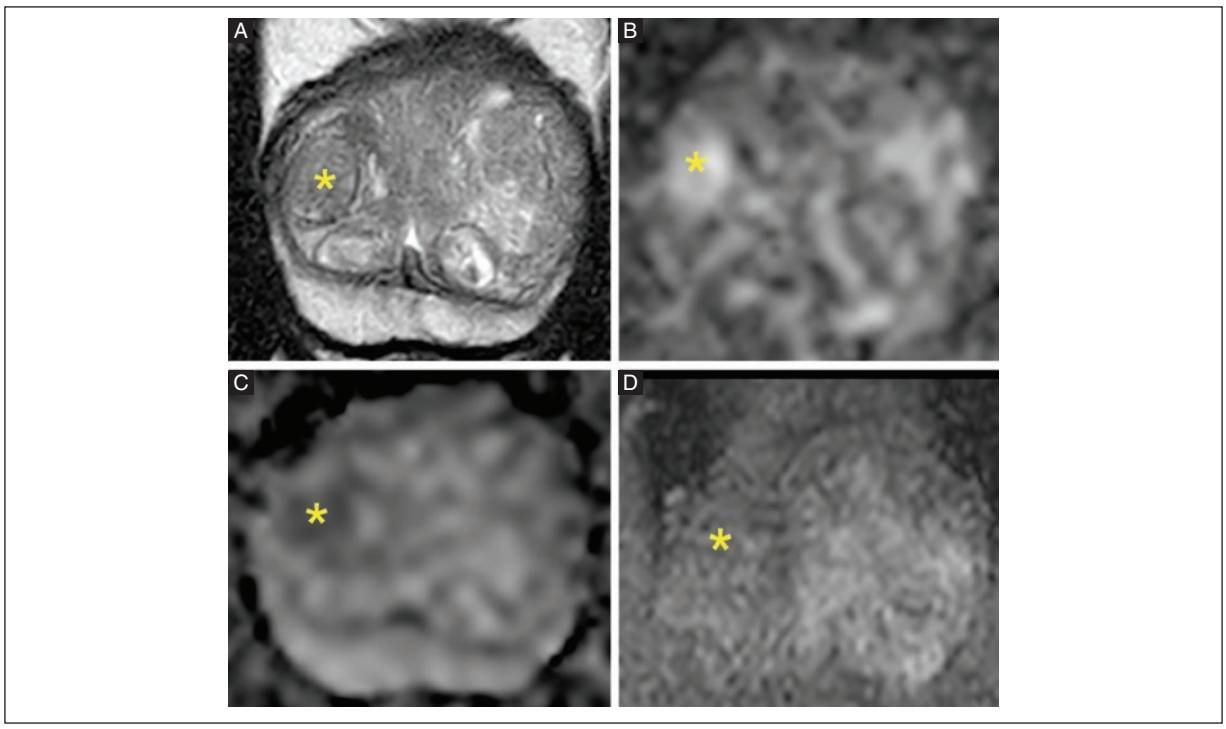

Figure 8. Prostate MRI with a PI-RADS score of 2 in TZ. **A:** an encapsulated nodule in the TZ of the mid-gland on the right (asterisk), with mild hypointensity in the axial T2W (asterisk). **B:** marked diffusion restriction, with high signal on DWI (asterisk). **C:** marked low signal on the ADC (asterisk). **D:** on the DCE image, the enhancement of the lesion is similar to the remaining TZ (asterisk). Follow-up examination showed stability for more than 2 years, probably a benign hyperplasia nodule.

ADC: apparent diffusion coefficient; DCE: dynamic contrast-enhanced; DWI: diffusion-weighted imaging; MRI: magnetic resonance imaging; PI-RADS: Prostate Imaging Reporting and Data System; PZ: peripheral zone; TZ: transition zone; T2W: T2-weighted.

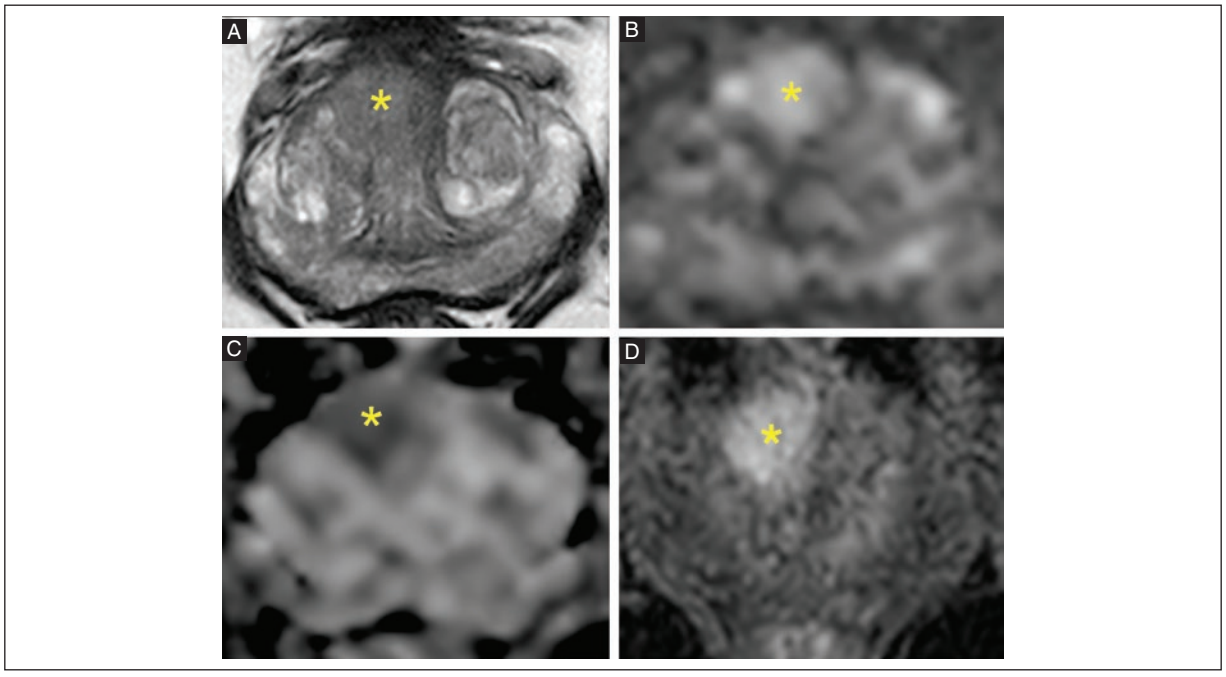

Figure 9. Prostate MRI with a PI-RADS score of 5 in the TZ. **A:** a non-encapsulated area in the anterior TZ extending through the entire mid-gland, including the PZ, with hypointensity in the axial T2W (asterisk). **B:** marked restriction, hyperintensity in the DWI (asterisk). **C:** hypointensity on the ADC map with a size of 1.5 cm in the axial plane (asterisk). **D.** post-contrast image with early enhancement of the lesion (asterisk).

ADC: apparent diffusion coefficient; DWI: diffusion-weighted imaging; MRI: magnetic resonance imaging; PI-RADS: Prostate Imaging Reporting and Data System; TZ: transition zone; T2W: T2-weighted.

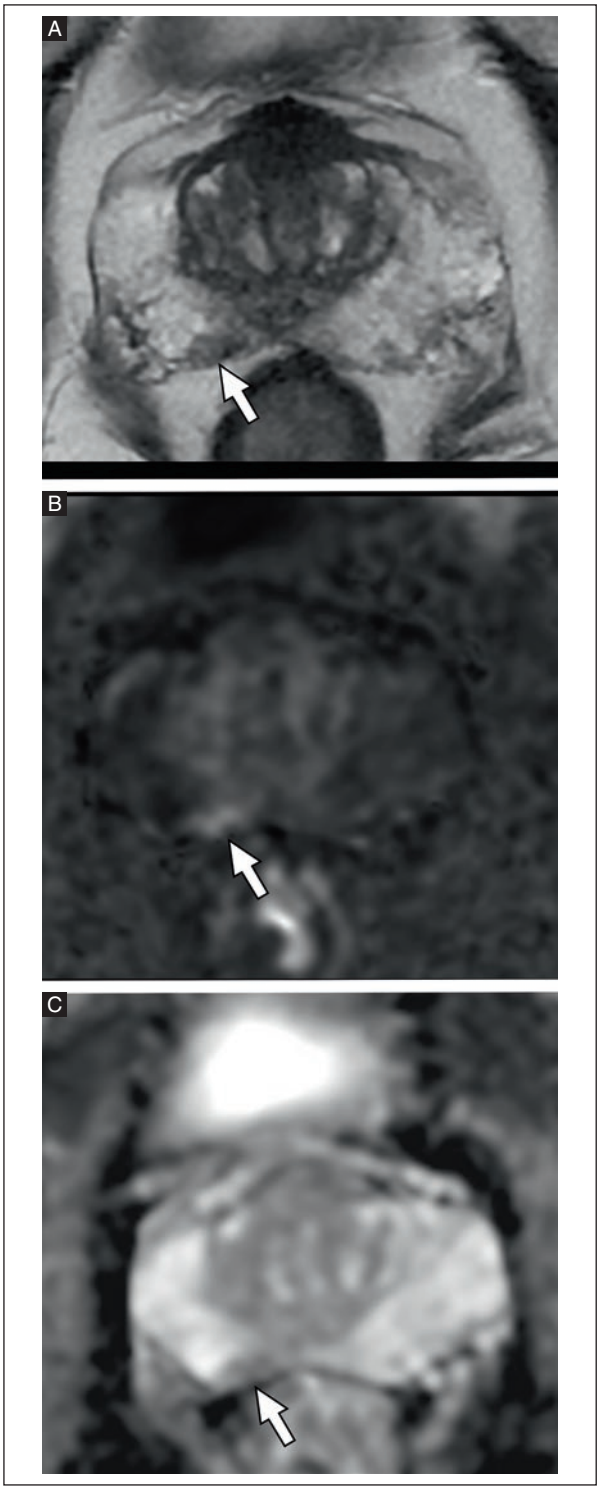

Figure 10. Prostate bpMRI of a PCa with a PI-RADS score of 4 in the PZ. **A:** a subcapsular, crescentic lesion is seen in the right mid-gland, paramedian, with low signal in axial T2W (arrow). **B:** high signal in the DWI (arrow). **C:** low signal in the ADC map (arrow). The subsequent fusion biopsy confirmed an ISUP 2 prostate adenocarcinoma.

ADC: apparent diffusion coefficient; DWI: diffusion-weighted imaging; bpMRI: biparametric magnetic resonance imaging; ISUP: International Society of Urological Pathology; PCa: prostate cancer; PZ: peripheral zone; PI-RADS: Prostate Imaging Reporting and Data System; T2W: T2-weighted.

explored the integration of artificial intelligence algorithms into bpMRI to improve its performance[26].

Application of PI-RADS in bpMRI

In the absence of DCE, PI-RADS assessment in bpMRI relies exclusively on T2W and DWI sequences (Figure 10). The protocol follows these guidelines:

Peripheral zone (PZ)

- DWI is the dominant sequence.
- Focal lesion with restricted diffusion, low signal in apparent diffusion coefficient (ADC) and high signal on DWI with high b-value is categorized as PI-RADS 4 or 5 depending on the degree of restriction and size of the lesion[27,28].
- Lesion without significant restriction or inconclusive DWI findings remain PI-RADS 3 and require correlation with other clinical data (e.g. prostate-specific antigen level)[23].

Transition zone (TZ)

- T2W is the dominant sequence.
- Suspicious lesions appear as poorly-defined hypointense areas with an infiltrative pattern or irregular margins[16].
- Well-encapsulated, homogeneous nodules are generally classified as PI-RADS 1 or 2.
- Lesions with poorly defined margins and moderate hypointensity can be classified as PI-RADS 3, with DWI restriction serving as a complementary criterion to increase malignant suspicious lesion (PI-RADS 4 or 5)[23,29].

Borderline lesion

- In inconclusive findings, bpMRI may be supplemented with additional clinical data or followed by mpMRI for diagnostic confirmation, especially in high-risk patients.

The application of PI-RADS in bpMRI requires expertise and a detailed understanding of the classification criteria[27]. Despite its limitations, bpMRI is a valuable alternative in settings where mpMRI is not feasible and offers a cost-effective and efficient approach to detecting clinically significant prostate cancer.

Score assignment is a challenging task that improves significantly with the radiologist´s experience. A detailed discussion of lesions that mimic PCa and the main

causes of missed lesions is beyond the scope of this article. However, readers can explore this topic further by consulting the reference by Purysko et al.[18].

DIAGNOSTIC ACCURACY OF PI-RADS V2.1

Although the diagnostic accuracy of a method depends on who performs it, it is always helpful to have reference values for the tool, even if these are derived from ideal scenarios with experienced examiners. The diagnostic accuracy of PI-RADS has shown considerable variation in the literature[30]. However, the average sensitivity and negative predictive value of PI-RADS consistently fall within highly favorable range, justifying its widespread use as an initial assessment tool for PCa[31,32]. It is worth noting that diagnostic accuracy values for MRI generally refer to clinically significant cancers, unless explicitly stated otherwise. Despite varying definitions in the literature, this generally refers to lesions with an International Society of Urological Pathology (ISUP) score of ≥ 2[33].

A recent meta-analysis and systematic review by Oerther et al.[34] focusing exclusively on PI-RADS version 2.1 data and clinically significant cancers has made an important contribution to this topic. This study analyzed data from over 70 studies with more than 13,000 patients. Using a PI-RADS cutoff score of ≥ 3, the study found a sensitivity of 96% and a specificity of 43%, with an area under the curve (AUC) of 0.86 (95% CI: 0.75-0.93). When the cutoff was adjusted to PI-RADS ≥ 4, sensitivity decreased to 89%, while specificity increased to 66%, resulting in an AUC of 0.89 (95% CI: 0.85-0.92).

The study by Oerther et al.[34] also highlighted a well-documented limitation of MRI and PI-RADS in the assessment of PCa: the low positive predictive value (PPV) of the method[35,36]. At a cut-off score of ≥ 3, the PPV for clinically significant lesions at the patient level was 63%. However, when the cut-off was raised to PI-RADS ≥ 4, the PPV decreased to 25%. These results are consistent with previous studies that emphasized the excellent sensitivity and negative predictive value of the method while acknowledging its limitation in terms of PPV[37].

Another critical parameter that provides useful guidance to practitioners is the cancer detection rate (CDR). Of course, the CDR varies according to the PI-RADS score assigned to each lesion[38]. In the study by Oerther et al.[34] the CDR for PI-RADS 1, 2, 3, 4, and 5 lesions was 6%, 5%, 19%, 54%, and 84%, respectively. These figures are consistent with those reported by Park et al.[39] in a 2021 systematic review, in which the CDR for scores 1 to 5 were 2%, 4%, 20%, 52% and 89%, respectively.

Another important consideration is the comparison between bpMRI and mpMRI techniques. Numerous previous studies have concluded that the diagnostic accuracy of the two approaches is equivalent. This result was also confirmed by Oerther et al.[34]. However, certain scenarios require the use of contrast-enhanced sequences to maximize the benefit of MRI. In cases where metallic prostheses are used in the pelvis (especially in the hip) causing magnetic susceptibility artifacts, or in obese and/or large patients with a reduced signal-to-noise ratio (SNR), gadolinium-based contrast-enhanced sequences are crucial to overcome the limitations of low-quality diffusion sequences in such situations[40].

FUTURE DEVELOPMENTS AND PERSPECTIVES FOR PI-RADS

The introduction of MRI in the management of PCa has standardized both image acquisition and reporting[35]. However, even with the current version 2.1 of PI-RADS, there is still considerable interobserver variability in examination description and conclusions, which affects patient risk stratification[30,33].

Advances related to MRI and PI-RADS include the development of the MRI Diagnostic Pathway[41]. This term refers to the diagnostic approach for patients with suspected PCa, that integrates epidemiologic data and imaging studies—particularly MRI—to determine the most effective strategy for either to confirm or rule out PCa[42]. Notably, international organizations already recommend MRI of the prostate as an initial diagnostic tool for patients, especially for those who have not undergone a prostate biopsy. Studies such as PROMIS[43], PRECISION[12] and MRI First[37] have demonstrated the benefits of MRI prior to biopsy, including higher detection rates of clinically significant cancers and lower detection of non-clinically significant ones.

Despite these advances, progress in the field continues and includes: a) the adoption of quality standards for image analysis; b) the use of more advanced post-processing techniques; c) the integration of artificial intelligence tools at different stages, from image acquisition to interpretation, and d) the development of systems in parallel with PI-RADS, such as Pi-QUAL[44] for image quality assessment and PRECISE[45] for

monitoring patients under active surveillance. Both systems have already reached their second version.

In this evolving context, discussions are underway about the necessity for a new version of PI-RADS that takes into account, if not all, at least some of these advancements. The American College of Radiology (ACR) committee responsible for RADS has adopted a more restrictive policy regarding changes to the scoring system it sponsors[46]. Nevertheless, there are a number of publications that highlight important considerations for a future version of PI-RADS. These considerations include: a) improvements to T2W and DWI sequences, particularly with the advent of synthetic diffusion techniques that improve the reliability of bpMRI examinations[47].

The Prime study, a prospective multi-institutional trial, is currently comparing the diagnostic accuracy of bpMRI and mpMRI and is expected to provide concrete data in this area; b) standardization of diagnostic approaches based on MRI findings. Many experts advocate integrating clinical data —such as prostate-specific antigen density (dPSA)— to improve diagnostic accuracy. For example, PI-RADS category 3 currently indicates an indeterminate likelihood of clinically significant prostate cancer, leaving clinicians uncertain whether to recommend a biopsy[48]. To address this issue, a new category (PI-RADS 3F) could be introduced that specifies follow-up protocols, similar to Breast Imaging Reporting and Data System (BI-RADS) category 3 in breast imaging, while reserving biopsies for cases with elevated dPSA; c) refinements to the lexicons developed for PI-RADS to improve the reproducibility of the classification and promote more consistent clinical practice.

CONCLUSION

After 13 years of use, PI-RADS has proven to be a powerful tool for classifying and stratifying PCa risk and has fundamentally changed patient assessment. Detailed knowledge of the imaging findings is still essential to accurately interpret the results and determine the best course of action. On a broader scale, PI-RADS contributes to the standardization of clinical practice. This article provides an overview of the principles that have promoted and sustained PI-RADS as an essential framework for the management of PCa.

Funding

The authors declare that they received no funding or support for this article.

Conflicts of interest

The authors declare no conflicts of interest.

Ethical considerations

Protection of humans and animals. The authors declare that no experiments involving humans or animals were conducted for this research.

Confidentiality, informed consent, and ethical approval. The study does not involve patient personal data nor requires ethical approval. The SAGER guidelines do not apply.

Declaration on the use of artificial intelligence. The authors declare that no generative artificial intelligence was used in the writing of this manuscript.

REFERENCES

1. Steyn JH, Smith FW. Nuclear magnetic resonance imaging of the prostate. Br J Urol 1982;54(6):726-728. doi: 10.1111/j.1464-410x.1982.tb13634.x.
2. Buonocore E, Hesemann C, Pavlicek W, Montie JE. Clinical and in vitro magnetic resonance imaging of prostatic carcinoma. AJR Am J Roentgenol. 1984;143(6):1267-1272. doi: 10.2214/ajr.143.6.1267.
3. Issa B. In vivo measurement of the apparent diffusion coefficient in normal and malignant prostatic tissues using echo-planar imaging. J Magn Reson Imaging. 2002;16 (2):196-200 doi: 10.1002/jmri.10139.
4. Edelman RR. The history of MR imaging as seen through the pages of radiology. Radiology. 2014;273(2Suppl):S181-S200. doi: 10.1148/radiol.14140706.
5. Cornfeld DM, Weinreb JC. MR imaging of the prostate: 1.5T versus 3T. Magn Reson Imaging Clin N Am. 2007;15(3):433-448, viii. doi: 10.1016/j.mric.2007.06.004.
6. Kim CK, Park BK, Kim B. Diffusion-weighted MRI at 3 T for the evaluation of prostate cancer. AJR Am J Roentgenol. 2010;194(6):1461-9. doi: 10.2214/AJR.09.3654.
7. Tanimoto A, Nakashima J, Kohno H, Shinmoto H, Kuribayashi S. Prostate cancer screening: the clinical value of diffusion-weighted imaging and dynamic MR imaging in combination with T2-weighted Imaging. J Magn Reson Imaging. 2007;25(1):146-152. doi: 10.1002/jmri.20793.
8. Kirkham APS, Emberton M, Allen C. How good is MRI at detecting and characterising cancer within the prostate? Eur Urol. 2006;50(6):1163-1175. doi: 10.1016/j.eururo.2006.06.025.
9. Barentsz JO, Richenberg J, Clements R, Choyke P, Verma S, Villeirs G, et al. European Society of Urogenital Radiology. ESUR prostate MR guidelines 2012. Eur Radiol. 2012;22(4):746-757. doi: 10.1007/s00330-011-2377-y.
10. Renard-Penna R, Mozer P, Cornud F, Barry-Delongchamps N, Bruguière E, Portalez D, et al. Prostate Imaging Reporting and Data System and Likert Scoring System: multiparametric MR Imaging Validation Study to Screen Patients for Initial Biopsy. Radiology. 2015;275(2):458-468. doi: 10.1148/radiol.14140184.
11. Weinreb JC, Barentsz JO, Choyke PL, Cornud F, Haider MA, Macura KJ, et al. PI-RADS Prostate Imaging - Reporting and Data System: 2015, Version 2. Eur Urol. 2016;69(1):16-40. doi: 10.1016/j.eururo.2015.08.052.
12. Kasivisvanathan V, Rannikko AS, Borghi M, Panebianco V, Mynderse LA, Vaarala MH, et al. PRECISION Study Group Collaborators. MRI-Targeted or Standard Biopsy for Prostate-Cancer Diagnosis. N Engl J Med. 2018;378(19):1767-1777. doi: 10.1056/NEJMoa1801993.
13. Prostate Cancer Guidelines. European Association of Urology. https://uroweb.org/guidelines/prostate-cancer/panel.
14. Wei JT, Barocas D, Carlsson S, Coakley F, Eggener S, Etzioni R, et al. Early Detection of Prostate Cancer: AUA/SUO Guideline Part I: Prostate Cancer Screening. J Urol. 2023;210(1):46–53. doi: 10.1097/JU.0000000000003491.
15. Schaeffer EM, Srinivas S, Adra N, An Y, Bitting R, Chapin B, et al. Prostate Cancer, Version 3.2024: Featured Updates to the NCCN Guidelines. J Nat Compr Cancer Network. 2024:22(3):140-150.

16. American College of Radiology® Committee on PI-RADS®. PI-RADS 2019 v2.1. Available at: https://www.acr.org/-/media/ACR/Files/RADS/PI-RADS/PIRADS-V2-1.pdf. American College of Radiology. Accessed on Jan. 31, 2025.
17. Turkbey B, Rosenkrantz AB, Haider MA, Padhani AR, Villeirs G, Macura KJ, et al. Prostate Imaging Reporting and Data System Version 2.1: 2019 Update of Prostate Imaging Reporting and Data System Version 2. Eur Urol. 2019;76(3):340-351. doi: 10.1016/j.eururo.2019.02.033.
18. Purysko AS, Childes BJ, Ward RD, Bittencourt LK, Klein EA. Pitfalls in Prostate MRI Interpretation: A Pictorial Review. Semin Roentgenol. 2021;56(4):391-405. doi: 10.1053/j.ro.2021.08.003.
19. Yilmaz EC, Lin Y, Belue MJ, Harmon SA, Phelps TE, Merriman KM, et al. PI-RADS Version 2.0 Versus Version 2.1: Comparison of Prostate Cancer Gleason Grade Upgrade and Downgrade Rates From MRI-Targeted Biopsy to Radical Prostatectomy. AJR Am J Roentgenol. 2024;222(1):e2329964. doi: 10.2214/AJR.23.29964.
20. Park SY, Woo S, Park KJ, Westphalen AC. A pictorial essay of PI-RADS pearls and pitfalls: toward less ambiguity and better practice. Abdom Radiol (NY). 2024;49(9):3190-3205. doi: 10.1007/s00261-024-04273-0.
21. Desai S, Costa DN. PI-RADS and Likert scales for structured reporting in multiparametric MR imaging of the prostate. Br J Radiol. 2022; 95(1131):20210758. doi: 10.1259/bjr.20210758.
22. Junker D, Steinkohl F, Fritz V, Bektic J, Tokas T, Aigner F, et al. Comparison of multiparametric and biparametric MRI of the prostate: are gadolinium-based contrast agents needed for routine examinations? World J Urol. 2019;37(4):691-699. doi: 10.1007/s00345-018-2428-y.
23. Gatti M, Faletti R, Calleris G, Giglio J, Berzovini C, Gentile F, et al P. Prostate cancer detection with biparametric magnetic resonance imaging (bpMRI) by readers with different experience: performance and comparison with multiparametric (mpMRI). Abdom Radiol (NY). 2019;44(5):1883-1893. doi: 10.1007/s00261-019-01934-3.
24. Stabile A, Giganti F, Rosenkrantz AB, Taneja SS, Villeirs G, Gill IS, et al. Multiparametric MRI for prostate cancer diagnosis: current status and future directions. Nat Rev Urol. 2020;17(1):41-61. doi: 10.1038/s41585-019-0212-4.
25. Cuocolo R, Verde F, Ponsiglione A, Romeo V, Petretta M, Imbriaco M, et al. Clinically Significant Prostate Cancer Detection With Biparametric MRI: A Systematic Review and Meta-Analysis. AJR Am J Roentgenol. 2021;216(3):608-621. doi: 10.2214/AJR.20.23219.
26. Thestrup KC, Logager V, Baslev I, Møller JM, Hansen RH, Thomsen HS. Biparametric versus multiparametric MRI in the diagnosis of prostate cancer. Acta Radiol Open. 2016;5(8):2058460116663046. doi: 10.1177/2058460116663046.
27. Scialpi M, Scialpi P, Martorana E, Torre R, Mancioli FA, D'Andrea A, et al. Biparametric MRI with simplified PI-RADS (S-PI-RADS) for prostate cancer detection and management: what do radiologist need to know. Radiol Med. 2021;126(12):1660-1661. doi: 10.1007/s11547-021-01343-x.
28. Boesen L, Nørgaard N, Løgager V, Balslev I, Bisbjerg R, Thestrup KC, et al. Assessment of the Diagnostic Accuracy of Biparametric Magnetic Resonance Imaging for Prostate Cancer in Biopsy-Naive Men: The Biparametric MRI for Detection of Prostate Cancer (BIDOC) Study. JAMA Netw Open. 2018;1(2):e180219. doi: 10.1001/jamanetworkopen.2018.0219.
29. Belue MJ, Yilmaz EC, Daryanani A, Turkbey B. Current Status of Biparametric MRI in Prostate Cancer Diagnosis: Literature Analysis. Life (Basel). 2022;12(6):804. doi: 10.3390/life12060804.
30. Westphalen AC, McCulloch CE, Anaokar JM, Arora S, Barashi NS, Barentsz JO, et al. Variability of the Positive Predictive Value of PI-RADS for Prostate MRI across 26 Centers: Experience of the Society of Abdominal Radiology Prostate Cancer Disease-focused Panel. Radiology. 2020;296(1):76-84. doi: 10.1148/radiol.2020190646.
31. Sathianathen NJ, Omer A, Harriss E, Davies L, Kasivisvanathan V, Punwani S, et al. Negative Predictive Value of Multiparametric Magnetic Resonance Imaging in the Detection of Clinically Significant Prostate Cancer in the Prostate Imaging Reporting and Data System Era: A Systematic Review and Meta-analysis. Eur Urol. 2020;78(3):402-414. doi: 10.1016/j.eururo.2020.03.048.
32. Stonier T, Simson N, Shah T, Lobo N, Amer T, Lee SM, et al. The "Is mpMRI Enough" or IMRIE Study: A Multicentre Evaluation of Prebiopsy Multiparametric Magnetic Resonance Imaging Compared with Biopsy. Eur Urol Focus. 2021;7(5):1027-1034. doi: 10.1016/j.euf.2020.09.012.
33. Mazzone E, Stabile A, Pellegrino F, Basile G, Cignoli D, Cirulli GO, et al. Positive Predictive Value of Prostate Imaging Reporting and Data System Version 2 for the Detection of Clinically Significant Prostate Cancer: A Systematic Review and Meta-analysis. Eur Urol Oncol. 2021;4(5):697-713. doi: 10.1016/j.euo.2020.12.004.
34. Oerther B, Nedelcu A, Engel H, Schmucker C, Schwarzer G, Brugger T, et al. Update on PI-RADS Version 2.1 Diagnostic Performance Benchmarks for Prostate MRI: Systematic Review and Meta-Analysis. Radiology 2024;312(2):e233337. doi: 10.1148/radiol.233337.
35. Padhani AR, Barentsz J, Villeirs G, Rosenkrantz AB, Margolis DJ, Turkbey B, et al. PI-RADS Steering Committee: The PI-RADS Multiparametric MRI and MRI-directed Biopsy Pathway. Radiology. 2019;292(2):464-474. doi: 10.1148/radiol.2019182946.
36. Haj-Mirzaian A, Burk KS, Lacson R, Glazer DI, Saini S, Kibel AS, et al. Magnetic Resonance Imaging, Clinical, and Biopsy Findings in Suspected Prostate Cancer: A Systematic Review and Meta-Analysis. JAMA Netw Open. 2024;7(3):e244258. doi: 10.1001/jamanetworkopen.2024.4258.
37. Rouvière O, Puech P, Renard-Penna R, Claudon M, Roy C, Mège-Lechevallier F, et al; MRI-FIRST Investigators. Use of prostate systematic and targeted biopsy on the basis of multiparametric MRI in biopsy-naive patients (MRI-FIRST): a prospective, multicentre, paired diagnostic study. Lancet Oncol. 2019;20(1):100-109. doi: 10.1016/S1470-2045(18)30569-2.
38. Oerther B, Engel H, Bamberg F, Sigle A, Gratzke C, Benndorf M. Cancer detection rates of the PI-RADS v2.1 assessment categories: systematic review and meta-analysis on lesion level and patient level. Prostate Cancer Prostatic Dis. 2022;25(2):256-263. doi: 10.1038/s41391-021-00417-1.
39. Park KJ, Choi SH, Kim MH, Kim JK, Jeong IG. Performance of Prostate Imaging Reporting and Data System Version 2.1 for Diagnosis of Prostate Cancer: A Systematic Review and Meta-Analysis. J Magn Reson Imaging. 2021;54(1):103-112. doi: 10.1002/jmri.27546.
40. Lin Y, Yilmaz EC, Belue MJ, Turkbey B. Prostate MRI and image Quality: It is time to take stock. Eur J Radiol. 2023;161:110757. doi: 10.1016/j.ejrad.2023.110757.
41. Padhani AR, Haider MA, Rouviere O. Balancing the benefits and harms of MRI-directed biopsy pathways. Eur Radiol. 2022;32(4):2326-2329. doi: 10.1007/s00330-21-08535-z.
42. Bittencourt LK, Guricova K, Zucker I, Durieux JC, Schoots IG. Risk-based MRI-directed diagnostic pathway outperforms non-risk-based pathways in suspected prostate cancer biopsy-naïve men: a large cohort validation study. Eur Radiol. 2022;32(4):2330-2339. doi: 10.1007/s00330-021-08407-6.
43. Ahmed HU, El-Shater Bosaily A, Brown LC, Gabe R, Kaplan R, Parmar MK, et al PROMIS study group. Diagnostic accuracy of multi-parametric MRI and TRUS biopsy in prostate cancer (PROMIS): a paired validating confirmatory study. Lancet. 2017;389(10071):815-822. doi: 10.1016/S0140-6736(16)32401-1.
44. de Rooij M, Allen C, Twilt JJ, Thijssen LCP, Asbach P, Barrett T, et al. PI-QUAL version 2: an update of a standardised scoring system for the assessment of image quality of prostate MRI. Eur Radiol. 2024;34(11):7068-7079. doi: 10.1007/s00330-024-10795-4.
45. Engelman C, Maffei D, Allen C, Kirkham A, Albertsen P, Kasivisvanathan V, et al. PRECISE Version 2: Updated Recommendations for Reporting Prostate Magnetic Resonance Imaging in Patients on Active Surveillance for Prostate Cancer. Eur Urol. 2024;86(3):240-255. doi: 10.1016/j.eururo.2024.03.014.
46. Davenport MS, Chatfield M, Hoang J, Maturen KE, Obuchowski N, Tse JR, et al. ACR-RADS Programs Current State and Future Opportunities: Defining a Governance Structure to Enable Sustained Success. J Am Coll Radiol. 2022;19(6):782-791. doi: 10.1016/j.jacr.2022.03.012.
47. Hermie I, Van Besien J, De Visschere P, Lumen N, Decaestecker K. Which clinical and radiological characteristics can predict clinically significant prostate cancer in PI-RADS 3 lesions? A retrospective study in a high-volume academic center. Eur J Radiol. 2019; 114:92-98. doi: 10.1016/j.ejrad.2019.02.031.
48. Barrett T. Updating PI-RADS Version 2.1-Point: The Time Is Now! AJR Am J Roentgenol. 2024. doi: 10.2214/AJR.24.32393. Epub ahead of print.

JMeXFRI

Journal of the Mexican Federation of Radiology and Imaging

Check for updates

FULL RESEARCH ARTICLE

Breast MRI acquisition and analysis protocol: a pictorial essay

I. Miranda Sanchez-Carenzo-Velez[1,2#], Yesika J. Davila-Zablah[1#], Elena Maria Sanchez-Siller[1#], Mané M. Ayala-Duran[1#], Ilany B. Lopez-Valdivia[2], Maria Guerra-Ayala[2], Jessica A. Perdomo-Galviz[2], Karla I. Soto-Valdez[2], Sofia Hurtado-Arellano[3], and Margarita L. Garza-Montemayor[1#]*

[1]*Diagnostic Breast Imaging Department, Hospital Zambrano Hellion Tec Salud;* [2]*Department of Radiology and Imaging, Tec Salud;* [3]*School of Medicine and Health Sciences, Tecnológico de Monterrey. Monterrey, Nuevo Leon, Mexico*

[#]*These authors contributed equally*

ABSTRACT

Breast cancer is a worldwide malignant disease that is heterogeneous in its macroscopic morphology and at the molecular level. Although mammography is the standard examination for diagnosis, breast magnetic resonance imaging (MRI) has the highest sensitivity for breast cancer detection. The indications for a breast MRI are diverse, with cancer staging being the most important. This pictorial essay presents a breast MRI acquisition and analysis protocol, supported by drawings of the morphologic features of mass and non-mass lesions based on the American College of Radiology Breast Imaging Reporting and Data System (BI-RADS) 5th Edition lexicon and the Kaiser score. Our institution includes the following sequences in the breast MRI protocol: T1-weighted spin-echo (SE), T2 fat-suppressed (FS), diffusion-weighted images (DWI), the apparent diffusion coefficient (ADC), T1 gradient echo (GE) with fat sat (FS), T1 dynamic contrast-enhanced (DCE) with gadolinium (Gd), time-signal intensity curve (kinetic curve), positive enhancement integral (PEI) values, maximum intensity projection (MIP) and the coronal T2 fast spin-echo (FSE). Experienced radiologists should interpret breast MRI in correlation with other imaging studies, such as a recent mammography and/or a breast ultrasound. This pictorial essay is published for educational purposes for radiologists and residents.

Keywords: *Breast magnetic resonance imaging. Kaiser score. Breast cancer. MRI lexicon.*

INTRODUCTION

The global incidence of breast cancer is increasing at a rate of 3.1% annually[1]. This reflects the importance of screening examinations such as mammography and ultrasound and other tools such as breast magnetic resonance imaging (MRI) with contrast medium. Breast MRI has a high sensitivity of 94-100% for detecting breast cancer[1,2]. The main indications for breast MRI are patients with a recent diagnosis of breast cancer for staging and treatment planning; the follow-up of women with a personal history of breast cancer to detect recurrence or a new tumor; women with an intermediate or high risk (15-20%) of breast cancer, and a positive gene test or a positive family history. This pictorial essay presents a breast MRI acquisition and analysis protocol, supported by drawings of the morphologic features of

Corresponding author:
I. Miranda Sanchez-Carenzo-Velez
E-mail: iamiranda7720@gmail.com

Received for publication: 18-11-2024
Accepted for publication: 17-12-2024
DOI: 10.24875/JMEXFRI.M25000097

Available online: 24-04-2025
J Mex Fed Radiol Imaging. 2025;4(1):16-27
www.JMeXFRI.com

mass and non-mass lesions based on the American College of Radiology Breast Imaging Reporting and Data System (BI-RADS) 5th Edition lexicon and the Kaiser score.

BREAST MRI ACQUISITION PROTOCOL

A 1.5T or higher MRI resonator is required to obtain images with higher spatial and temporal resolution. A dedicated breast coil is also essential to obtain images of adequate quality. Breast coils usually have between 4 and 16 channels[3,4].

Acquisition protocols may vary from institution to institution, but essential sequences such as T1-weighted spin echo (SE), T2 fat-suppressed (FS), diffusion-weighted images (DWI), T1 dynamic contrast-enhanced (DCE) with gadolinium (Gd), and kinetic curve must be performed[3,5,6]. Some additional sequences are performed in some centers, such as Ultrafast and T2 turbo inversion recovery magnitude (TIRM)[5,6].

Our institution includes the following sequences in the breast MRI protocol: T1-weighted SE, T2 FS, DWI, apparent diffusion coefficient (ADC), T1 gradient echo (GE) with FS, T1 DCE with Gd, T1 DCE with Gd and subtraction, maximum intensity projection (MIP), positive enhancement integral (PEI) values, coronal T2 fast-spin echo (FSE) and kinetic curve.

BREAST MRI ANALYSIS

After adequate and complete sequence acquisition, an image visualization and interpretation protocol is performed[6]. Interpretation should be performed by radiologists with experience in breast imaging[3]. Breast MRI should be interpreted in correlation with other imaging studies such as a recent mammography and/or breast ultrasound[7]. Image visualization should be performed on medical-grade monitors.

We recommend the following sequence screen arrangement with 8 simultaneous images in two rows: an upper row with 4 images and a lower row with 4 images. The sequences in the upper row, from left to right, are T1 weighted SE, T2 FS, DWI, and ADC. The sequences in the bottom row are T1 DCE with Gd, T1 DCE with Gd and subtraction, PEI, and coronal T2 FSE, from left to right. The images should be linked so they can be displayed simultaneously and dynamically. This sequence visualization protocol allows for accurate and efficient breast MRI interpretation. Breast MRI analysis should emphasize the advantages and benefits of each sequence.

The T1-weighted SE sequence is useful to assess normal breast anatomy (Figure 1). Fatty tissue appears hyperintense (bright), while lesions with fluid content, such as cysts or ectatic ducts, appear hypointense (dark). In the T2 FS sequence, fluids appear hyperintense, which allows the identification of cysts, edema, or inflammatory processes (mastitis).

DWI measures water molecule movement through tissues and helps differentiate benign and malignant lesions. Cancer cells generally have a higher cell content and, therefore, restrict the movement of water molecules, which leads to a more intense DWI sequence signal. The ADC map is derived from the DWI sequence and represents the degree of diffusion of water molecules within tissues. A low ADC indicates a high cell density, which suggests a malignant breast lesion. Conversely, a high ADC value suggests a benign breast lesion[2,4].

The T1 DCE with Gd highlights the areas where contrast is administered. This helps identify and characterize breast tissue lesions based on their vascularity. It is particularly useful for detecting malignant tumors, as these usually have higher blood flow and more contrast uptake than benign lesions.

The PEI sequence graphically represents a numerical value that measures the tissue perfusion of a contrast medium to highlight differences between normal and abnormal tissue. It can facilitate lesion detection and help differentiate between benign and malignant tumors. Kinetic curves characterize breast lesions by showing specific contrast uptake patterns and clearance. The coronal T2 FSE assesses the axillary lymph nodes in their three levels and the internal mammary chains.

BREAST MRI DESCRIPTION WITH THE ACR BI-RADS LEXICON

The general description of the composition based on the ACR BI-RADS 5th Edition[8] includes the amount of fibroglandular tissue and background parenchymal enhancement. On the other hand, the description of abnormal findings includes focus, mass, non-mass lesion, intramammary lymph nodes, skin lesions, associated features (non-enhancing findings, fat-containing lesions), the location, size, abnormal enhancement descriptors, and the kinetic curve[8].

Suspected malignant lesions are difficult to describe. To facilitate and not forget the features to be identified and described on the breast MRI, we developed the chart in figure 2. The chart includes the descriptors of mass and non-mass lesions, the distribution patterns

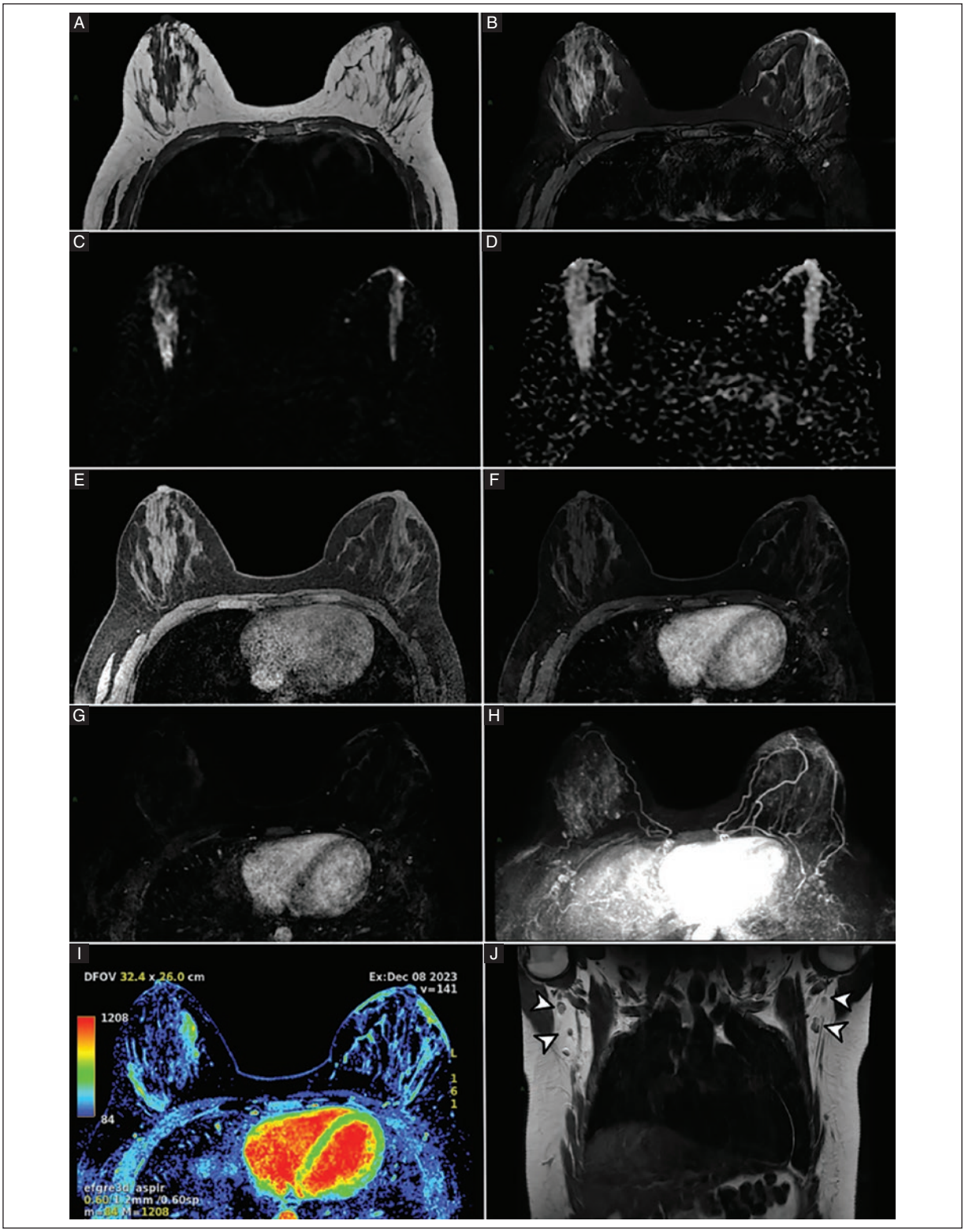

Figure 1. Normal breast MRI findings. **A:** T1 weighted SE with heterogeneous fibroglandular tissue. **B:** T2 FS without hyperintense findings. **C:** DWI sequence and **D:** ADC with no restrictive lesion. **E:** T1 GE with FS shows normal breast tissue and no suspicious findings. **F:** T1 DCE with Gd and physiologic enhancement. **G:** T1 DCE with Gd and subtraction. No abnormal lesions are present. **H:** MIP with normal fibroglandular tissue and vascular enhancement. **I:** PEI without correlation of time-signal intensity curves and no suspicious findings. **J**: coronal T2 FSE with normal axillary lymph nodes (arrowheads).

ADC: apparent diffusion coefficient; DCE: dynamic contrast-enhanced; DWI: diffusion-weighted images; FS: fat suppressed; FSE: fast spin echo; Gd: gadolinium; GE: gradient echo; MRI: magnetic resonance imaging; MIP: maximum intensity projection; PEI: positive enhancement integral; SE: spin echo.

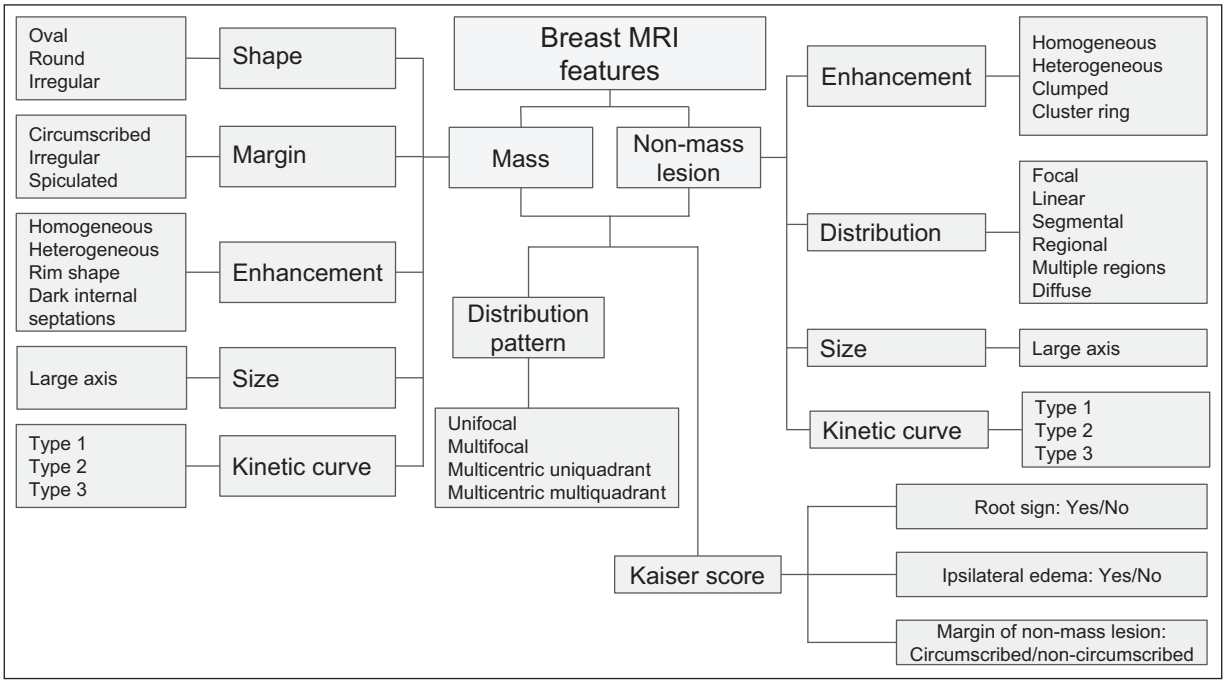

Figure 2. Diagram showing the features of lesions examined by breast MRI according to BI-RADS lexicon. The characteristics described include those of a mass, namely the shape (oval, round and irregular), followed by the margin (circumscribed, irregular and spiculated), mass enhancement (homogeneous, heterogeneous, rim shape, dark internal septations), the size which must be measured in the long axis and expressed in millimeters or centimeters, and the kinetic curve type (1, 2, 3). For non-mass lesions, the descriptors are enhancement (homogeneous, heterogeneous, clumped and cluster ring), distribution (focal, linear, segmental, regional, multiple regions and diffuse), size, which must be measured in its longitudinal axis and reported in millimeters or centimeters and the kinetic curve type (1, 2, 3). The distribution pattern of the malignant lesion should be described (unifocal, multifocal, multicentric uniquadrant, or multicentric multiquadrant). As an additional tool, the Kaiser score of the lesions should be determined, considering some characteristics not mentioned in the BI-RADS, such as root sign (yes/no), ipsilateral edema (yes/no), and non-mass lesion margin (circumscribed and non-circumscribed).

BI-RADS: Breast Imaging Reporting and Data System; MRI: magnetic resonance imaging.

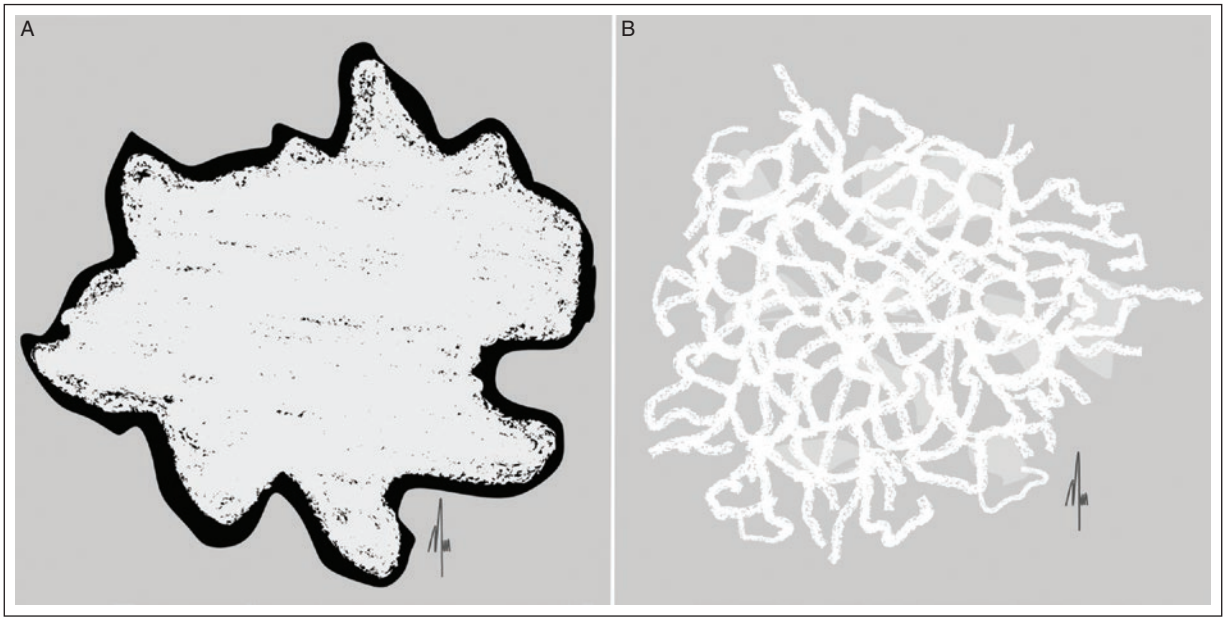

Figure 3. Drawings showing the difference between breast lesions. **A:** the mass is a three-dimensional, space-occupying lesion in the breasts. **B:** a non-mass lesion is an area of enhancement that does not meet the criteria for a mass, with a non-convex margin, interspersed fat, or fibroglandular tissue between the enhancement components.

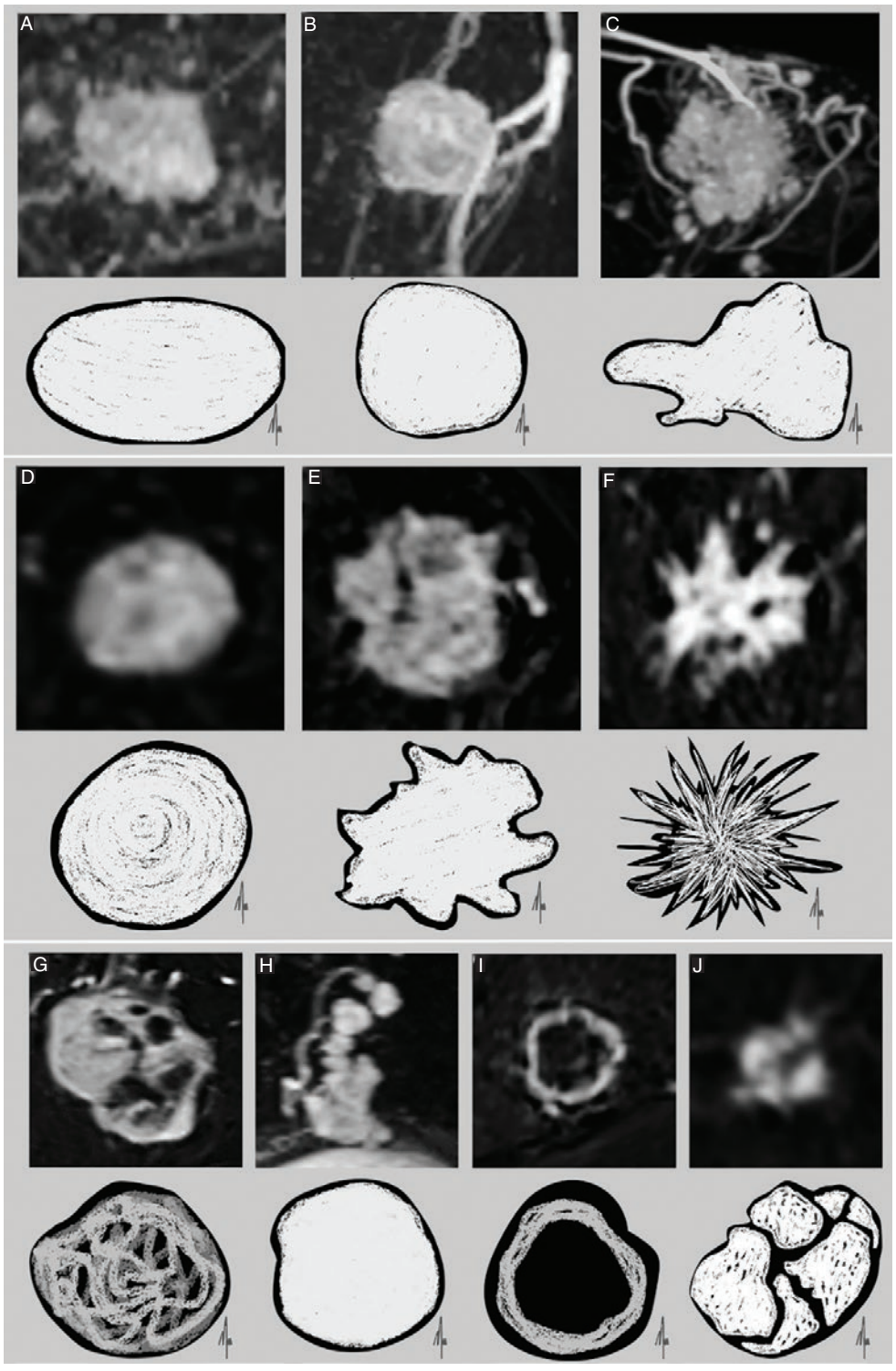

Figure 4. T1 DCE with Gd and drawings showing the three types of mass lesion morphology, the three types of margins, and the classification of mass lesion enhancement. **Morphology. A:** oval, elliptical, or ovoid shape with two or three undulations. **B:** round: spherical, circular, or globular. **C:** irregular, neither round nor oval, usually represents a suspicious malignant finding. **Margin. D:** circumscribed with a clear delimitation; an abrupt transition between the lesion and surrounding tissue is recognizable. The entire margin must be well-defined. **E:** irregular is pointed but not spiculated. **F:** spiculated with lines that radiate from the center to the periphery. This is a suspicious malignant lesion. **Enhancement. G:** heterogeneous with non-uniform enhancement but showing areas of varying signal intensity. **H:** homogeneous with uniform and confluent enhancement. **I:** rim shape is most pronounced at the periphery of the mass. **J:** dark internal septations with dark hypointense internal septa with non-enhancing lines located within a mass.

DCE: dynamic contrast-enhanced; Gd: gadolinium.

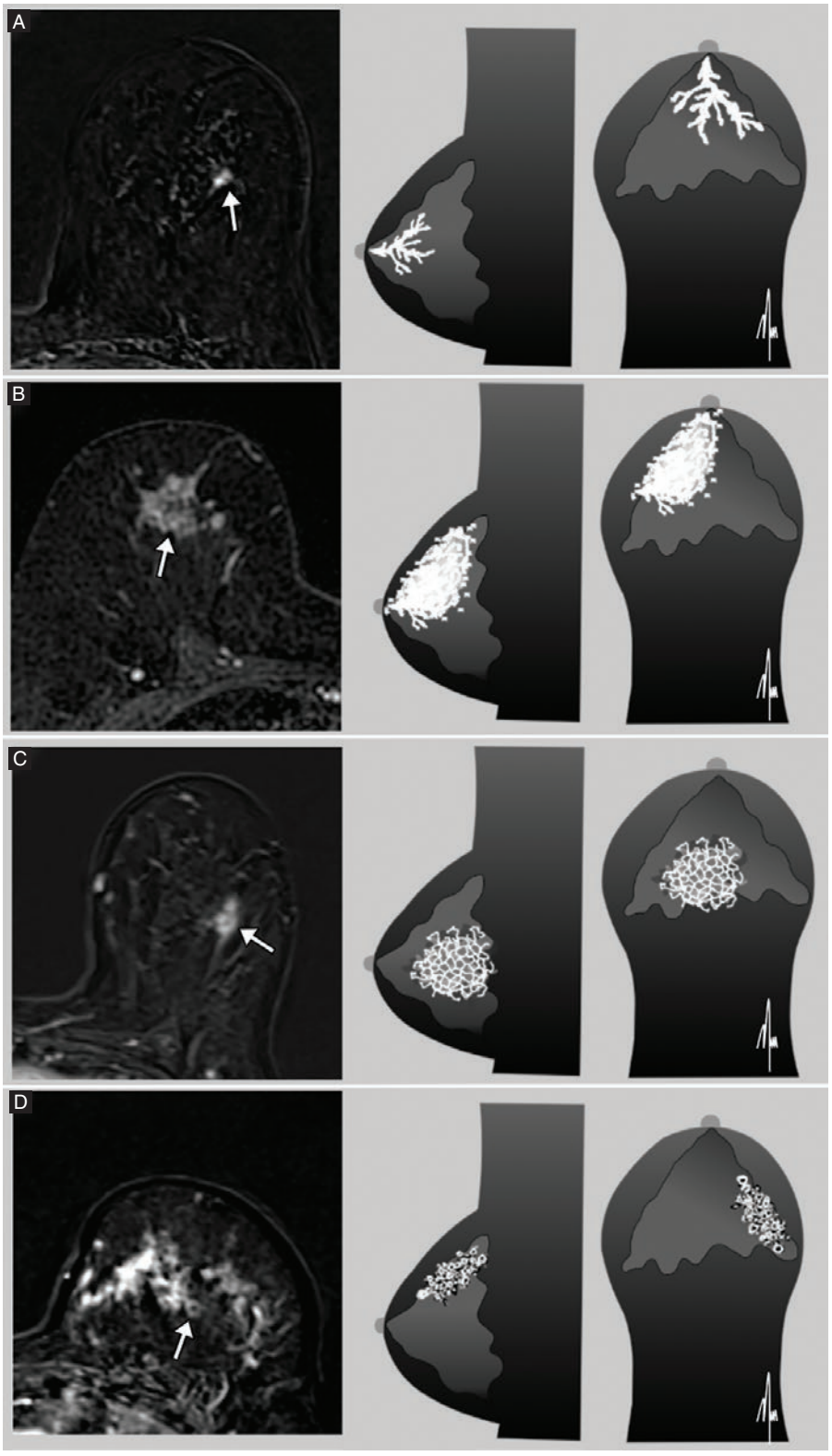

Figure 5. T1 DCE with Gd and drawings of the different types of non-mass lesion enhancement. **A:** homogeneous is confluent and uniform (arrow). **B:** heterogeneous is not uniform. It has a random distribution separated by areas of normal or fatty breast parenchyma (arrow). **C:** clumped with enhancement in lumps of different shapes and sizes and some confluent areas. It is suspicious of a malignant lesion (arrow). **D:** cluster ring with thin enhancement rings grouped around the ducts. It is suspicious of a malignant lesion (arrow).

DCE: dynamic contrast-enhanced; Gd: gadolinium.

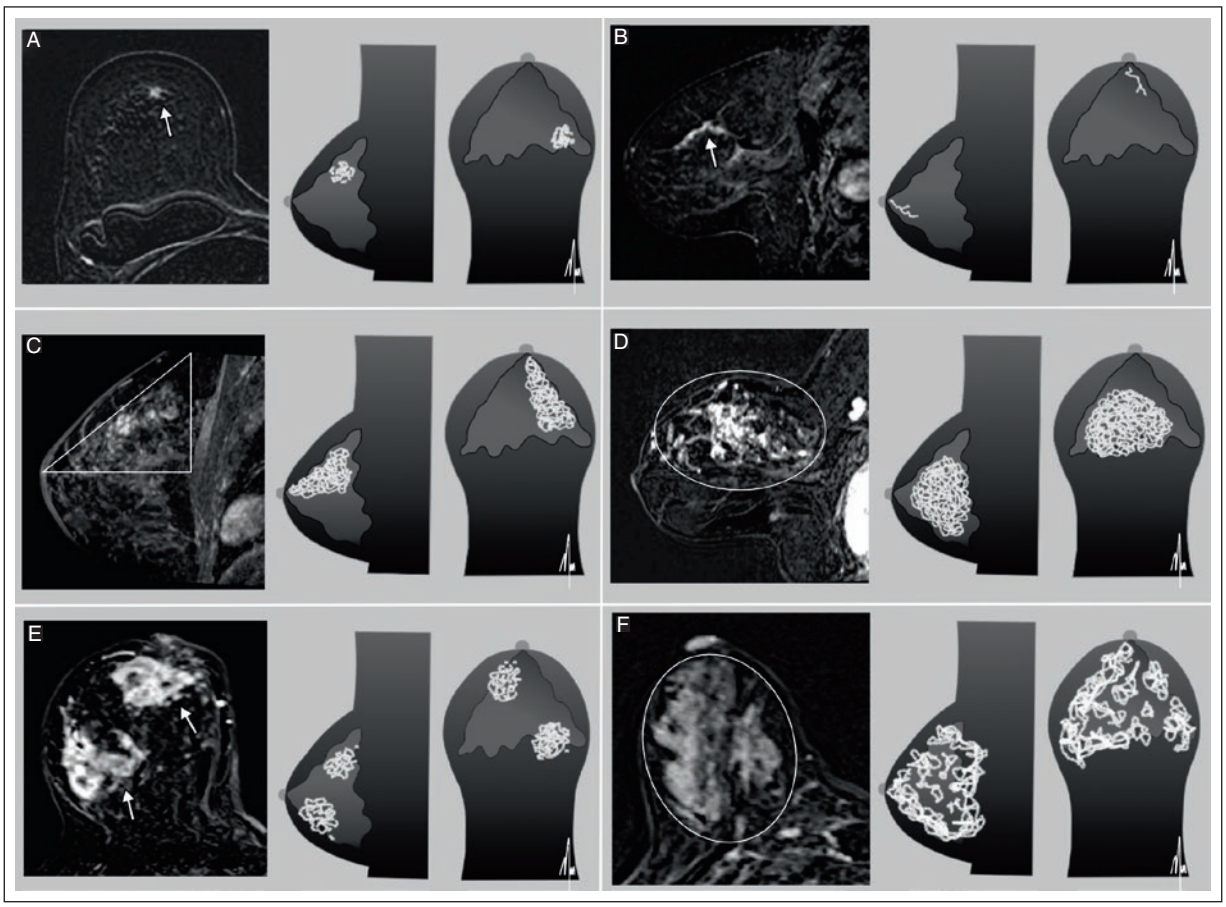

Figure 6. T1 DCE with Gd and drawings of the distribution of non-mass lesions: **A:** focal is limited to a sector with internal enhancement that is not considered nodular (arrow). **B:** linear with appearance of a straight line or a line those branches (arrow). **C:** segmentary is triangular or conical with the apex towards the nipple (triangle). **D:** regional, comprising more than one duct system, occupies at least one quadrant) (circle). **E:** multiple regions with several regions of enhancement in two large sectors separated from normal tissue (arrows). **F:** diffuse is randomly distributed over the entire breast (circle).

DCE: dynamic contrast-enhanced; Gd: gadolinium.

of malignant breast lesions[8,9], the Kaiser score, and its unique descriptors[10-12].

According to the chart, the first step is to differentiate between a mass and non-mass lesion, keeping in mind that a mass is a three-dimensional, space-occupying lesion in the breast and a non-mass lesion is an area of enhancement that does not meet the criteria for a mass or focus, such as a non-convex margin or interspersed fat or fibroglandular tissue between the enhancement components[8] (Figure 3).

The features of the mass described are shape, margin, enhancement, size, and kinetic curve. The unique and distinctive characteristics of the mass are its shape, margin, and enhancement. The shape may be oval (lobulated, elliptical, or ovoid, without or with two or three undulations), round (spherical, circular, or globular), or irregular, neither round nor oval, and is usually a suspicious, malignant finding (Figure 4). The margin may be circumscribed if there is a clear delimitation, with an abrupt transition between the lesion and surrounding tissue, and the entire margin must be well defined; irregular if they are pointed but not spiculated; and spiculated on this type of lesion shows lines radiating from the center to the periphery and is a suspicious finding. Enhancement may indicate the likelihood of a malignant lesion. Homogeneous and dark internal septations are usually benign, non-suspicious lesions, in contrast to heterogeneous margin enhancement, which is a suspicious finding for malignancy[8].

Enhancement, distribution, size, and kinetic curve are descriptive features that distinguish non-mass lesions. Enhancement can be homogeneous if it is confluent

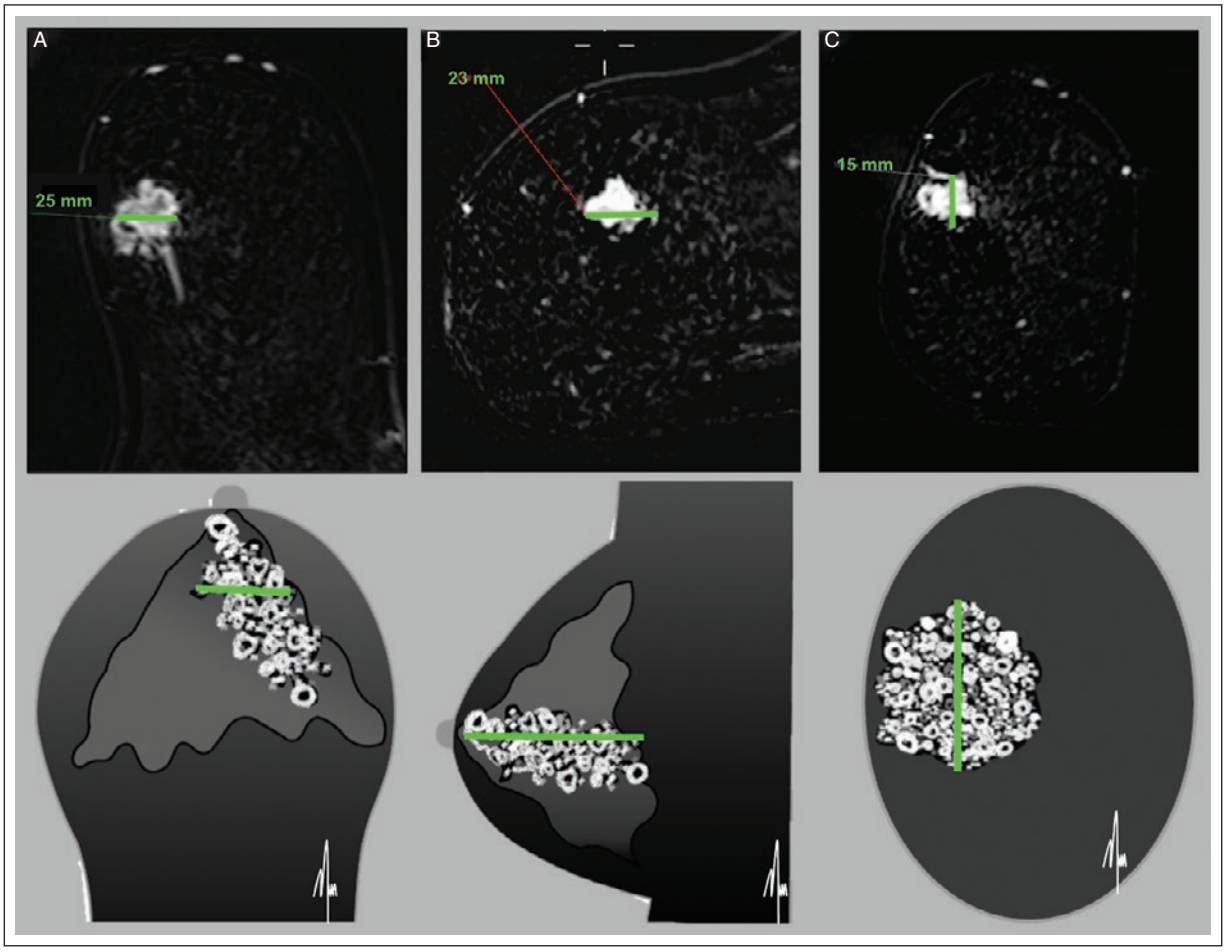

Figure 7. Drawing and T1 DCE with Gd show how the lesion's diameter is measured in the three planes. **A:** transverse diameter in the axial plane (green line). **B:** anteroposterior diameter in the sagittal plane (green line). **C:** cephalocaudal diameter in the coronal plane (green line). DCE: dynamic contrast-enhanced; Gd: gadolinium.

and uniform and heterogeneous if it is not uniform, has a random distribution, and is separated by areas of normal or fatty breast parenchyma. Clumped enhancement, a suspicious malignant finding, occurs in clumps of different shapes and sizes and some confluent areas develop. Clustered ring enhancement occurs when thin rings of enhancement are grouped around the ducts, it is a suspicious malignant finding (Figure 5).

The distribution can be focal, linear, segmental, in multiples regions, or diffuse. The term focal means it is confined to one sector of internal enhancement and is not considered nodular. By definition, it occupies less than one breast quadrant[8] (Figure 6). Linear if the appearance is a straight or branching line; segmental, if it is triangular or conical with the tip pointing towards the nipple; regional if it involves more than one ductal system and occupies at least one quadrant; multiple regions if several regions of enhancement are separated from normal tissue in two large sectors; diffuse if it is randomly distributed throughout the breast.

Features that are similar between mass and non-mass lesions and evaluated similarly are size and the kinetic curve. Size must be measured in the three axes where the largest diameter is determined and expressed in millimeters or centimeters (Figure 7).

The kinetic curves are those in which DCE MRI uses a temporal signal intensity curve obtained from repeated MRI scans after the injection of a contrast agent. They are useful for detecting breast cancer due to their high sensitivity[3]. The behavior of the initial phase (slow, medium, or fast) and the late phase (persistent, plateau, or washout) is analyzed. The kinetic curve can be presented in three types (Figure 8). The persistent curve (type 1) shows a progressive increase in the

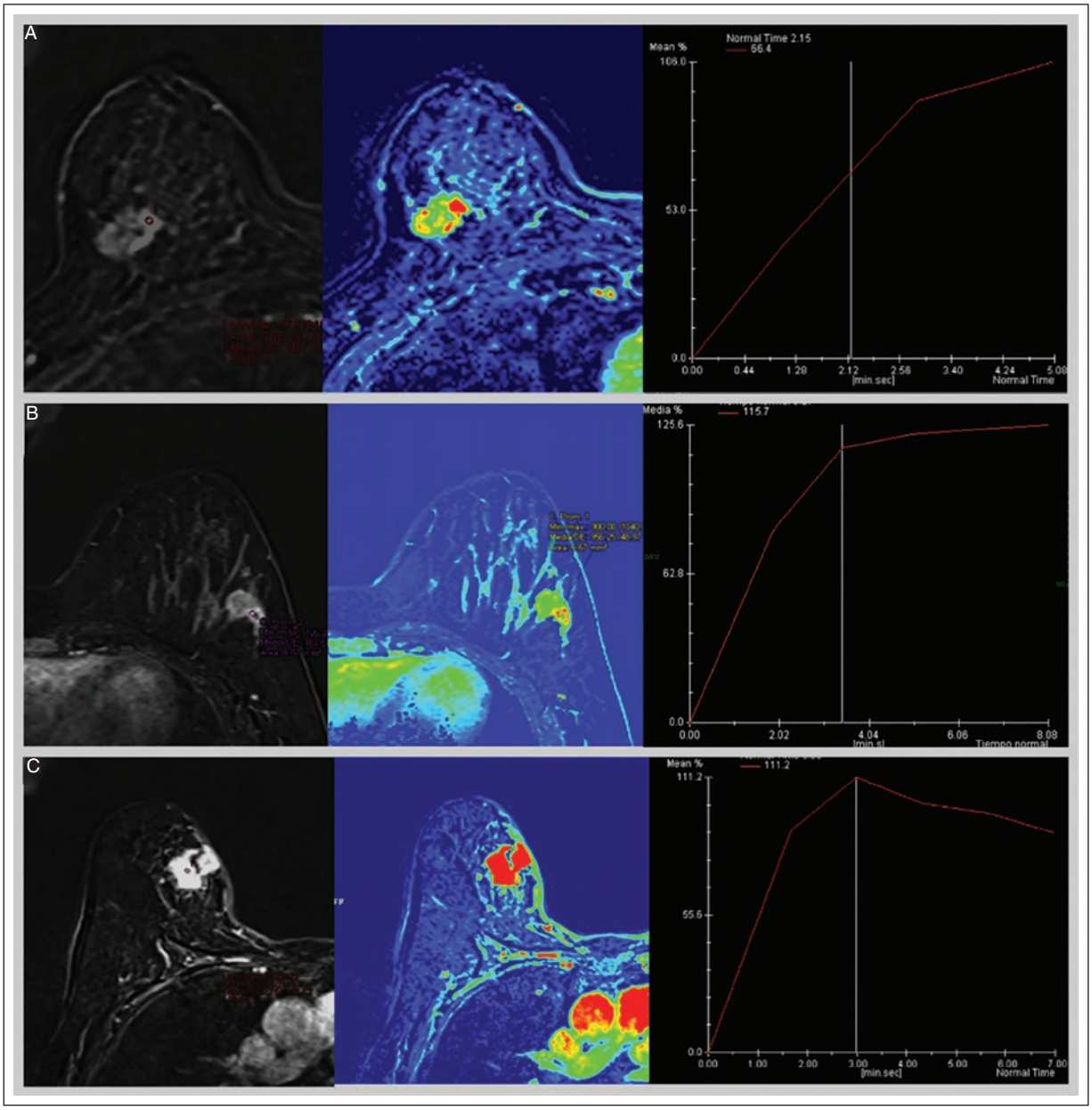

Figure 8. Examples of the different types of kinetic curves with their respective T1 DCE with Gd and PEI values. **A:** type 1, persistent curve, Kaiser score of 6, BI-RADS category 4. **B:** type 2, plateau curve, Kaise score of 7, BI-RADS category 4. **C:** type 3, washout curve, Kaiser score of 11, BI-RADS category 5.

BI-RADS: Breast Imaging Reporting and Data System; DCE: dynamic contrast-enhanced; Gd: gadolinium; PEI: positive enhancement integral.

enhancement curve in the early and delayed T1-weighted SE. It is not considered suspicious of breast malignancy. The plateau curve (type 2), if there is no further increase in signal intensity on T1-weighted SE images in the delayed phase after the early signal increase, is considered doubtful for malignancy, and the washout curve (type 3) if the signal intensity on delayed images decreases after the early signal increase. It is considered suspicious for malignancy[12].

DISTRIBUTION PATTERNS OF MALIGNANT BREAST LESIONS

Four distribution patterns of malignant breast lesions have been described[9]: a unifocal pattern (UF): a single lesion in a single breast regardless of its location; a multifocal pattern (MF): ≥ 2 lesions in a single breast in a single quadrant with a distance < 5 cm; a multicentric uniquadrant pattern (MCUQ): ≥ 2 lesions in a single

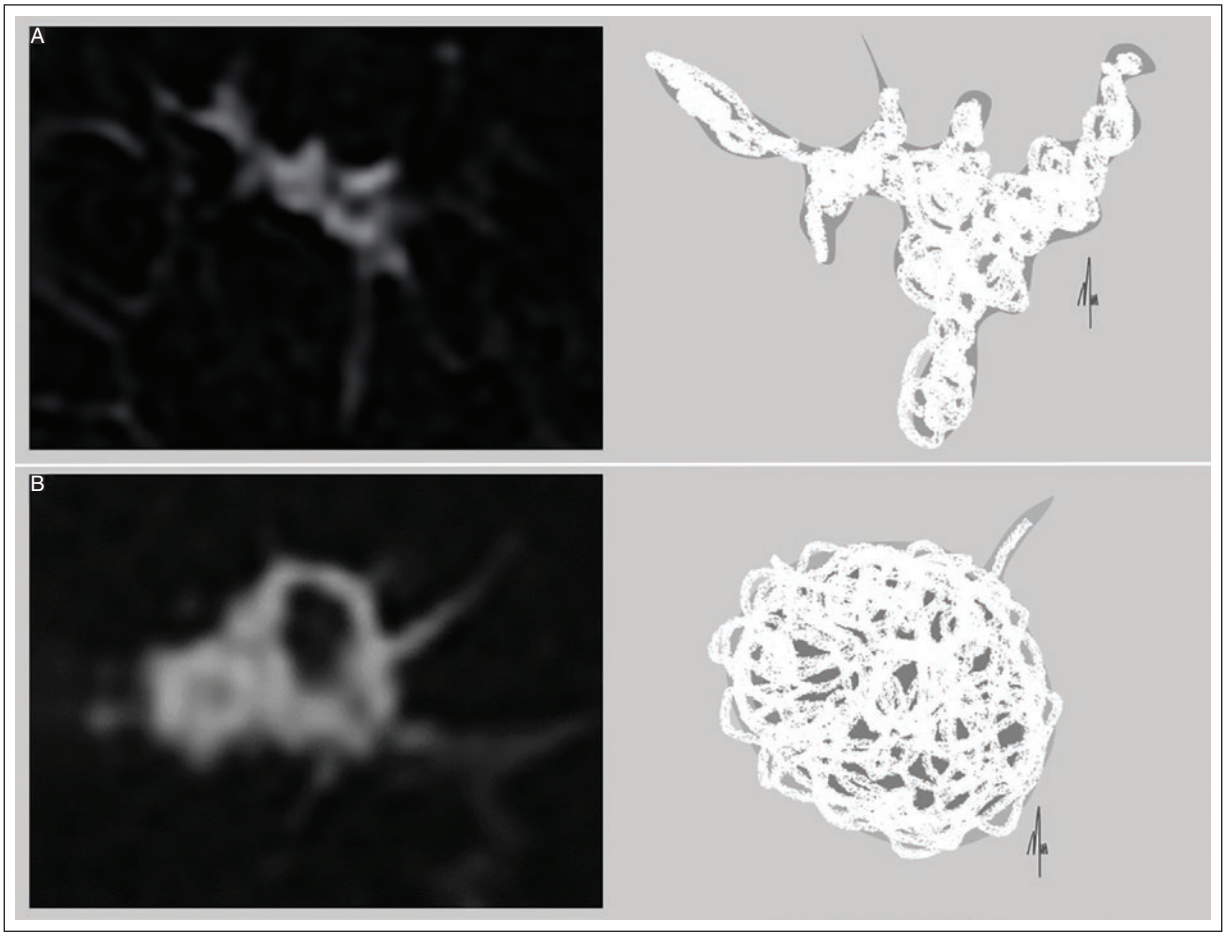

Figure 9. The root sign is an additional tool described in the Kaiser score. It is a spiculated extension of the lesion margin, even if the rest is smooth. It can help differentiate malignant from benign lesions. The presence of the root sign increases the probability of malignancy. **A:** T1 DCE with Gd showing a non-mass focal lesion with a root sign. **B:** T1 DCE with Gd with an irregular mass with a root sign.

DCE: dynamic contrast-enhanced; Gd: gadolinium.

breast in a single quadrant with a distance > 5 cm; and a multicentric multiquadrant pattern (MCMQ): ≥ 2 lesions in a single breast in ≥ 2 quadrants regardless of their distance.

DESCRIPTION OF THE KAISER SCORE

The Kaiser score includes some morphologic and kinetic characteristics of the BI-RADS lexicon to rate breast MRI lesions, such as enhancement (present or not), margin in masses (circumscribed, irregular, or spiculated), and the kinetic curve (type 1, 2, or 3). The Kaiser score also includes the root sign, edema, and the margin of a non-mass lesion (circumscribed or non-circumscribed)[10,11,13,14].

The root sign, a spiculated extension from the margin of the lesion, even if the rest of the margin is smooth, can vary from a single spike to multiple spiculations. This finding increases the likelihood of breast malignancy[12-14] (Figure 9).

Another feature that the Kaiser score considers is ipsilateral edema (present or not), which is seen as a high signal intensity on T2 FS images; only if it is ipsilateral or not is it considered (Figure 10). It is important to know if it is focal, which can indicate greater tumor invasiveness. There are three types of focal edema: peritumoral, prepectoral, and subcutaneous. Benign and malignant etiologies can cause diffuse edema.

The Kaiser score is determined with a virtual calculator available at https://school-of-radiology.com/kaiser-score/[15]. This calculator follows a flowchart practically and functionally as a step-by-step guide that asks key questions about the described breast characteristics. The questionnaire first asks if the lesion enhances or not.

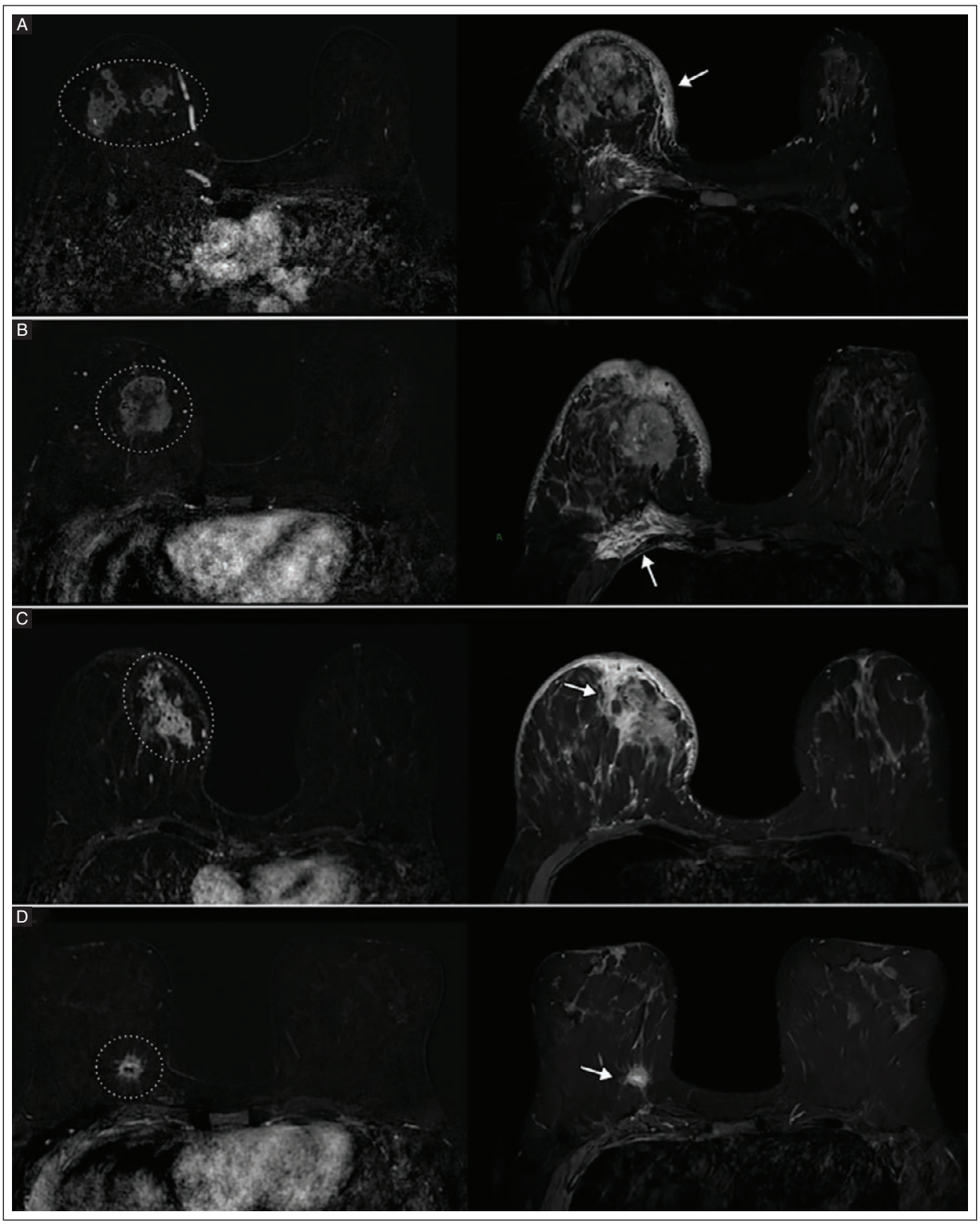

Figure 10. T1 DCE with Gd (left column) and T2 FS (right column) examples of the types of enhancement and edema. **A:** multiple irregular, oval masses in the right breast with rim shape enhancement (dotted circle). There is associated subcutaneous edema (white arrow). **B:** an irregular, oval mass in the right breast with heterogeneous enhancement (dotted circle). Prepectoral edema is associated (white arrow). **C:** irregular mass lesion in the right breast with heterogeneous enhancement (dotted circle). There is associated peritumoral edema (white arrow). **D:** irregular and spiculated mass in the right breast with rim shape enhancement. There is no edema (white arrow).

DCE: dynamic contrast-enhanced; FS: fat suppressed; Gd: gadolinium.

If not, the Kaiser score is not applicable and will be ended. If the answer is yes, it proceeds to the second question in which a distinction is made between mass and non-mass lesions[15]. If the lesion is a mass, it will ask if it has spiculations, referring to the root sign. The next question will be the type of kinetic curve (1, 2, or 3). If you select 1, the questionnaire will end. If you select curves 2 or 3, you will proceed to the last question, which defines if there is ipsilateral edema. This is the end of the questionnaire[15].

When the answer is a non-mass lesion, the next question will be if it has spiculations, referring again to the root sign. The next question is the type of kinetic curve (1, 2, or 3). If you select 1 or 2, it will ask you one last question about whether the margins are circumscribed. After this, it will finish and give you a result; however, if the answer is curve 3, the next and last question will change to confirm if there is homogeneous centrifugal or non-homogeneous centripetal enhancement. The questionnaire ends at this point[15].

Each of these findings has a score, and the combination of these criteria sums up to a Kaiser score of 1 to 11, which can be related to the probability of malignancy. It is translated into a BI-RADS categories: Kaiser score of 1-4 = BI-RADS category 2 or 3; Kaiser score of 5-7 = BI-RADS category 4; and Kaiser score of 8-11 = BI-RADS category 5.

CONCLUSION

This pictorial essay presents a breast MRI acquisition and analysis protocol, supported by drawings of the morphologic features of mass and non-mass lesions based on the updated ACR BI-RADS 5th Edition lexicon and Kaiser scoring. This pictorial essay is published for educational purposes for radiologists and residents.

Acknowledgments

The authors thank Professor Ana M. Contreras-Navarro for her guidance in preparing and writing this scientific paper.

Funding

This research received no external funding.

Conflicts of interest

The authors declare that they have no conflicts of interest.

Ethical considerations

Protection of humans and animals. The authors declare that the procedures followed complied with the ethical standards of the responsible human experimentation committee and adhered to the World Medical Association and the Declaration of Helsinki. The procedures were approved by the institutional Ethics Committee.

Confidentiality, informed consent, and ethical approval. The authors have followed their institution's confidentiality protocols, obtained informed consent from patients, and received approval from the Ethics Committee.

Declaration on the use of artificial intelligence. The authors declare that no generative artificial intelligence was used in the writing of this manuscript.

REFERENCES

1. Harbeck N, Gnant M. Breast cancer. Lancet. 2017;389(10074): 1134-1150. doi: 10.1016/S0140-6736(16)31891-8.
2. Pérez-Zúñiga I, Villaseñor-Navarro Y, Perez-Badillo MP, Cruz-Morales R, Pavon-Hernandez C, Aguilar-Cortazar L. Breast magnetic resonance and its applications. (Spanish). Gac Mex Oncol. 2012;11(4):268-280.
3. Mann RM, Cho N, Moy L. Breast MRI: State of the Art. Radiology. 2019; 292(3):520-536. doi: 10.1148/radiol.2019182947.
4. Fischer U. Breast MRI - The champion in the millimeter league: MIO breast MRI - The method of choice in women with dense breasts. Eur J Radiol. 2023;167:111053. doi: 10.1016/j.ejrad.2023.111053.
5. Pinker K, Helbich TH, Morris EA. The potential of multiparametric MRI of the breast. Br J Radiol. 2017;90(1072):20160715e. doi: 10.1259/bjr.20160715.e.
6. Camps Herrero J. Breast magnetic resonance imaging: state of the art and clinical applications. Radiologia. 2011;53(1):27-38. Spanish. doi: 10.1016/j.rx.2010.08.009.
7. Edwards SD, Lipson JA, Ikeda DM, Lee JM. Updates and revisions to the BI-RADS magnetic resonance imaging lexicon. Magn Reson Imaging Clin N Am. 2013;21(3):483-93. doi: 10.1016/j.mric.2013.02.005.
8. American College of Radiology. (2013). ACR Breast Imaging Reporting and Data System (BIRADS). Reston, VA: American College of Radiology.
9. Lopez-Mendez JMI, Delgadillo-Cisterna R, Rodriguez-Pulido G. Unifocal, multifocal, or multicentric breast cancer distribution patterns on multiplanar breast MRI: a technical note. J Mex Fed Radiol Imaging. 2024;3(1): 56-61. doi: 10.24875/JMEXFRI.24000001.
10. Wang Q, Fu F, Chen Y, Yang D, Zhang J, Yu H, Su L. Application of the Kaiser score by MRI in patients with breast lesions by ultrasound and mammography. Diagn Interv Radiol. 2022;28(4):322-328. doi: 10.5152/dir.2022.201075.
11. Zhou XZ, Liu LH, He S, Yao HF, Chen LP. Diagnostic value of Kaiser score combined with breast vascular assessment from breast MRI for the characterization of breast lesions. Front Oncol. 2023;13:1165405. doi: 10.3389/fonc.2023.1165405.
12. Woitek R, Spick C, Schernthaner M, Rudas M, Kapetas P, Bernathova M. A simple classification system (the Tree flowchart) for breast MRI can reduce the number of unnecessary biopsies in MRI-only lesions. Eur Radiol. 2017;27(9):3799-3809. doi: 10.1007/s00330-017-4755-6.
13. Baltzer PAT, Dietzel M, Gröschel T, Kaiser WA. A simple and robust classification tree for differentiation between benign and malignant lesions in MR-mammography. Eur J Radiol. 2012;81 Suppl 1: S4-5. doi: 10.1016/S0720-048X(12)70002-5.
14. Dietzel M, Baltzer PAT. How to use the Kaiser score as a clinical decision rule for diagnosis in multiparametric breast MRI: a pictorial essay. Insights Imaging. 2018;9(3):325-335. doi: 10.1007/s13244-018-0611-8.
15. Baltzer PA, Dietzel M. Kaiser Score [Internet]. Friburgo (DE). University Hospital Freiburg of Germany, School of Radiology; 2023 [updated: 2021 Dec 6; cited: 2024 Nov 6]. Available from: https://school-of-radiology.com/kaiser-score/.

JMeXFRI

Journal of the Mexican Federation of Radiology and Imaging

Check for updates

FULL RESEARCH ARTICLE

Standardized structured breast MRI report: a technical note

I. Miranda Sanchez-Carenzo-Velez[1,2#], Yesika J. Davila-Zablah[1#], Elena Maria Sanchez-Siller[1#], Mane M. Ayala-Duran[1#], Ilany B. Lopez-Valdivia[2], Maria Guerra-Ayala[2], Jessica A. Perdomo-Galviz[2], Karla I. Soto-Valdez[2], Sofia Hurtado-Arellano[3], and Margarita L. Garza-Montemayor[1#]*

[1]*Diagnostic Breast Imaging Department, Hospital Zambrano Hellion Tec Salud;* [2]*Department of Radiology and Imaging, Tec Salud;* [3]*School of Medicine and Health Sciences Tecnologico de Monterrey. Monterrey, Nuevo Leon, Mexico*

[#]*These authors contributed equally.*

ABSTRACT

Currently, the American College of Radiology (ACR) Breast Imaging Reporting and Data System (BI-RADS) 5th Edition lexicon is widely used for the interpretation of breast lesions on magnetic resonance imaging (MRI). It is known worldwide and should be used by all radiologists who specialize in breast imaging. However, it is not always easy to interpret the specific imaging features of the BI-RADS ACR categories. In addition, other systematic methods can improve the diagnostic accuracy of breast MRI, such as the Kaiser score, a widely used clinical decision aid based on the BI-RADS lexicon, which has a high diagnostic accuracy in classifying mass and non-mass breast lesions. The MRI report should be concise, clear and provide important details about the breast lesions. This technical note aims to provide a standardized structured report template using the ACR BI-RADS 5th Edition lexicon and Kaiser score to increase clarity and completeness.

Keywords: *Breast magnetic resonance imaging. Breast Imaging Reporting and Data System. Kaiser score. Breast cancer. MRI lexicon.*

INTRODUCTION

A tree-shaped evaluation of breast magnetic resonance imaging (MRI) findings to differentiate benign from malignant imaging findings was first described in 1997 by Nuñez et al.[1] with a model based on architectural features of breast lesions. Another approach was proposed in 2002 by the Göttingen group with 5 criteria to define and evaluate a category for contrast-enhanced MRI[2] that mimics the categories used in mammography[3]. In 2003, the American College of Radiology (ACR) included a chapter in the fourth edition of the Breast Imaging Reporting and Data System (BI-RADS) describing breast MRI with a lexicon and categories for mass and non-mass breast lesions. This chapter was updated in the 5th edition of 2013[4]. On the other hand, the Kaiser score diagnostic criteria align with the BI-RADS lexicon for MRI were published in 2013. The Kaiser score has proven its value in aiding radiologists in clinical decision making and in differentiating between benign and malignant enhanced lesions on breast MRI[5]. The Kaiser score has shown a high specificity

Corresponding author:
I. Miranda Sanchez-Carenzo-Velez
E-mail: iamiranda7720@gmail.com

Received for publication: 18-11-2024
Accepted for publication: 17-12-2024
DOI: 10.24875/JMEXFRI.M25000096

Available online: 24-04-2025
J Mex Fed Radiol Imaging. 2025;4(1):28-36
www.JMeXFRI.com

for lesion detection of 87.4% and a positive predictive value of 94%[6-8]. This technical note aims to provide a standardized structured reporting template using the BI-RADS 5th Edition lexicon and the Kaiser score to increase clarity and completeness.

RECOMMENDATIONS FOR A STANDARDIZED STRUCTURED BREAST MRI REPORT

The BI-RADS 5th Edition provides a standardized lexicon for the interpretation and classification of breast MRI lesions[4,9-14]. The lexicon contains appropriate terms for enhancement features and a standardized classification of breast lesions. A general description of breast composition includes the amount of fibroglandular tissue and parenchymal enhancement in the background. The description of the findings includes focus, mass, non-mass lesion, abnormal enhancement descriptors, intramammary lymph nodes, skin lesions, associated features (non-enhancing findings and fat-containing lesions), location, size and kinetic curve, and the presence of implants.

The Kaiser score, on the other hand, combines criteria from the BI-RADS lexicon and other findings into a flowchart with 11 criteria for categorizing mass and non-mass breast lesions[6,7]. The Kaiser score has been validated and there is a freely available online calculator at https://school-of-radiology.com/kaiser-score[8]. The higher values of the Kaiser score reflect the increasing likelihood of malignancy and, together with the clinical context, aid in individual decision-making and are useful for therapeutic decision-making and prognosis[6,7,15-17].

STANDARDIZED STRUCTURED BREAST MRI REPORT

We propose a standardized template for a structured breast MRI report, which is divided into several sections that are filled in with patient information in a specific order (Table 1) (Supplementary material, Table 1).

The first section is the simplest and shortest and includes the full name of the imaging examination and whether it is simple (unenhanced) or contrasted breast MRI.

The second section states the reason for the examination: screening, diagnosis, staging, complementary, treatment evaluation and/or follow-up of breast cancer.

The third section contains information about the patient's medical history, such as family and/or personal history. If breast cancer has been recently diagnosed, the histopathologic diagnosis and the date and location of previous imaging examinations should be included.

The fourth section contains information on the sequences and techniques used, including post-processing.

The fifth section contains a general description starting with the breast composition: the amount of fibroglandular tissue, parenchymal enhancement in the background, and whether implants and/or artifacts are present.

The sixth section is one of the most important. Here the features of the visualized lesions are described. At this point, we proposed add the features described in the BI-RADS lexicon and the features taken into account in the Kaiser score, whether they are mass and/or non-mass lesions. This paragraph should include the affected side, the location (quadrant) of the breast lesion, the radius and the distance to the nipple. Mass features include shape, margin, root sign (yes/no), enhancement, kinetic curve, size measured in the three axes, and ipsilateral edema (yes/no). The non-mass features include enhancement, distribution, margins (circumscribed or not), root sign (yes/no), kinetic curve, size measured in three axes and ipsilateral edema (yes/no).

The seventh section describes the distribution pattern: unifocal pattern, a multifocal pattern, a multicentric uniquadrant, or a multicentric multiquadrant[18]. The distribution pattern is only specified for malignant lesions. A digital blank template of breast MRI diagrams for reporting distribution patterns is provided (Supplementary material, Table 2).

The eighth section describes other associated features such as non-enhancing findings and fat-containing lesions and types of findings such as cysts, lipomas, hemangiomas, benign solid nodules, scars, benign skin lesions, or tissue marker clips.

The ninth and tenth sections contain information on other soft tissue findings, including the skin, nipple, and nipple-areola complex[19]. For example, the skin may show edema, thickening, tumor involvement, invasion, and/or retraction. The nipple and nipple-areola complex may have tumor involvement, invasion, and/or retraction.

The eleventh section describes the axillary nodes in three levels and the internal mammary chain; in the case of abnormal lymph nodes, the number and the levels in which they are located.

The twelfth section contains further abnormalities that are relevant to the clinical context, such as metastases.

Table 1. Standardized structured breast MRI report template

Description	Patient information
Date and place:	
Name of the patient:	
Name of the referring physician:	
1. Name of the imaging examination.	
2. Indication: screening, diagnosis, staging, complementary examination, evaluation of treatment or follow-up of breast cancer.	
3. Medical history: family and/or personal. If there is a history of breast cancer, indicate the histopathologic diagnosis and the date and location of previous examinations.	
4. Examination technique: indicate the sequences performed and the techniques used for post-processing.	
5. General description of breast composition: indicate the amount of fibroglandular tissue and parenchymal enhancement in the background.	
6. Description of imaging findings including the ACR BI-RADS lexicon and features assessed by the Kaiser score, applies to each lesion(s) identified: Mass: location (side, radius by clock time), distance from nipple, morphology, shape, margin, root sign (yes/no), enhancement, type of kinetic curve, size measured in the three axes, and ipsilateral edema (yes/no). Non-mass: location (radius by clock time), distance from nipple, enhancement, distribution, margin (circumscribed or not), root sign (yes/no), type of kinetic curve and size measured on three axes and ipsilateral edema (yes/no).	
7. Distribution pattern (only indicated for malignant lesions): unifocal pattern, multifocal pattern, multicentric uniquadrant pattern, or multicentric multiquadrant pattern.	
8. Description of other associated features: non-enhancing findings and fat-containing lesions and types of findings, such as cysts, lipomas, hemangiomas, benign solid nodules, scars, benign skin lesions, or tissue marker clips.	
9. Description of the skin: edema, thickening, tumor involvement, invasion, and/or retraction.	
10. Description of the nipple and nipple-areola complex: tumor involvement, invasion, and/or retraction.	
11. Description of the axillary lymph nodes, three levels and the internal mammary chain: in the case of abnormal lymph nodes, indicate the number and levels in which they are located.	
12. Description of other abnormalities relevant to the clinical context, e.g., metastases.	
13. Conclusion: the most important information from the breast MRI examination is summarized.	
14. Kaiser score[a,b]	
15. BI-RADS: add the category based on findings, including recommendations.	
16. Name, signature, and license number of the radiologist who performed the breast MRI.	

[a]Baltzer PA et al.[8]; [b]https://school-of-radiology.com/kaiser-score/[8].

ACR: American College of Radiology; BI-RADS: Breast Imaging Reporting and Data System; MRI: magnetic resonance imaging.

Note: If your facility allows you to store important breast MRI images in the system, you should do so; the attending physicians will be grateful.

Table 2. Example of a standardized structured breast MRI report for a benign lesion (Figure 1)

Description	Patient information: example
Date and place:	
Name of the patient:	
Name of the referring physician:	
1. Name of the imaging examination.	Contrast-enhanced breast MRI
2. Indication: screening, diagnosis, staging, complementary examination, evaluation of treatment or follow-up of breast cancer.	Diagnostic
3. Medical history: family and/or personal. If there is a history of breast cancer, indicate the histopathologic diagnosis and the date and location of previous imaging examinations.	25-year-old female patient with a palpable lump in both breasts. She has a positive familial risk factor for breast cancer (her sister was diagnosed at the age of 26).
4. Examination technique: indicate the sequences performed and the techniques used for post-processing.	T1-weighted SE, T2 FS, DWI, ADC, T1 GE with FS, T1 DCE with Gd, T1 DCE with Gd and subtraction, kinetic curve, PEI values, MIP and coronal T2 FSE sequences were performed.
5. General description of breast composition: indicate the amount of fibroglandular tissue and parenchymal enhancement in the background.	The breast composition is almost entirely fat, with mild and symmetrical background parenchyma enhancement.
6. Description of imaging findings including the ACR BI-RADS lexicon and features assessed by Kaiser score, applies to each lesion(s) identified: Mass: location (side, radius by clock time), distance from nipple, morphology, shape, margin, root sign (yes/no), enhancement, type of kinetic curve, size measured in the three axes, and ipsilateral edema (yes/no). Non-mass: location (radius by clock time), distance from nipple, enhancement, distribution, margin (circumscribed or not), root sign (yes/no), type of kinetic curve and size measured on three axes and ipsilateral edema (yes/no).	In the right breast, the main mass is located in the upper inner quadrant, in the radius at 11:00, 6 cm from the nipple; it is oval, circumscribed, without root sign and shows enhancement with dark internal septations without edema. Type 2 kinetic plateau curve. The mass measures 3.2 cm in anteroposterior diameter x 3.4 cm in craniocaudal diameter x 2.0 cm in transverse diameter. Multiple oval, circumscribed masses in both breasts with the same features described.
7. Distribution pattern (only indicated for malignant lesions): unifocal pattern, multifocal pattern, multicentric uniquadrant, or multicentric multiquadrant pattern.	Not applicable.
8. Description of other types of findings: cyst, lipoma, hemangioma, benign solid mass, scar, benign skin lesion, tissue marker clip, non-enhancing findings and whether implants are present.	None
9. Description of the skin: edema, thickening, tumor involvement, invasion and/or retraction.	None
10. Description of the nipple and nipple-areola complex: tumor involvement, invasion and/or retraction.	None
11. Description of the axillary lymph nodes, three levels and the internal mammary chain: in the case of abnormal lymph nodes, indicate the number and levels in which they are located.	None
12. Description of other abnormalities relevant to the clinical context, e.g., metastases.	None
13. Conclusion: the most important information from the breast MRI examination is summarized.	Multiple oval and circumscribed masses in both breasts contain benign features.
14. Kaiser score[a,b]	2
15. BI-RADS: add the category based on findings, including recommendations.	Category BI-RADS 2 Benign -Essentially 0% likelihood of malignancy Recommendations: consider clinical monitoring and, depending on the clinical findings, performing a breast ultrasound.
16. Name, signature, and license number of the radiologist who performed the breast MRI.	

[a]Baltzer PA et al.[8]; [b]https://school-of-radiology.com/kaiser-score/[8].

ACR: American College of Radiology; ADC: apparent diffusion coefficient; BI-RADS: Breast Imaging Reporting and Data System; DCE: dynamic contrast-enhanced; DWI: diffusion-weighted imaging; FS: fat suppressed; FSE: fast spin echo; Gd: gadolinium; GE: gradient echo; MIP: maximum intensity projection; MRI: magnetic resonance imaging; PEI: positive enhancement integral; SE: spin echo.

Note: If your facility allows you to store important breast MRI images in the system, you should do so; the attending physicians will be grateful.

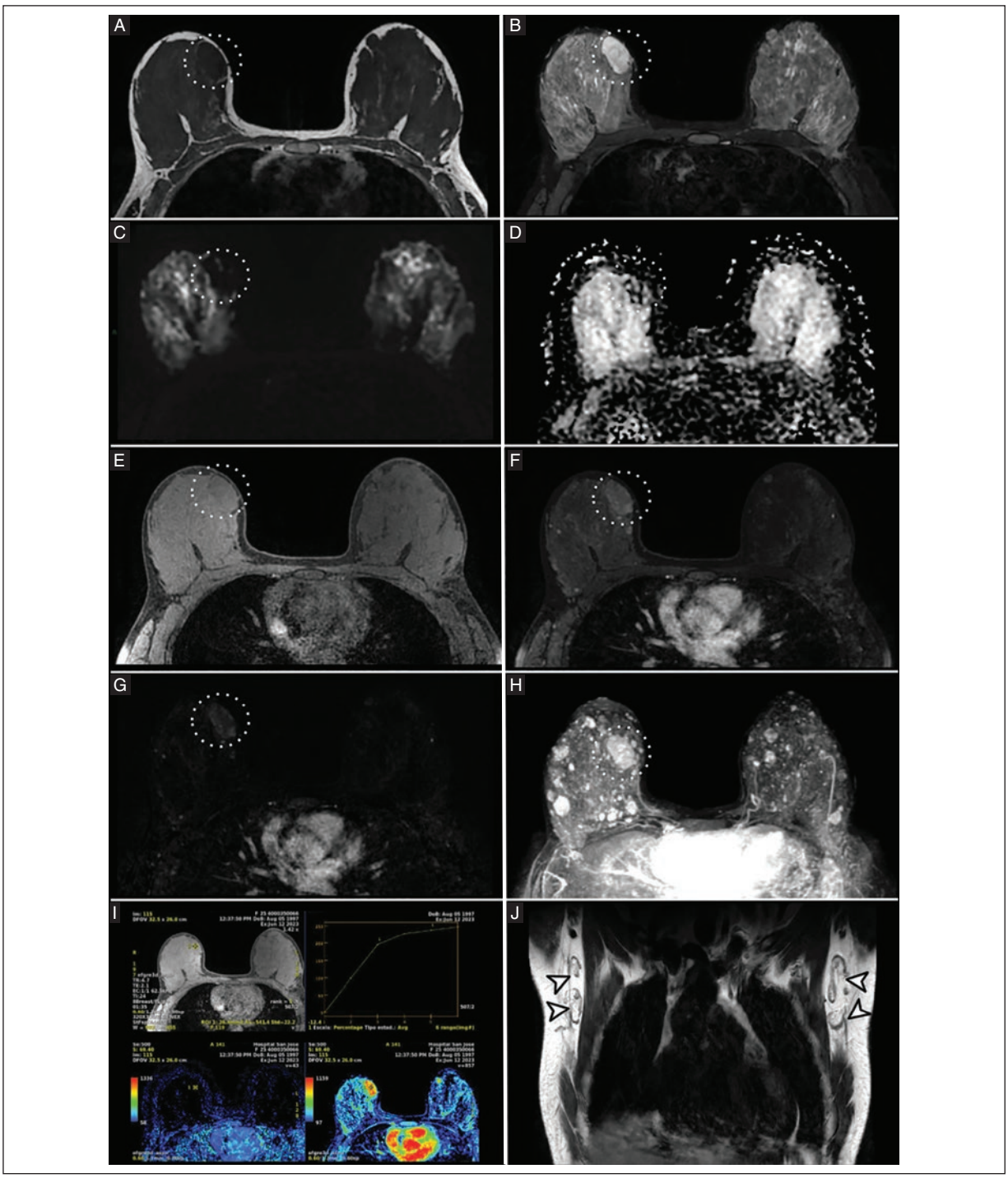

Figure 1. Breast MRI lesion in a 25-year-old woman with a palpable mass and a histopathologic diagnosis of fibroadenoma. **A:** T1 weighted SE shows a hypointense oval circumscribed mass in the upper inner quadrant of the right breast (dotted circle). **B:** T2 FS with hyperintense oval circumscribed mass in the upper inner quadrant of the right breast (dashed circle). **C:** DWI sequence and **D:** ADC without restriction in the topography of the lesion (dotted circles). **E:** T1 GE with FS shows an isointense oval circumscribed mass in the upper inner quadrant of the right breast (dotted circle). **F:** T1 DCE with Gd and **G:** T1 DCE with Gd with subtraction with the lesion of interest in the right breast showing enhancement with dark internal septations (dotted circles). **H:** MIP with multiple oval and circumscribed masses in both breasts. Some show enhancement with dark internal septations, others show homogeneous uptake. The largest mass is 3.4 cm in size and is located in the inner upper quadrant of the right breast (dotted circle). **I:** PEI with correlation of time-signal intensity curves performed on the main lesion shows a type II plateau curve. **J:** coronal T2 FSE with normal lymph nodes in the axillary level (white arrowheads). This mass corresponds to a Kaiser score of 2, BI-RADS category 2.

ADC: apparent diffusion coefficient; BI-RADS: Breast Imaging Reporting and Data System; DCE: dynamic contrast-enhanced; DWI: diffusion-weighted images; FS: fat suppressed; FSE: fast spin echo; GE: gradient echo; Gd: gadolinium; MIP: maximum intensity projection; MRI: magnetic resonance imaging; PEI: positive enhancement integral; SE: spin echo.

Table 3. Example of a standardized structured breast MRI report for a malignant breast lesion (Figure 2)

Description	Patient information: example
Date and place:	
Name of the patient:	
Name of the referring physician:	
1. Name of the imaging examination.	Contrast-enhanced breast MRI
2. Indication: screening, diagnosis, staging, complementary examination, evaluation of treatment or follow-up of breast cancer.	Diagnostic
3. Medical history: family and/or personal. If there is a history of breast cancer, indicate the histopathologic diagnosis and the date and location of previous imaging examinations.	34-year-old female patient with a palpable lump in the right breast. She has a positive family history of breast cancer (her sister was diagnosed at the age of 40).
4. Examination technique: indicate the sequences performed and the techniques used for post-processing.	T1 weighted SE, T2 FS, DWI, ADC, T1 GE with FS, T1 DCE with Gd, T1 DCE with Gd and subtraction, kinetic curve, PEI values, MIP and coronal T2 FSE sequences were performed.
5. General description of breast composition: indicate the amount of fibroglandular tissue and parenchymal enhancement in the background.	The breast composition is heterogeneous fibroglandular tissue with minimal and symmetrical background parenchyma enhancement.
6. Description of imaging findings including the ACR BI-RADS lexicon and features assessed by Kaiser score, applies to each lesion(s) identified: Mass: location (side, radius by clock time), distance from nipple, morphology, shape, margin, root sign (yes/no), enhancement, type of kinetic curve, size measured in the three axes, and ipsilateral edema (yes/no). Non-mass: location (radius by clock time), distance from nipple, enhancement, distribution, margin (circumscribed or not), root sign (yes/no), type of kinetic curve and size measured on three axes and ipsilateral edema (yes/no).	There are three masses in the right breast: mass #1 is located in the upper outer quadrant at 10:00, 5 cm from the nipple, is irregular in morphology and margin, without root sign, with heterogeneous enhancement and has a late plateau phase (kinetic curve type 2). It measures 4.3 cm in anteroposterior diameter, 3.1 cm in craniocaudal diameter, and 2.4 cm in transverse diameter. Mass #2 is located in the upper inner quadrant, at 2:00 of the clock, 4 cm from the nipple, and is irregular in morphology and margin, with root sign, heterogeneous enhancement and a late plateau phase (kinetic curve type 2). It measures 2.7 cm in anteroposterior diameter, 4.5 cm in craniocaudal diameter and 2.7 cm in transverse diameter. Mass #3 is located in the lower inner quadrant at 8:00 of the clock, 2 cm from the nipples and is irregular in morphology and margin, without root sign, heterogeneous enhancement and a late plateau phase (kinetic type 2 curve). It measures 4.6 cm in anteroposterior diameter, 4.0 cm in craniocaudal diameter, and 4.0 cm in transverse diameter. There is ipsilateral edema. They show diffusion restriction with a very low ADC value between 0.480 and 0.633 x 10^{-3} mm^2/s. In addition, further small irregular hyperenhanced masses are observed in both upper quadrants. These findings are associated with diffuse subcutaneous prepectoral edema and pectoral edema.
7. Distribution pattern (only indicated for malignant lesions): unifocal pattern, multifocal pattern, multicentric uniquadrant, or multicentric multiquadrant pattern.	Multicentric multiquadrant pattern.
8. Description of other associated features: cyst, lipoma, hemangioma, benign solid mass, scar, benign skin lesion, tissue marker clip, non-enhancing findings and whether implants are present.	None
9. Description of the skin: edema, thickening, tumor involvement, invasion, and retraction.	There is thickening of the skin.
10. Description of the nipple and nipple-areola complex: tumor involvement, invasion, and retraction.	Thickening of the nipple-areola complex.
11. Description of the axillary lymph nodes, three levels and the internal mammary chain: in case of abnormal lymph nodes, indicate the number and levels in which they are located.	Three abnormal lymph nodes with cortical thickening of up to 7 mm at level I are observed in the right axillary region.

(Continued)

Table 3. Example of a standardized structured breast MRI report for a malignant breast lesion (Figure 2) *(continuation)*

Description	Patient information: example
12. Description of other abnormalities relevant to the clinical context, e.g., as metastases.	No other relevant abnormalities were found in the anatomical structures.
13. Conclusion: the most important information from the breast MRI examination is summarized.	Highly suggestive of a malignancy in the right breast, multicentric multiquadrant pattern with ipsilateral lymph node involvement. It is also associated with diffuse thickening and edema of the skin and nipple-areola complex.
14. Kaiser score[a,b]	10
15. BI-RADS: add the category based on findings, including recommendations.	Category BI-RADS 5 Highly suggestive of malignancy, ≥ 95% likelihood of malignancy. A breast biopsy is recommended.
16. Name, signature, and license number of the radiologist who performed the breast MRI.	

[a]Baltzer PA et al.[8]; [b]https://school-of-radiology.com/kaiser-score/[8].
ADC: apparent diffusion coefficient; ACR: American College of Radiology; BI-RADS: Breast Imaging Reporting and Data System; DCE: dynamic contrast-enhanced; DWI: diffusion-weighted imaging; FS: fat suppressed; FSE: fast spin echo; Gd: gadolinium; GE: gradient echo; MIP: maximum intensity projection; MRI: magnetic resonance imaging; PEI: positive enhancement integral; SE: spin echo.
Note: If your facility allows you to store important breast MRI images in the system, you should do so; the attending physicians will be grateful.

The thirteenth section is the conclusion, which summarizes the most important information about the main breast MRI lesion(s).

The Kaiser score is added in section fourteen. It can be accessed on the virtual platform: https://school-of-radiology.com/kaiser-score[14]. It is easy to use and contains intuitive questions about specific lesion features. When the algorithm is completed, the result of the Kaiser score for a specific case and the corresponding BI-RADS recommendation is displayed.

The BI-RADS categories and recommendations are described in section fifteen[4]: Category 1: Negative – Essentially 0% likelihood of malignancy; Category 2: Benign – Essentially 0% likelihood of malignancy; Category 3: Probably benign – ≥ 0% but ≤ 2% likelihood of malignancy; Category 4: Suspicious – > 2% but < 95% likelihood of malignancy; Category 5: Highly suggestive of malignancy – ≥ 95% likelihood of malignancy; and Category 6: Known biopsy-proven malignancy N/A.

Finally, in section sixteen, the radiologist who interpreted the breast MRI provides name, signature, and license number.

Table 2 describes the standardized structured template for the breast MRI report using the example of a 25-year-old woman with multiple lumps in the breast and a histopathologic diagnosis of benign fibroadenoma (Figure 1).

Table 3 describes the standardized structured breast MRI report template using the example of a 34-year-old woman with a breast mass and a histopathologic diagnosis of no special type (NST) luminal B infiltrating carcinoma (Figure 2).

CONCLUSION

This evidence-based technical note provides a standardized structured report template using the ACR BI-RADS 5th Edition lexicon and Kaiser score to improve clarity and completeness. A supplemental digital template for the standardized structured breast MRI report and the breast cancer distribution patterns are available for download.

Acknowledgments

The authors thank Professor Ana M. Contreras-Navarro for her guidance in preparing and writing this scientific paper.

Funding

This research received no external funding.

Conflicts of interest

The authors declare that they have no conflicts of interest.

Ethical considerations

Protection of humans and animals. The authors declare that the procedures followed complied with the

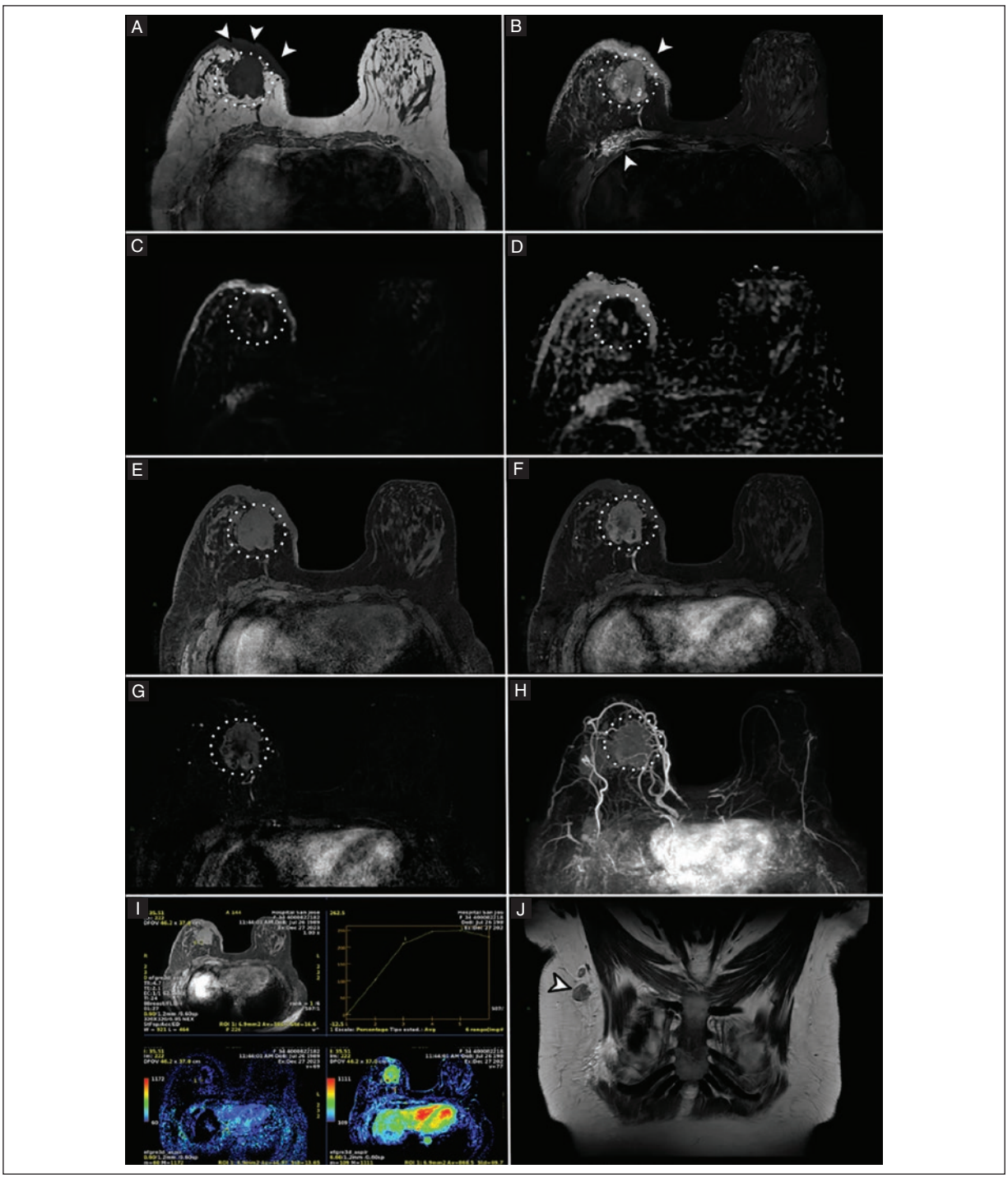

Figure 2. Breast MRI lesion in a 34-year-old woman with a palpable lump. The histopathologic diagnosis was NST luminal B infiltrating carcinoma. **A:** T1 weighted SE with scattered fibroglandular tissue. There is an irregular hypointense mass in the inner lower quadrant of the right breast with skin thickening and retraction (white arrowheads). **B:** T2 FS with the same irregular oval mass showing some internal hyperintense areas with associated subcutaneous and prepectoral edema (white arrowheads). **C:** DWI and **D:** ADC with restriction and very low ADC value (dotted circles). **E:** T1 GE with FS shows an irregular mass with subcutaneous edema (dotted circle). **F:** T1 DCE with Gd and **G:** T1 DCE with Gd with subtraction show the irregular oval mass with heterogeneous enhancement (dashed circles). **H:** MIP shows an irregular mass with increased vessels compared to the contralateral side (dashed circle). **I:** PEI with time-signal intensity for the finding of interest showing a type 2 kinetic curve. **J:** coronal T2 FSE with abnormal lymph nodes in axillary level I (white arrowhead). This mass corresponds to a Kaiser score of 10, BI-RADS category 5. Multicentric multiquadrant distribution pattern (not shown).

ADC: apparent diffusion coefficient; BI-RADS: breast imaging reporting and data system; DCE: dynamic contrast-enhanced; DWI: diffusion-weighted images; FS: fat suppressed; FSE: fast spin echo; Gd: gadolinium; GE: gradient echo; MIP: maximum intensity projection; MRI: magnetic resonance imaging; NST: not-special type; PEI: positive enhancement integral; SE: spin echo.

ethical standards of the responsible human experimentation committee and adhered to the World Medical Association and the Declaration of Helsinki. The procedures were approved by the institutional Ethics Committee.

Confidentiality, informed consent, and ethical approval. The authors have followed their institution's confidentiality protocols, obtained informed consent from patients, and received approval from the Ethics Committee.

Declaration on the use of artificial intelligence. The authors declare that no generative artificial intelligence was used in the writing of this manuscript.

Supplementary data

Supplementary data are available online in the Journal online DOI: 10.24875/JMEXFRI.M25000096. These data are provided by the corresponding author and published online for the reader's benefit. The contents of supplementary data are the sole responsibility of the authors.

REFERENCES

1. Nuñes LW, Schnall MD, Orel SG, Hochman MG, Langlotz CP, Reynolds CA. Breast MR imaging: interpretation model. Radiology. 1997;202(3):833-841. doi: 10.1148/radiology.202.3.9051042.
2. Baum F, Fischer U, Vosshenrich R, Grabbe E. Classification of hypervascularized lesions in CE MR imaging of the breast. Eur Radiol. 2002;12(5):1087-1092. doi: 10.1007/s00330-001-1213-1.
3. Fischer U. Breast MRI - The champion in the millimeter league: MIO breast MRI - The method of choice in women with dense breasts. Eur J Radiol. 2023;167:111053. doi: 10.1016/j.ejrad.2023.111053.
4. American College of Radiology (2013). ACR Breast Imaging Reporting and Data System (BIRADS). Reston, VA: American College of Radiology.
5. Pötsch N, Vatteroni G, Clauser P, Rainer E, Kapetas P, Milos R. Using the Kaiser Score as a clinical decision rule for breast lesion classification: Does computer-assisted curve type analysis improve diagnosis? Eur J Radiol. 2024;170:111271. doi: 10.1016/j.ejrad.2023.111271.
6. Dietzel M, Baltzer PAT. How to use the Kaiser score as a clinical decision rule for diagnosis in multiparametric breast MRI: a pictorial essay. Insights Imaging. 2018; 9(3):325-335. doi: 10.1007/s13244-018-0611-8.
7. Wang Q, Fu F, Chen Y, Yang D, Zhang J, Yu H, et al. Application of the Kaiser score by MRI in patients with breast lesions by ultrasound and mammography. Diagn Interv Radiol. 2022;28(4):322-328. doi: 10.5152/dir.2022.201075.
8. Baltzer PA, Dietzel M. Kaiser Score [Internet]. Friburgo (DE). University Hospital Freiburg of Germany, School of Radiology; 2023 [updated: 2021 Dec 6; cited: 2024 Nov 6]. Available from: https://school-of-radiology.com/kaiser-score/.
9. Harbeck N, Gnant M. Breast cancer. Lancet. 2017;389(10074):1134-1150. doi: 10.1016/S0140-6736(16)31891-8.
10. Pérez-Zúñiga I, Villaseñor-Navarro Y, Perez-Badillo MP, Cruz-Morales R, Pavon-Hernandez C, Aguilar-Cortazar L. Breast magnetic resonance and its applications. (Spanish). Gac Mex Oncol. 2012;11(4):268-280.
11. Mercado CL. BI-RADS update. Radiol Clin North Am. 2014;52(3):481-487. doi: 10.1016/j.rcl.2014.02.008.
12. Mann RM, Cho N, Moy L. Breast MRI: State of the Art. Radiology. 2019;292(3):520-536. doi: 10.1148/radiol.2019182947.
13. Molleran V, Mahoney MC. The BI-RADS breast magnetic resonance imaging lexicon. Magn Reson Imaging Clin N Am. 2010;18(2):171-185, vii. doi: 10.1016/j.mric.2010.02.001.
14. Shin K, Phalak K, Hamame A, Whitman GJ. Interpretation of Breast MRI Utilizing the BI-RADS Fifth Edition Lexicon: How Are We Doing and Where Are We Headed? Curr Probl Diagn Radiol. 2017;46(1):26-34. doi: 10.1067/j.cpradiol.2015.12.00.
15. Baltzer PAT, Dietzel M, Gröschel T, Kaiser WA. A simple and robust classification tree for differentiation between benign and malignant lesions in MR-mammography. Eur J Radiol. 2012;81 Suppl 1: S4-5. doi: 10.1016/S0720-048X(12)70002-5.
16. Zhou XZ, Liu LH, He S, Yao HF, Chen LP. Diagnostic value of Kaiser score combined with breast vascular assessment from breast MRI for the characterization of breast lesions. Front Oncol. 2023; 13:1165405. doi: 10.3389/fonc.2023.1165405.
17. Woitek R, Spick C, Schernthaner M, Rudas M, Kapetas P, Bernathova M. A simple classification system (the Tree flowchart) for breast MRI can reduce the number of unnecessary biopsies in MRI-only lesions. Eur Radiol. 2017;27(9):3799-3809. doi: 10.1007/s00330-017-4755-6.
18. Lopez-Mendez JMI, Delgadillo-Cisterna R, Rodriguez-Pulido G. Unifocal, multifocal, or multicentric breast cancer distribution patterns on multiplanar breast MRI: a technical note. J Mex Fed Radiol Imaging. 2024;3(1):56-61. doi: 10.24875/JMEXFRI.24000001.
19. Eghtedari M, Chong A, Rakow-Penner R, Ojeda-Fournier H. Current Status and Future of BI-RADS in Multimodality Imaging, From the AJR Special Series on Radiology Reporting and Data Systems. AJR Am J Roentgenol. 2021;216(4):860-873. doi: 10.2214/AJR.20.24894.

JMeXFRI

Journal of the Mexican Federation of Radiology and Imaging

Check for updates

FULL RESEARCH ARTICLE

Diagnostic performance of an experienced radiologist and Quantra artificial intelligence software in the assessment of mammographic breast density

Beatriz E. Gonzalez-Ulloa, Claudia B. Corona-Gonzalez, and Rosa L. Molina-Gutierrez*

Breast Imaging Department, Centro de Diagnostico Especializado por Imagen, Zapopan, Jalisco, Mexico

ABSTRACT

Introduction: *The diagnostic performance of the current version of Quantra artificial intelligence (AI) software has not been evaluated. This study aimed to compare the diagnostic performance of an experienced radiologist and Quantra AI in assessing mammographic breast density (MBD).* **Material and methods:** *In this prospective cohort study, a radiologist with 32 years of experience interpreting breast images and AI Quantra v2.2.2 assessed MBD in 2D mammograms and tomosynthesis of women over 35. Four and two MBD categories based on American College of Radiology (ACR) Breast Imaging Reporting and Data System (BI-RADS) 5th Edition lexicon were analyzed. Diagnostic performance parameters of Quantra AI and an experienced radiologist were calculated and compared as the gold standard for MBD.* **Results:** *The highest sensitivity of Quantra AI compared to an experienced radiologist as the gold standard in four MBD categories was in category d, and the lowest was in category b. In contrast, specificity was high in categories a and b. The accuracy of Quantra AI was highest in categories a and d. Sensitivity in two categories was best for dense breasts and specificity for non-dense breasts. The accuracy was the same for both categories. When the Quantra AI was the gold standard, the experienced radiologist showed the best sensitivity in category b and the lowest in category d. Specificity was higher in categories a and d and accuracy was better in category c. In two MBD categories, sensitivity was highest for non-dense breasts and specificity for dense breasts. The accuracy was equally high in both categories.* **Conclusion:** *The diagnostic performance of Quantra AI was good with the current software version in four and two MBD categories compared to an experienced radiologist as the gold standard. On the other hand, the experienced radiologist showed good sensitivity and specificity for non-dense and dense breasts and a wide range of results in diagnostic performance in four MBD categories compared to Quantra AI as the gold standard. Even if the radiologist is experienced, subjectivity still exists, and the help of a tool like AI can be valuable.*

Keywords: *Mammographic breast density. Artificial intelligence. Radiologist. BI-RADS. Quantra.*

INTRODUCTION

Mammographic breast density (MBD) is the proportion of the breast composed of fibroglandular tissue. The current reference standard for radiologists to classify MBD categories is the American College of Radiology (ACR) Breast Imaging Reporting and Data System (BI-RADS), but this standard is subjective, and its variability reduces reproducibility[1]. It is important to

***Corresponding author:**
Beatriz E. Gonzalez-Ulloa
E-mail: betyglez@yahoo.com

Received for publication: 08-10-2024
Accepted for publication: 17-12-2024
DOI: 10.24875/JMEXFRI.M25000094

Available online: 24-04-2025
J Mex Fed Radiol Imaging. 2025;4(1):37-43
www.JMeXFRI.com

differentiate non-dense breasts from dense breasts since it may be a determining factor in the decision to perform additional examinations such as ultrasound, tomosynthesis, contrast-enhanced mammography, or breast magnetic resonance imaging (MRI) in women with a higher breast cancer risk. A high MBD is an independent risk factor for breast cancer and reduces the sensitivity of mammography by masking underlying lesions[2-4].

Literature reports have shown that the diagnostic performance of artificial intelligence (AI) is comparable to that of radiologists, suggesting a synergy between radiologists and AI[1,5-10]. However, risks in using AI independent of the radiologist's experience have been described, such as automation due to lower reader performance and commission and omission errors[8]. On the other hand, BI-RADS categorization depends on the radiologist's perception of MBD. Radiologists may have distracting factors when reading imaging studies that can favor or amplify diagnostic errors[11]; thus, an automated AI method such as Quantra software may have greater reproducibility and accuracy in classifying MBD. Few clinical studies have reported the diagnostic performance of AI Quantra (v2.0) software[5,6] in assessing MBD, and none of the current version of AI Quantra (v2.2.2). This study compared the diagnostic performance of an experienced radiologist and AI Quantra software v2.2.2 in assessing MBD using BI-RADS 5th Edition. Both were compared as the gold standard for MBD.

MATERIAL AND METHODS

This prospective cohort study was conducted from May 2 to June 30, 2022, in the Breast Imaging Department of the Centro de Diagnostico Especializado por Imagen in Zapopan, Jalisco, Mexico. An experienced radiologist trained in breast imaging with current certification from the Mexican Council of Radiology and Imaging participated in the study. Informed consent was obtained.

Study development and variables

Mammograms from a previously published study were reviewed[12]. Screening or diagnostic mammograms of women 35 years or older were evaluated in four MBD categories (a, b, c, d) and two MBD categories (a+b, non-dense) and (c+d, dense) based on the ACR BI-RADS 5th Edition. The diagnostic performance of AI Quantra with an experienced radiologist and the experienced radiologist with AI Quantra were compared as the gold standard. Sex, age, and years of experience as a radiologist performing breast imaging examinations were recorded.

Protocol for image acquisition and analysis

Digital mammography and digital breast tomosynthesis

Images were acquired with Selenia Dimensions equipment (Hologic, Bedford, MA, USA) and automatic acquisition parameters. Images were stored and reviewed in a PACS system (SecureView, Diagnostic Workstation Bedford, MA, USA). Conventional projections of both breasts were acquired: two craniocaudal (CC) and two lateral-medial-oblique (LMO). MBD was classified based on the densest area of fibroglandular tissue: Category a, almost entirely fat; Category b, scattered fibroglandular tissue; Category c, heterogeneously dense; and Category d, extremely dense[13,14].

AI Quantra software

The mammography images were analyzed with AI Quantra version 2.2.2 (Hologic Inc., Bedford, MA. USA). Its assessment is based on the distribution and texture of the fibroglandular tissue pattern with an estimate of breast composition based on dense tissue by choosing the densest category classified according to BI-RADS 5th Edition[13-15].

Statistical analysis

Sensitivity, specificity, positive predictive value (PPV), negative predictive value (NPV), positive and negative likelihood ratios, and accuracy were calculated to determine the diagnostic performance of AI Quantra compared to an experienced radiologist as the gold standard. A comparison between an experienced radiologist and AI Quantra as the gold standard, was also performed. Data analysis was performed with SPSS v.25.0 (IBM Corp., Armonk, NY, USA).

RESULTS

The experienced radiologist has 32 years of experience interpreting breast images; interprets approximately 90 mammograms per week, and spends 50 hours performing various breast examinations and procedures (including mammography, ultrasound, MRI, biopsies, and breast marking). Six hundred eighty-five mammograms were analyzed.

Table 1. Diagnostic performance of AI Quantra compared to an experienced radiologist as the gold standard in the assessment of four MBD categories using the BI-RADS 5th Edition

Parameter	AI Quantra vs. experienced radiologist			
	Category a	Category b	Category c	Category d
Sensitivity, % (95% CI)	67.3 (52.5-80.0)	42.4 (36.1-49.0)	63.4 (57.7-68.8)	85.2 (76.1-91.9)
Specificity, % (95% CI)	95.9 (94.0-97.3)	95.4 (93.1-97.2)	71.7 (66.9-76.2)	78.8 (75.3-82.0)
PPV, % (95% CI)	55.9 (45.4-66.0)	83.5 (76.2-88.8)	64.4 (60.1-68.5)	37.5 (33.4-41.8)
NPV, % (95% CI)	97.4 (96.2-98.3)	75.4 (73.3-77.4)	70.8 (67.3-74.0)	97.3 (95.6-98.3)
Positive LR, mean (min-max)	16.3 (10.7-24.9)	9.3 (5.9-14.7)	2.2 (1.9-2.7)	4.0 (3.4-4.8)
Negative LR, mean (min-max)	0.3 (0.2-0.5)	0.6 (0.5-0.7)	0.5 (0.4-0.6)	0.2 (0.1-0.3)
Accuracy, % (95% CI)	93.8 (91.7-95.5)	76.8 (73.5-80.0)	68.0 (64.3-71.5)	79.6 (76.4-82.6)

AI: artificial intelligence; BI-RADS: Breast Imaging Reporting and Data System; CI: confidence interval; LR: Likelihood ratio; min-max: minimum-maximum; MBD: mammographic breast density; NPV: negative predictive value; PPV: positive predictive value.

The diagnostic performance of AI Quantra compared to an experienced radiologist as the gold standard in assessing four MBD categories

The highest sensitivity of AI Quantra compared to the radiologist was observed in category d (85.2%) and the lowest in category b (42.4%) (Table 1). In contrast, specificity was high in categories a and b (95.9 and 95.4%). The accuracy of AI Quantra was highest in categories a (93.8%) and d (79.6%). Figure 1 shows the assessment of the four MBD categories by the experienced radiologist and AI Quantra with the same results. In contrast, Figure 2 shows that the AI Quantra underestimated or overestimated MBD compared to the experienced radiologist.

The diagnostic performance of an experienced radiologist compared to AI Quantra as the gold standard in assessing four MBD categories

The highest sensitivity of the experienced radiologist was in category b (83.4%), and the lowest in category d (37.5%) compared to AI Quantra as the gold standard (Table 2). Specificity was high in categories a and d (97.4 and 97.3%, respectively), while it was lower in category c (70.8%). The highest accuracy of the experienced radiologist was in categories a and d (93.8% and 79.7%, respectively) while the lowest was for category c (68.0%). Figure 3 shows the overestimation of MBD categories by AI Quantra compared to the experienced radiologist.

The diagnostic performance of AI Quantra compared to an experienced radiologist as the gold standard in assessing two MBD categories

The sensitivity of AI Quantra was high (95.9%) in dense breasts compared to the experienced radiologist as the gold standard, while sensitivity was low (57.1%) in non-dense breasts (Table 3). In contrast, the specificity of AI Quantra™ was high in non-dense breasts (95.9%) and low in dense breasts (57.1%). The accuracy was the same for both categories (79.5%). Figure 4 shows the classification of MBD in categories a and d, with the same results by the experienced radiologist and AI Quantra. This scenario makes recognizing the difference between non-dense and dense breasts easier.

The diagnostic performance of an experienced radiologist compared to AI Quantra as the gold standard in assessing two MBD categories

The sensitivity of the experienced radiologist in non-dense breasts was high (91.1%) compared to AI Quantra as the gold standard (Table 4). Specificity was higher in dense breasts (91.1%). Diagnostic accuracy was 79.5% for both the non-dense and dense categories. Figure 5 shows the classification of MBD in categories b and c, where the experienced radiologist and AI Quantra agreed. In this case, it was easier to differentiate the two categories, non-dense and dense MBD.

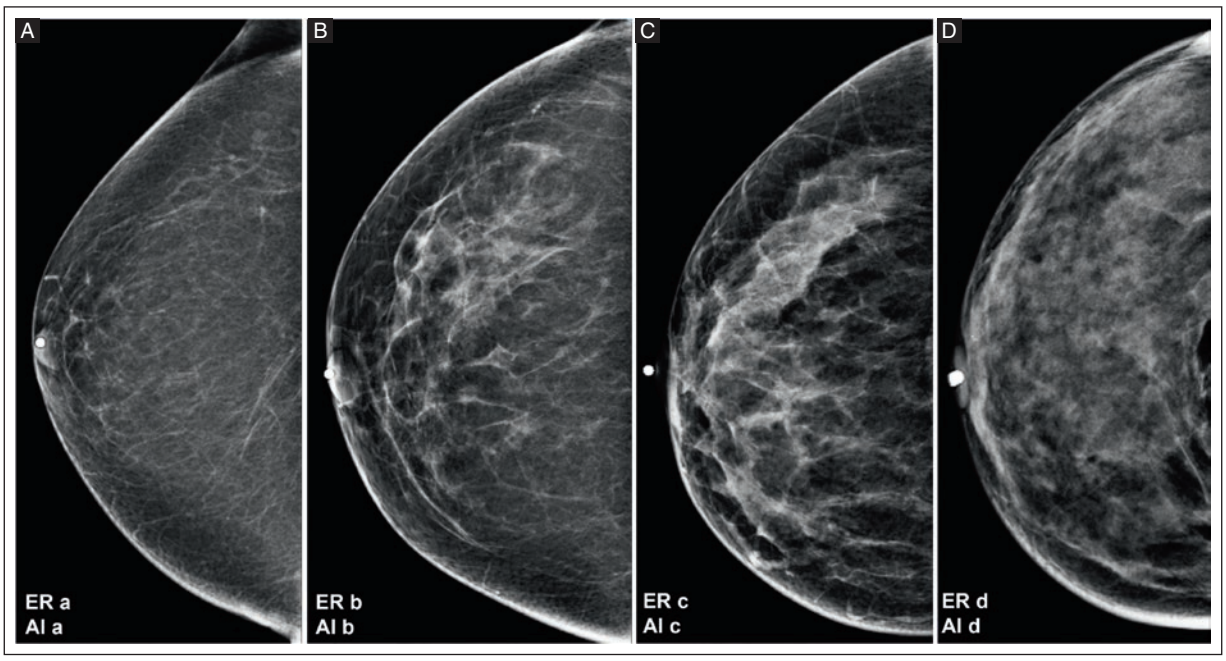

Figure 1. Mammography shows the MBD classification by an ER and AI Quantra using BI-RADS 5th Edition. **A, B, C,** and **D:** CC views of the right breast, an ER and AI Quantra with equal results for four MBD categories.

AI: artificial intelligence; BI-RADS: Breast Imaging Reporting and Data System; CC: craniocaudal; ER: experienced radiologist; MBD: mammography breast density.

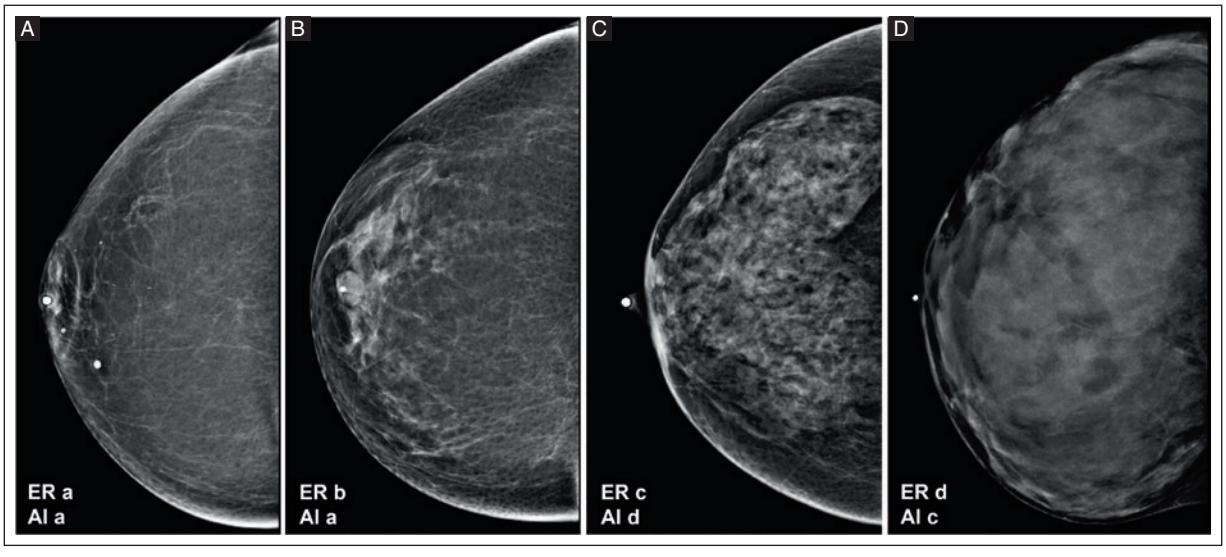

Figure 2. Mammography shows the MBD classification by an ER and AI Quantra using BI-RADS 5th Edition. **A, B, C,** and **D**: CC views of the right breast, an ER and AI Quantra with differences in classification in four MBD categories.

AI: artificial intelligence; BI-RADS: Breast Imaging Reporting and Data System; CC: craniocaudal; ER: experienced radiologist; MBD: mammography breast density.

DISCUSSION

In our study, AI Quantra showed diagnostic performance with good accuracy compared to an experienced radiologist, as the gold standard in four and two MBD categories. On the other hand, the experienced radiologist showed good sensitivity and specificity in diagnostic performance for non-dense and dense breasts and a wide variety of results when all categories were assessed with AI Quantra as the gold

Table 2. Diagnostic performance of an experienced radiologist compared to AI Quantra as the gold standard in the assessment of four MBD categories using the BI-RADS 5th Edition

Parameter	Experienced radiologist vs. AI Quantra			
	Category a	Category b	Category c	Category d
Sensitivity, % (95% CI)	55.9 (42.4-68.8)	83.8 (75.6-89.6)	64.4 (58.7-69.9)	37.5 (30.8-44.6)
Specificity, % (95% CI)	97.4 (95.8-98.5)	75.4 (71.6-78.9)	70.8 (65.9- 75.3)	97.3 (95.4-98.5)
PPV, % (95% CI)	67.4 (54.7-77.9)	42.4 (38.5-46.5)	63.4 (59.2-67.4)	85.2 (76.6-91.0)
NPV, % (95% CI)	95.9 (94.6-96.9)	95.5 (93.4-96.9)	71.7 (68.3-75.0)	78.8 (77.0-80.6)
Positive LR, mean (min-max)	21.6 (12.7-36.9)	3.4 (2.9-4.0)	2.2 (1.8-2.6)	13.8 (7.8-24.3)
Negative LR, mean (min-max)	0.45 (0.34-0.60)	0.22 (0.15-0.33)	0.5 (0.43-0.59)	0.64 (0.58-0.72)
Accuracy, % (95% CI)	93.8 (91.7-95.5)	76.8 (73.5-78.0)	68.0 (64.3-71.5)	79.7 (76.4-82.6)

AI: artificial intelligence; BI-RADS: Breast Imaging Reporting and Data System; CI: confidence interval; LR: Likelihood ratio; min-max: minimum-maximum; MBD: mammographic breast density; NPV: negative predictive value; PPV: positive predictive value.

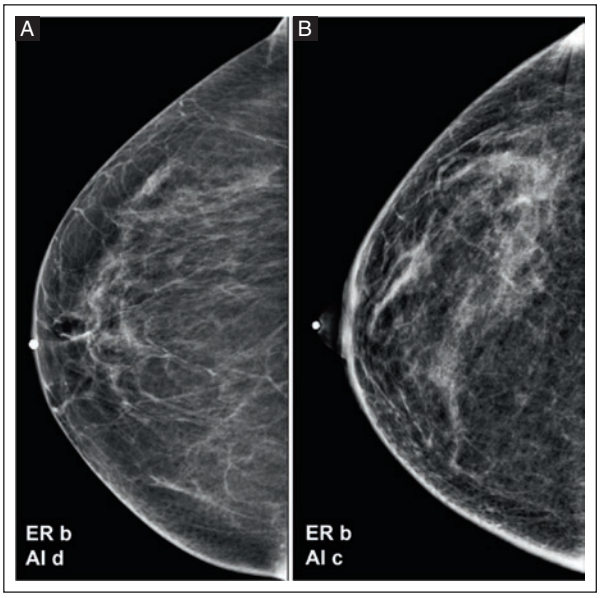

Figure 3. Mammography shows the MBD classification of an ER and AI Quantra with BI-RADS. **A-B:** CC views, the MBD results were different for both.

AI: artificial intelligence; BI-RADS: Breast Imaging Reporting and Data System; CC: craniocaudal; ER: experienced radiologist; MBD: mammography breast density.

standard. This exploratory study is the first to use AI Quantra as the gold standard for assessing the diagnostic performance of an experienced radiologist.

There are few articles[1,5,6] regarding the diagnostic performance of AI Quantra in assessing MBD. Epko et al.[5] compared the previous version of AI Quantra (v2.0) to a majority report as the gold standard. They found a sensitivity of 35.7%, 91.2%, 88.6%, and 50.3% for the four MBD categories: a, b, c, and d, respectively. The sensitivity was 91.3% and the specificity 83.6%, respectively, for the two MBD categories (a-b vs. c-d). They concluded that AI Quantra only partially reproduces the BI-RADS classification for four MBD categories but does very well in two MBD categories. Other studies[1,6] with the previous version of AI Quantra reported better sensitivity and specificity for the two MBD categories than the four MBD categories. In our study, the current AI Quantra version (v2.2.2) compared to an experienced radiologist as the gold standard showed a sensitivity of 67.3%, 42.4%, 63.4%, and 85.2% for categories a, b, c, and d, respectively. The specificity was 95.9%, 95.4%, 71.7%, and 78.8% respectively. Two-category sensitivity was highest in dense breasts (95.9%), while specificity was best in non-dense breasts (95.9%). Our results differed from Epko et al.[5] as we had better results on the diagnostic performance of AI Quantra in assessing MBD regarding sensitivity in categories a and d (67.3% vs. 25.4% and 85.2% vs. 56.7%, respectively) and higher specificity in categories b and c (95.4% vs. 75.4% and 78.8% vs. 61.3%, respectively). This could be because we used a more recent version of AI Quantra software based on the 5th edition BI-RADS. Furthermore, we found a comparable diagnostic performance of AI Quantra with all the MBD categories and two MBD categories. Using an automated AI tool can lead to better performance in assessing MBD, greater efficiency in daily work through report standardization, and greater MBD reproducibility.

No articles were found on the evaluation of MDB by radiologists compared to the results of AI Quantra as the

Table 3. Diagnostic performance of AI Quantra compared to an experienced radiologist as the gold standard in the assessment of two MBD categories using the BI-RADS 5th Edition

Parameter	AI Quantra vs. experienced radiologist	
	Non-dense categories[a]	Dense categories[a]
Sensitivity, % (95% CI)	57.1 (51.2-62.9)	95.9 (93.4-97.6)
Specificity, % (95% CI)	95.9 (93.4-97.6)	57.1 (51.1-62.9)
PPV, % (95% CI)	91.1 (86.3-94.4)	75.3 (72.7-77.7)
NPV, % (95% CI)	75.3 (72.7-77.7)	91.1 (86.2-94.3)
Positive LR, mean (min-max)	13.7 (8.5-22.8)	2.2 (1.9-2.56)
Negative LR, mean (min-max)	0.4 (0.4-0.5)	0.07 (0.04-0.12)
Accuracy, % (95% CI)	79.5 (76.3-82.5)	79.5 (76.2-82.4)

[a]Two categories: a+b (non-dense) and c+d (dense).

AI: artificial intelligence; BI-RADS: Breast Imaging Reporting and Data System; CI: confidence interval; LR: Likelihood ratio; min-max: minimum-maximum; NPV: negative predictive value; MBD: mammographic breast density; PPV: positive predictive value.

Table 4. Diagnostic performance of an experienced radiologist compared to AI Quantra as the gold standard in the assessment of two MBD categories using the BI-RADS 5th Edition

Parameter	AI Quantra vs experienced radiologist	
	Non-dense categories[a]	Dense categories[a]
Sensitivity, % (95% CI)	91.1 (86.0-94.8)	75.3 (71.3-79.0)
Specificity, % (95% CI)	75.3 (71.3- 89.0)	91.1 (86.0-94.8)
PPV, % (95% CI)	57.1 (53.2-61.0)	95.9 (93.6-97.4)
NPV, % (95% CI)	95.9 (93.6-97.4)	57.1 (53.2-61.0)
Positive LR, mean (min-max)	3.7 (3.1-4.3)	8.47 (5.3-13.6)
Negative LR, mean (min-max)	0.12 (0.07-0.19)	0.27 (0.23-0.32)
Accuracy, % (95% CI)	79.5 (76.3-82.5)	79.5 (76.3-82.5)

[a]Two categories: a+b (non-dense) and c+d (dense).

AI: artificial intelligence; BI-RADS: Breast Imaging Reporting and Data System; CI: confidence interval; LR: Likelihood ratio; MBD: mammographic breast density; NPV: negative predictive value; PPV: positive predictive value.

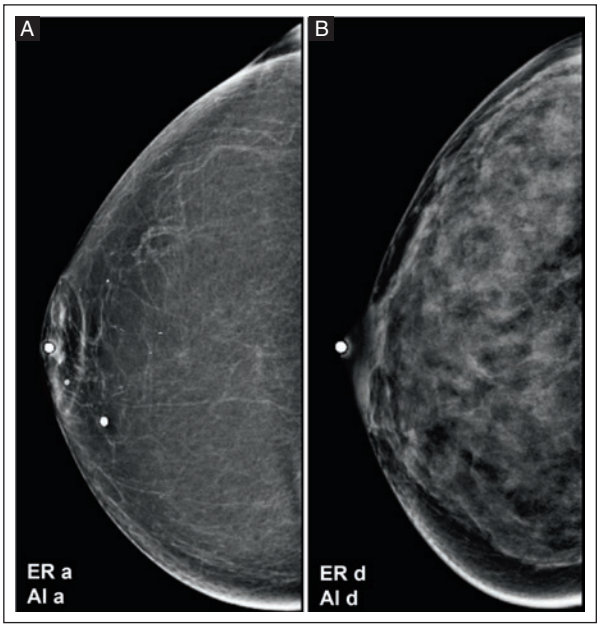

Figure 4. Mammography showing a comparison of MBD BI-RADS categories a and d by an ER and AI Quantra. **A and B**: CC views, the categories were comparable.

AI: artificial intelligence; BI-RADS: Breast Imaging Reporting and Data System; CC: craniocaudal; ER: experienced radiologist; MBD: mammography breast density.

gold standard. The experienced radiologist in our study had a wide range of results in diagnostic performance when assessing all MBD categories compared to AI Quantra as the gold standard. The experienced radiologist showed higher sensitivity in non-dense breasts (91.1%) and better specificity in dense breasts (91.1%) in the two MBD categories. There is insufficient evidence to recommend AI Quantra as the gold standard for assessing MBD, although AI may be superior to radiologists in classifying MBD in some categories[5,6,12]. As AI is constantly fed with images and thus its learning ability can be perfected, its accuracy could be superior to that of the human eye. It can certainly be used as a gold standard in assessing MBD in the future and be a useful tool in the radiologist's daily workflow[7,10].

The prospective design and the large sample size are the strengths of this study. However, the study had some limitations. It was a single-center study, and a single mammography unit acquired all mammograms. On the other hand, AI Quantra was the only AI software available at the center, only one experienced radiologist participated, and no consensus report for MBD assessment was included.

CONCLUSION

This study found better results in the diagnostic performance of the current AI Quantra (v.2.2.2) software in all MBD categories and two MBD categories than previously published with the previous version[5,6]. On the other hand, an experienced radiologist showed good sensitivity and specificity for both non-dense and dense breasts and a wide range of results in diagnostic

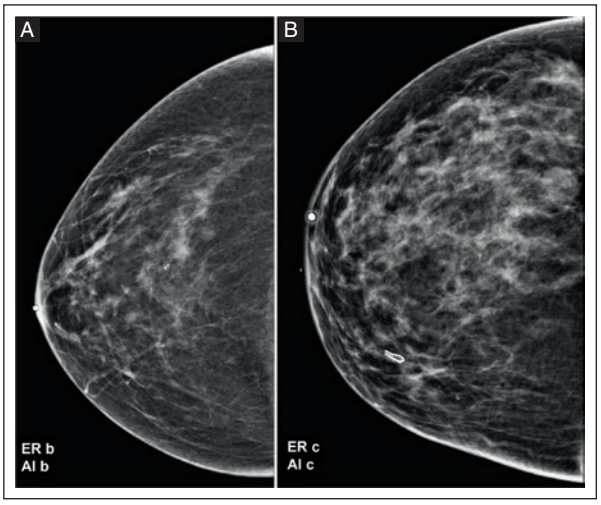

Figure 5. Mammography showing a comparison of MBD BI-RADS categories b and c by an ER and AI Quantra. **A and B:** CC views both have the same result.

AI: artificial intelligence; BI-RADS: Breast Imaging Reporting and Data System; CC: craniocaudal; ER: experienced radiologist; MBD: mammography breast density.

performance for four MBD categories compared with the AI Quantra as the gold standard. Since the assessment of MBD is subjective and depends on many factors, AI is a tool that radiologists can use to make better decisions about the follow-up of patients. Radiologists need to learn to use AI for MBD assessment with its benefits, even if it is not yet considered the gold standard. It is important to remember that AI algorithms do not work equally well in all subpopulations or patient groups[7]. Further studies evaluating MBD with AI Quantra are needed to validate the reliability and application of this method in routine clinical practice.

Acknowledgments

The authors thank Professor Ana M. Contreras-Navarro for her guidance in preparing and writing this scientific paper.

Funding

This research received no external funding.

Conflicts of interest

The authors declare that they have no conflicts of interest.

Ethical considerations

Protection of humans and animals. The authors declare that the procedures followed complied with the ethical standards of the responsible human experimentation committee and adhered to the World Medical Association and the Declaration of Helsinki.

Confidentiality, informed consent, and ethical approval. The authors have followed their institution's confidentiality protocols.

Declaration on the use of artificial intelligence. The authors declare that no generative artificial intelligence was used in the writing of this manuscript.

REFERENCES

1. Richard-Davis G, Whittemore B, Disher A, Rice VM, Lenin RB, Dollins C, et al. Evaluation of Quantra Hologic Volumetric Computerized Breast Density Software in Comparison with Manual Interpretation in a Diverse Population. Breast Cancer (Auckl). 2018;12:1178223418759296. doi: 10.1177/1178223418759296.
2. Ekpo EU, Hogg P, Highnam R, McEntee MF. Breast composition: measurement and clinical use. Radiography 2015; 21(4): 324-333. doi: 10.1016/j.radi.2015.06.006.
3. Freer PE. Mammographic breast density: impact on breast cancer risk and implications for screening. RadioGraphics 2015;35(2):302-315. doi: 10.1148/rg.352140106.
4. McCormack VA, dos Santos Silva I. Breast density and parenchymal patterns as markers of breast cancer risk: a meta-analysis. Cancer Epidemiol Biomarkers Prev. 2006;15(6):1159-1169. doi: 10.1158/1055-9965. EPI-06-0034.
5. Ekpo EU, McEntee MF, Rickard M, Brennan PC, Kunduri J, Demchig D, et al. Quantra™ should be considered a tool for two-grade scale mammographic breast density classification. Br J Radiol. 2016;89(1060): 20151057. doi: 10.1259/bjr.20151057.
6. Pahwa S, Hari S, Thulkar S, Angraal S. Evaluation of breast parenchymal density with QUANTRA software. Indian J Radiol Imaging 2015; 25: 391-396. doi: 10.4103/0971-3026.169458.
7. Taylor CR, Monga N, Johnson C, Hawley JR, Patel M. Artificial Intelligence Applications in Breast Imaging: Current Status and Future Directions. Diagnostics (Basel). 2023;13(12):2041. doi: 10.3390/diagnostics 13122041.
8. Dratsch T, Chen X, Rezazade Mehrizi M, Kloeckner R, Mähringer-Kunz A, Püsken M, et al. Automation Bias in Mammography: The Impact of Artificial Intelligence BI-RADS Suggestions on Reader Performance. Radiology. 2023;307(4): e222176. doi: 10.1148/radiol.222176.
9. Rahmat K, Ab Mumin N, Ramli Hamid MT, Fadzli F, Ng WL, Muhammad Gowdh NF. Evaluation of automated volumetric breast density software in comparison with visual assessments in an Asian population: A retrospective observational study. Medicine (Baltimore). 2020;99(39): e22405. doi: 10.1097/MD.0000000000022405.
10. Ciatto S, Bernardi D, Calabrese M, Durando M, Gentilini MA, Mariscotti G, et al. A first evaluation of breast radiological density assessment by QUANTRA software as compared to visual classification. Breast. 2012; 21(4):503-506. doi: 10.1016/j.breast.2012.01.005.
11. Ornelas-Cortinas G, Luna-Marroquin A. Diagnostic errors in radiology: where are we? J Mex Fed Radiol Imaging. 2024;3(4):205-207. doi: 10.24875/JMEXFRI.M24000085.
12. Gonzalez-Ulloa B, Corona-Gonzalez C, Molina-Gutierrez R, Salas Aguirre S. Mammography breast density assessment with Quantra artificial intelligence software: intra and interobserver agreement with radiologist. J Mex Fed Radiol Imaging. 2024;3(4):221-230. doi:10.24875/JMEXFRI. M24000088.
13. D'Orsi C, Sickles EA, Mendelson EB, Morris EA. Breast Imaging Reporting and Data System: ACR BI-RADS breast imaging atlas. 5th Edition. Reston: American College of Radiology. 2013.
14. American College of Radiology. ACR BI-RADS Atlas: Breast Imaging Reporting and Data System. 5th. Reston, VA: American College of Radiology; 2013. ACR BI-RADS® - Mammography.
15. Hologic Inc. Understanding Quantra 2.2 user guide for Cenova 3.0.1 English Man 05503-302 rev 002. Hologic; Bedford, MA, USA: 2019. https://www.hologic.com.

JMeXFRI

Journal of the Mexican Federation of Radiology and Imaging

Check for updates

FULL RESEARCH ARTICLE

High diagnostic accuracy of non-restricted diffusion in breast DWI to predict benign BI-RADS category 4 lesions can avoid unnecessary breast biopsies

Jahel D. Quiroga-Ayma[1,2], *David F. Perez-Montemayor*[1,2]*, *and Karla G. Garcia-Alvarez*[3]

[1]*Centro de Imagenologia Integral IMAX;* [2]*Instituto de Estudios Superiores de Tamaulipas, Universidad Anahuac;* [3]*Laboratorio de Patologia, Hospital Beneficiencia Española de Tampico. Tampico, Tamaulipas, Mexico*

ABSTRACT

Introduction: *Breast diffusion-weighted imaging (DWI) can reclassify a significant number of suspicious breast images as benign, thus avoiding unnecessary biopsies. This study evaluated the diagnostic performance of breast DWI in differentiating benign and malignant BI-RADS category 4 lesions with histopathologic confirmation.* **Material and Methods:** *This cross-sectional study included women with a BI-RADS category 4 breast lesion with suspected malignancy on mammography and/or ultrasound. BI-RADS subcategories 4a, 4b, and 4c were recorded. Breast DWI was performed to assess non-restricted and restricted diffusion. Sensitivity, specificity, positive predictive value (PPV), negative predictive value (NPV), and accuracy of breast DWI for predicting benign and malignant lesions were calculated. Percutaneous breast biopsy was the gold standard.* **Results:** *Seventy-three women with a mean age of 49.4 ± 13.9 years with BI-RADS category 4 lesions were included. There were 48 benign, 2 benign with upgrade potential (BWUP), and 23 malignant lesions with histopathologic confirmation. Most of the benign lesions (n = 41, 85.4%) showed non-restricted diffusion, while only 7 (14.6 %) showed restricted diffusion (p < 0.001). In contrast, all of the malignant lesions (n = 23, 100%) showed restricted diffusion (p < 0.001). Non-restricted diffusion had a sensitivity of 85.4% and a specificity of 96.0% for predicting benign BI-RADS category 4 lesions. The PPV was 97.6% and the NPV 77.4%. The diagnostic accuracy was 89.0%.* **Conclusion:** *Our study shows that non-restricted diffusion in breast DWI has a high diagnostic accuracy in predicting benign BI-RADS category 4 breast lesions. This improved lesion characterization by breast DWI can reduce the number of false positive results and unnecessary biopsies in benign breast lesions.*

Keywords: *Diagnostic breast imaging. Breast diffusion-weighted imaging. Magnetic resonance imaging. Non-restricted diffusion. Benign breast lesion. Breast biopsy.*

INTRODUCTION

Breast cancer is a leading cause of mortality in women worldwide[1]. Early detection and diagnosis are essential for effective treatment and a better prognosis. Conventional diagnostic imaging methods, such as mammography and ultrasound, are limited in their ability to differentiate between benign and malignant lesions. Therefore, category 4 or 5 lesions based on the American College of Radiology (ACR) Breast

***Corresponding author:**
David F. Perez-Montemayor
E-mail: dfperez@prodigy.net.mx

Received for publication: 04-10-2024
Accepted for publication: 12-12-2024
DOI: 10.24875/JMEXFRI.M25000098

Available online: 24-04-2025
J Mex Fed Radiol Imaging. 2025;4(1):44-52
www.JMeXFRI.com

Imaging and Reporting Data System (BI-RADS) are categorized as suspicious for malignancy with an indication for breast biopsy[2].

In the evaluation of breast lesions based on morphologic, kinetic, and biological aspects, breast magnetic resonance imaging (MRI) provides complementary information. In particular, the functional sequence of diffusion-weighted imaging (DWI) shows high specificity in characterizing breast lesions[3,4]. DWI was described in the mid-1980s and has become an essential modern diagnostic imaging method. DWI observes water diffusion *in vivo*, which is "hindered" by numerous tissue components at the microscopic level, such as cell membranes, fibers, or macromolecules, compared to free water. Therefore, DWI reflects the microstructure of the tissue and is often used for cancer imaging since restricted diffusion is usually greater in malignant tissue[4]. In addition, the apparent diffusion coefficient (ADC) map obtained from the DWI sequence quantifies the extent of restricted diffusion of water molecules, which is related to tissue microstructure and cellularity[3,4]. In its first consensus, the International Breast DWI Group of the European Society of Breast Imaging defined the appearance of the lesion (non-restricted or restricted diffusion) and the ADC value of normal tissue, and benign and malignant lesions based on breast DWI[3].

Breast DWI may reclassify a significant number of breast MRI findings suspicious for malignancy as benign and thereby reduce unnecessary biopsies[5]. Due to the high number of BI-RADS category 4 lesions that are negative for malignancy after biopsy, an imaging tool capable of distinguishing benign and malignant lesions before biopsy would be useful to avoid the risks and complications of biopsies[5]. Therefore, this study evaluated the diagnostic performance of breast DWI in differentiating between benign and malignant BI-RADS category 4 lesions with histopathologic confirmation.

MATERIAL AND METHODS

This cross-sectional study was conducted from May to December 2024 at the Centro de Imagenologia Integral IMAX in Tampico, Tamaulipas, Mexico. Women with an indication for biopsy of a BI-RADS category 4 breast lesion classified as suspicious for malignancy on mammography and/or ultrasound and referred for breast MRI and biopsy were included. We excluded women with claustrophobia, aneurysm clips, cardiac pacemakers, or metal implants. Data were collected as part of routine medical care; thus, informed consent was not required. The institutional research and research ethics committees approved the study.

Study development and variables

Information was obtained from clinical records. Age, breast lesion laterality, and BI-RADS subcategories 4a, 4b, and 4c were recorded. Diagnosis was confirmed by histopathologic examination of a breast biopsy, which was classified as benign, benign with upgrade potential (BWUP), and malignant.

Image acquisition and analysis protocol

Breast DWI was performed using a Philips Ingenia 1.5 T MRI (Philips Inc., Best, Netherlands) with a dedicated breast coil. The breast DWI sequence was acquired in the axial plane using an echoplanar imaging sequence with a *b*-value of 800 s/mm^2 with fat suppression, a diffusion time > 25 ms, a slice thickness of 2 mm, and an acquisition time of 2 minutes.

Lesions with non-restricted diffusion were hyperintense on the DWI and ADC map. Lesions with restricted diffusion were hyperintense on the DWI and hypointense on the ADC map. For lesions with restricted diffusion on the DWI, the ADC value was determined by plotting the average of the three region of interest (ROI) values on the darkest part of the ADC map, avoiding necrotic, noisy, or non-enhancing lesion voxels.

Percutaneous breast biopsy

An ultrasound-guided core needle biopsy (14G) was performed. The histopathologic diagnosis of the lesions was the gold standard for evaluating the diagnostic performance of breast DWI. The pathologist had no knowledge of the imaging findings.

Statistical analysis

Quantitative variables are presented as central tendency and dispersion measures, and categorical variables as absolute and relative frequencies. The Mann-Whitney U test was used to analyze differences in ADC values between non-restricted and restricted diffusion. The Kruskal-Wallis test assessed differences in ADC between BI-RADS subcategories 4a, 4b, and 4c. The analysis was adjusted with post-hoc comparisons using the Bonferroni method. Categorical variables were analyzed with the chi-squared and Fisher´s exact tests to evaluate the association between non-restricted and restricted lesion diffusion

Table 1. Characteristics of women with BI-RADS category 4 breast lesions related to breast DWI non-restriction and restriction diffusion and ADC value

Description	Total (n = 73)	Non-restriction diffusion (n = 42)	Restriction diffusion (n = 31)	p
Age, years (mean ± SD)	49.4 ± 13.9	49.0 ± 14.8	49.9 ± 12.8	0.268
Left breast / Right breast	39 (53.4) / 34 (46.6)	27 (64.2%) / 15 (35.7%)	12 (38.7%) / 19 (61.3%)	0.027
BI-RADS category 4				
Subcategory 4a	30	23 (76.7%)	7 (23.3%)	< 0.001
Subcategory 4b	34	18 (52.9%)	16 (47.1%)	0.678
Subcategory 4c	9	1 (11.1%)	8 (88.9%)	< 0.001
ADC (mean ± SD)	1.17 ± 0.40	1.38 ± 0.34	0.88 ± 0.27	< 0.001

ADC: apparent diffusion coefficient; BI-RADS: Breast Imaging and Reporting Data System; DWI: diffusion-weighted imaging; SD: standard deviation.

Table 2. BI-RADS 4 subcategories and their relationship to benign, BWUP, or malignant breast lesions with histopathologic confirmation

Description	Total (n = 73)	Benign breast lesions, (n = 48)	BWUP (n = 2)	Malignant breast lesions, (n = 23)	p
BI-RADS					
Subcategory 4a, n (%)	30	27 (90.0)	0	3 (10.0)	0.001
Subcategory 4b, n (%)	34	20 (58.8)	2 (5.9)	12 (35.3)	0.218
Subcategory 4c, n (%)	9	1 (11.1)	0	8 (88.9)	0.001

BI-RADS: Breast Imaging and Reporting Data System; BWUP: benign with upgrade potential.

in breast DWI and the breast lesion diagnosis (benign, BWUP, or malignant). Sensitivity, specificity, positive predictive value (PPV), negative predictive value (NPV), and accuracy of breast DWI for predicting benign and malignant lesions were determined. The 95% confidence interval was calculated. A p value < 0.05 was significant. SPSS version 25 (IBM Corp., Armonk, NY. USA) was used for analyses.

RESULTS

Seventy-three women with a mean age of 49.4 ± 13.9 years with BI-RADS category 4 breast lesions were included (Table 1). Lesions were more common in the left breast (n = 39, 53.4%) than in the right breast (n = 34, 46.6%). BI-RADS subcategories 4a, 4b, and 4c were compared with non-restricted and restricted diffusion in breast DWI and ADC values. There were 30 breast lesions in the BI-RADS 4a subcategory, 34 in the BI-RADS 4b subcategory, and 9 in the BI-RADS 4c subcategory. Subcategory 4a lesions with non-restricted diffusion were significantly more common (n = 23, 76.7%) than lesions with restricted diffusion (n = 7, 23.3%) (p < 0.001). The frequency of non-restricted and restricted diffusion was comparable (p = 0.678) in subcategory 4b. In contrast, subcategory 4c lesions with restricted diffusion (n = 8, 88.9%) were significantly more frequent than those with non-restricted diffusion (n = 1, 11.1%) (p < 0.001). On the other hand, the ADC value was significantly higher in non-restricted diffusion lesions (mean 1.3 ± 0.3) than in lesions with restricted diffusion (mean 0.8 ± 0.2) (p < 0.001).

BI-RADS 4 subcategories and their relationship to histopathologically confirmed benign, BWUP, or malignant breast lesions

There were 48 benign, 2 BWUP, and 23 malignant histopathologically confirmed breast lesions (Table 2). Twenty-seven (90.0%) of 30 breast lesions in subcategory 4a were benign. In contrast, only 3 (10.0%) were malignant (p < 0.001). On the other hand, only 1 (11.1%)

Table 3. Association of benign, BWUP, or malignant breast lesions BI-RADS category 4 with breast DWI non-restriction and restriction diffusion

Description	Total (n = 73)	Non-restriction diffusion (n = 42)	Restriction diffusion (n = 31)	p
Benign breast lesion, n (%)	48	41 (85.4)	7 (14.6)	< 0.001
BWUP, n (%)	2	1 (50.0)	1 (50.0)	0.672
Malignant breast lesion, n (%)	23	0	23 (100)	< 0.001

BI-RADS: Breast Imaging and Reporting Data System; BWUP: benign with upgrade potential; DWI: diffusion-weighted imaging.

Table 4. ADC value comparison of benign, BWUP, and malignant breast lesions related to BI-RADS 4 subcategories

Description	n	Subcategory 4a ADC value, mean ± SD	Subcategory 4b ADC value, mean ± SD	Subcategory 4c ADC value, mean ± SD	p
Benign breast lesion	48	1.3 ± 0.4	1.3 ± 0.3	1.3 ± 0.3	0.662
BWUP	2	0	1.3 ± 0	0	0.317
Malignant breast lesion	23	0.9 ± 0.2	0.8 ± 0.1	0.6 ± 0.1	0.007

BI-RADS: Breast Imaging and Reporting Data System; BWUP: benign with upgrade potential; ADC: apparent diffusion coefficient; SD: standard deviation.

of 9 breast lesions in subcategory 4c were benign, and 8 (88.9%) were malignant (p < 0.001). In subcategory 4b, there was no significant difference between benign, BWUP, and malignant lesions (p = 0.218).

Association of benign, BWUP, or malignant BI-RADS category 4 breast lesions with non-restricted and restricted diffusion in breast DWI

Most benign lesions (n = 41, 85.4%) had non-restricted diffusion, while only 7 (14.6%) had restricted diffusion (p < 0.001) (Table 3). In contrast, all malignant lesions (23, 100%) had restricted diffusion (p < 0.001). Of the two BWUP lesions, one showed non-restricted diffusion and the other restricted diffusion.

Comparison of the ADC value in benign, BWUP, and malignant breast lesions in relation to the BI-RADS 4 subcategories

Benign breast lesions had significantly higher ADC values than malignant breast lesions. Benign breast lesions in subcategories 4a, 4b, and 4c had the same ADC value (1.3×10^{-3} mm^2/s) (Table 4) and were similar for BWUP lesions (1.3×10^{-3} mm^2/s). In contrast, the ADC value in malignant lesions was low: 0.9×10^{-3} mm^2/s, 0.8×10^{-3} mm^2/s, and 0.6×10^{-3} mm^2/s for subcategories 4a, 4b, and 4c, respectively (p < 0.007).

In figure 1, the breast DWI shows a non-mass lesion, hyperintense with non-restricted diffusion. The ADC value was 2.1×10^{-3} mm^2/s. The histopathologic diagnosis was fibrocystic breast disease. The breast DWI in figure 2 shows an oval, hyperintense mass with restricted diffusion. The ADC map shows a hypointense mass with a central hyperintense area. The ADC value was 1.2×10^{-3} mm^2/s. The histopathologic diagnosis was breast fibroadenoma. The breast DWI in figure 3 shows an oval, hyperintense mass with non-restricted diffusion. The ADC value was 1.9×10^{-3} mm^2/s. The histopathologic diagnosis was a biphasic lesion with extensive stromal fibrosis with atypical ductal hyperplasia with papilloma (BWUP). The breast DWI in figure 4 shows an irregular, predominantly hyperintense mass with restricted diffusion. The ADC value was 0.79×10^{-3} mm^2/s. The histopathologic diagnosis was ductal carcinoma non-special type.

Diagnostic performance of non-restricted diffusion in breast DWI for predicting a benign BI-RADS category 4 breast lesion

Non-restricted diffusion in breast DWI showed a sensitivity of 85.4% and a specificity of 96.0% for predicting a benign BI-RADS category 4 lesion (Table 5). The PPV was 97.6%, with an NPV of 77.4%. The diagnostic accuracy was 89.0%.

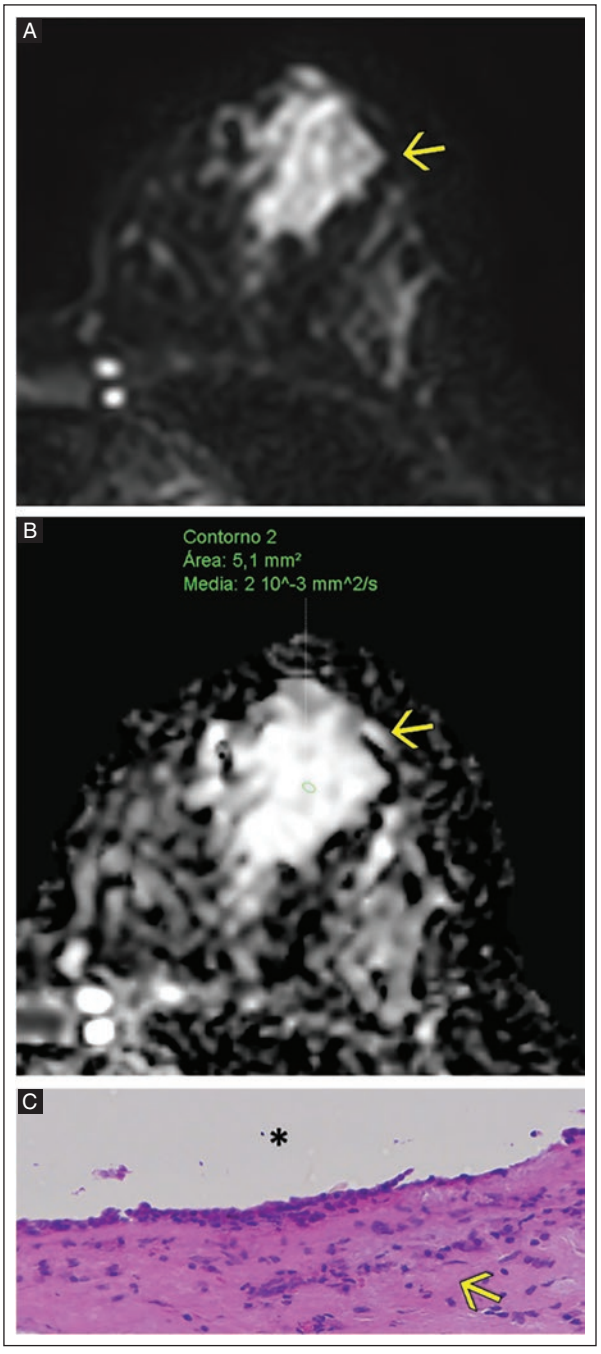

Figure 1. Breast DWI of a 37-year-old woman with a palpable lump in the left breast. Mammography (not shown) with BI-RADS subcategory 4a. **A:** axial DWI view of the left breast shows an irregular hyperintense non-mass lesion with non-restricted diffusion (arrow). **B:** an ADC map showing a hyperintense, retroareolar non-mass lesion (arrow). ROI with an ADC value of 2.1 × 10^{-3} mm^2/s (green circle). **C:** breast biopsy (H&E 40x) shows a duct with extensive microhemorrhage, inflammation, fibrin, peripheral fibrosis (arrow), and cystic dilatation (black asterisk). The histopathologic diagnosis was fibrocystic breast disease.

ADC: apparent diffusion coefficient; BI-RADS: Breast Imaging and Reporting Data System; DWI: diffusion-weighted imaging; H&E: hematoxylin and eosin; ROI: region of interest.

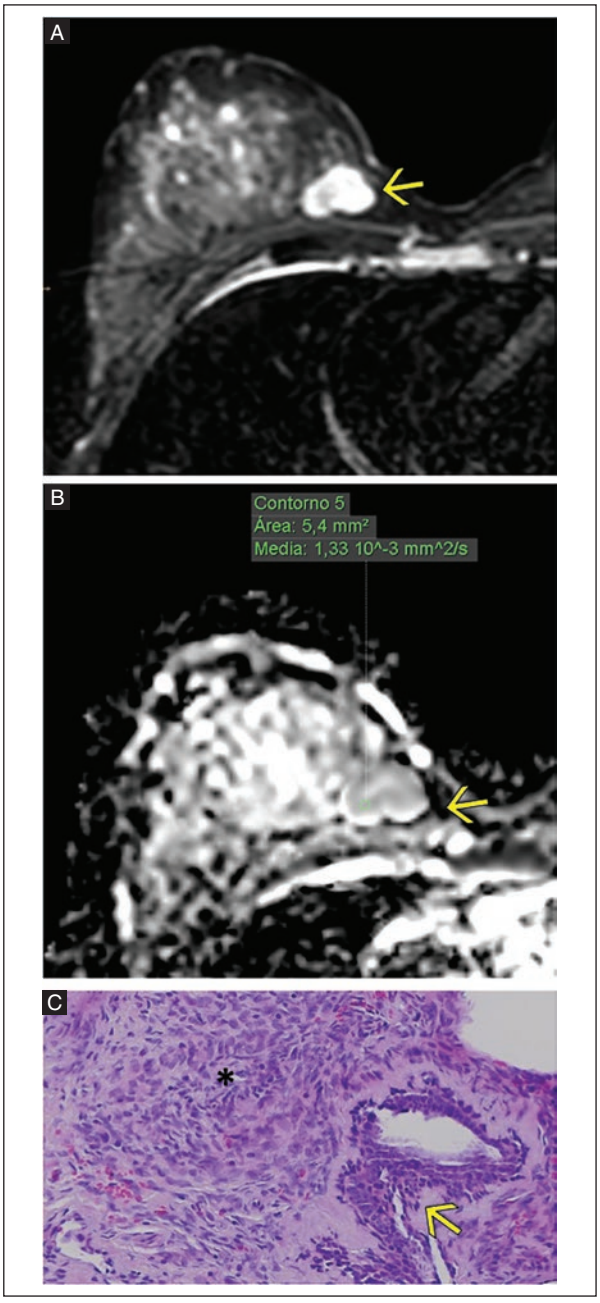

Figure 2. Breast DWI of a 26-year-old woman with a palpable lump in the right breast. Ultrasound (not shown) with BI-RADS subcategory 4b. **A:** axial DWI view shows an oval heterogeneous mass with a circumscribed margin in the posterior third of the inner quadrant of the right breast, hyperintense with restricted diffusion and central hypointense lines (arrow). **B:** the ADC map shows a hypointense mass with a central hyperintense area. The ROI with an ADC value of 1.2 × 10^{-3} mm^2/s (arrow). **C:** breast biopsy (H&E, 40x) shows a fusocellular lesion (asterisk), with stromal hyperplasia and isolated dilated hyperplastic ducts (arrow), dilated and congestive capillaries, without atypical mitoses or marked pleomorphism. The histopathologic diagnosis was breast fibroadenoma.

ADC: apparent diffusion coefficient; BI-RADS: Breast Imaging and Reporting Data System; DWI: diffusion-weighted imaging; H&E: hematoxylin and eosin; ROI: region of interest.

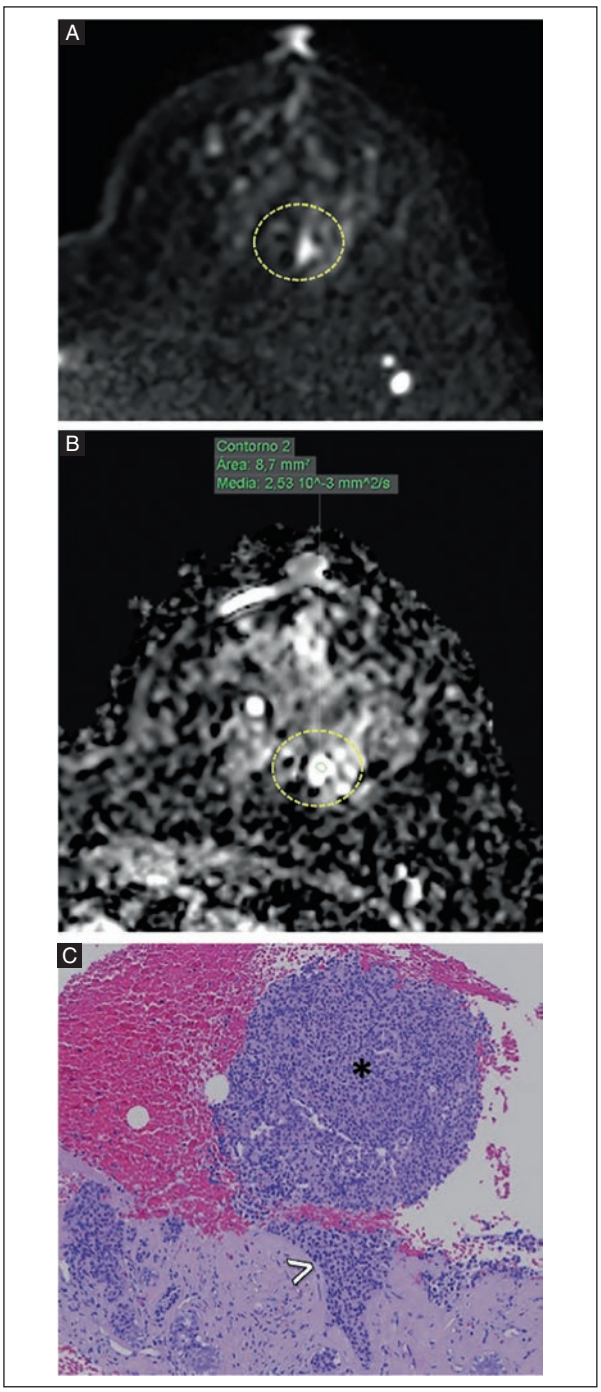

Figure 3. Breast DWI of a 45-year-old woman with a mass in the left breast. Mammography and US (not shown) with BI-RADS category 4b. **A:** axial DWI view with an oval mass and a microlobulated margin, located in the posterior third of the interline of the lower quadrant of the left breast, hyperintense with non-restricted diffusion. **B:** the ROI with an ADC value of 1.9×10^{-3} mm^2/s (dotted circles). **C:** the breast biopsy (H&E 40x) shows dense fibrous tissue (asterisk), with atypical ductal hyperplasia (arrowhead) and areas of adenosis and papillary proliferation within a duct with microhemorrhage. The histopathologic diagnosis was biphasic lesion with extensive stromal fibrosis with atypical ductal hyperplasia with papilloma (BWUP).

ADC: apparent diffusion coefficient; BI-RADS: Breast Imaging and Reporting Data System; BWUP: benign with upgrade potential; DWI: diffusion-weighted imaging; H&E: hematoxylin and eosin; ROI: region of interest; US: ultrasound.

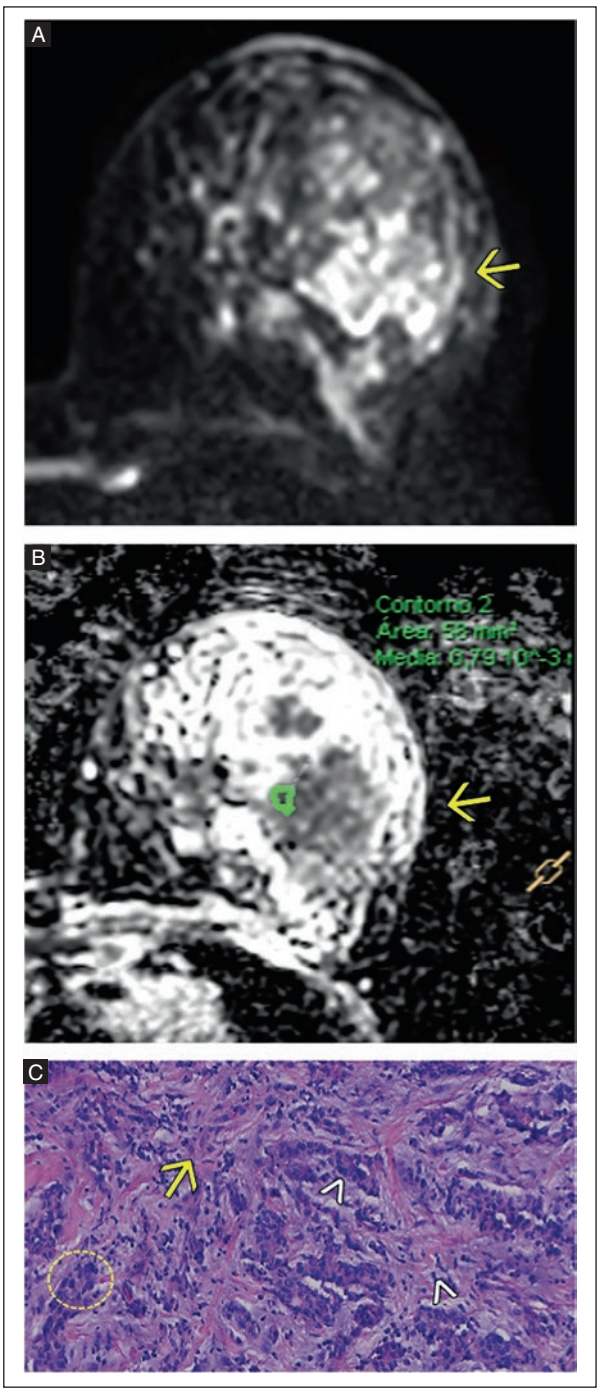

Figure 4. Breast DWI in a 45-year-old woman with a palpable lump in the left breast. Ultrasound (not shown) BI-RADS category 4c. **A:** axial DWI view shows an irregular mass, non-circumscribed margin, heterogeneous, occupying the outer quadrants of the left breast, predominantly hyperintense with restricted diffusion (arrow). **B:** ADC map with a hypointense mass (arrow). ROI (green circle) with an ADC value of 0.7×10^{-3} mm^2/s. **C:** breast biopsy (H&E 40x) showing a malignant lesion with ductal configuration, accentuated atypia, and pleomorphism (arrow), with atypical mitoses (dotted circle) in a desmoplastic stroma (arrowheads). The histopathologic diagnosis was ductal carcinoma of non special type.

ADC: apparent diffusion coefficient; BI-RADS: Breast Imaging and Reporting Data System; DWI: diffusion-weighted imaging; H&E: hematoxylin and eosin; ROI: region of interest.

Table 5. Diagnostic performance of breast DWI non-restriction diffusion for predicting a benign BI-RADS category 4 breast lesion

Description	Parameter
Sensitivity, % (95% CI)	85.4 (72.2-93.9)
Specificity, % (95% CI)	96.0 (79.6-99.9)
PPV, % (95% CI)	97.6 (85.7-99.6)
NPV, % (95% CI)	77.4 (63.2-87.2)
Accuracy, % (95% CI)	89.0 (79.5-95.1)

BI-RADS: Breast Imaging and Reporting Data System; CI: confidence interval; DWI: diffusion-weighted imaging; NPV: negative predictive value; PPV: positive predictive value.

Table 6. Diagnostic performance[a] of breast DWI restriction diffusion for predicting a malignant BI-RADS category 4 breast lesion

Description	Parameter
Sensitivity, % (95% CI)	96.0 (79.6-99.9)
Specificity, % (95% CI)	85.4 (72.2-93.9)
PPV, % (95% CI)	77.4 (63.2-87.2)
NPV, % (95% CI)	97.6 (85.7-99.6)
Accuracy, % (95% CI)	89.0 (79.5-95.1)

OR: 6.58 (3.30-13.11). [a]Includes 2 BWUP breast lesions.

BI-RADS: Breast Imaging and Reporting Data System; BWUP: benign with upgrade potential; CI: confidence interval; DWI: diffusion-weighted imaging; NPV: negative predictive value; PPV: positive predictive value.

Diagnostic performance of restricted diffusion in breast DWI for the prediction of a BI-RADS category 4 malignant breast lesion

The presence of restricted diffusion in breast DWI for predicting a BI-RADS category 4 malignant lesion showed a sensitivity of 96.0% and a specificity of 85.4% (Table 6). The PPV was 77.4% and the NPV 97.6%. The diagnostic accuracy was 89.0%. Restricted diffusion in the breast DWI showed an increased risk of malignancy (OR: 6.58, 95% CI, 3.30-13.11).

DISCUSSION

Our study shows that non-restricted diffusion has a high diagnostic accuracy (89.0%) for predicting benign breast lesions in BI-RADS category 4 lesions. Non-restricted diffusion in breast DWI is useful for differentiating between benign and malignant BI-RADS category 4 lesions. Breast DWI improves lesion characterization and reduces false-positive results and unnecessary breast benign biopsies.

Breast DWI has a high specificity for characterizing lesions, and the sensitivity of DWI alone can be equal or even higher than commonly used screening techniques such as mammography and ultrasound[3]. Shi et al.[6] evaluated the diagnostic performance of breast DWI in distinguishing malignant and benign lesions in a systematic review and meta-analysis. Forty-one studies using a 1.5T MR unit with 3501 patients and 3867 breast lesions were included. They showed a pooled sensitivity and specificity of 91% and 86%, respectively. In the 17 studies with a 3.0T MR unit, which included 1227 patients and 1338 breast lesions, the pooled sensitivity and specificity were 88% and 84%, respectively. The authors concluded that breast DWI has comparable sensitivity and specificity in 1.5T and 3.0T MR units. Our study of the diagnostic performance of non-restricted diffusion for predicting benign BI-RADS category 4 lesions found comparable results with a sensitivity of 85.4%, a specificity of 96.0%, and a high diagnostic accuracy (89.0%) using a 1.5T MR unit. We identified 48 benign BI-RADS category 4 lesions with histopathologic confirmation; 41 (85.4%) had non-restricted and 7 (14.6%) restricted diffusion. Applying the criterion of non-restricted diffusion in BI-RADS category 4 lesions to avoid breast biopsies could significantly reduce the number of benign biopsies. Based on our results, 41 non-restricted breast lesions would not have been biopsied. Only restricted diffusion lesions would have required a breast biopsy; thus, breast DWI would have reduced the overall biopsy rate by 51.2% (41/73). According to our results, breast DWI can distinguish a significant number of benign (non-restricted diffusion) from malignant (restricted diffusion) BI-RADS category 4 lesions.

The International Breast DWI Group of the European Society of Breast Imaging proposes a standardizing the ADC value for benign ($1.3\text{-}1.7 \times 10^{-3}$ mm^2/s) and malignant ($\leq 0.9 \times 10^{-3}$ mm^2/s) breast lesions as intermediate and very low diffusion levels, respectively, based on the recent meta-analysis of studies evaluating DWI to differentiate benign from malignant[3,6]. Ramírez-Galván et al.[7], in a Mexican study that included 36 BI-RADS category 4 breast lesions, found 21 (58.3%) benign and 15 (41.7%) malignant lesions. The ADC value of the benign lesions

was significantly higher (1.4×10^{-3} mm^2/s) than that of malignant ones (0.8×10^{-3} mm^2/s) ($p < 0.001$). Their study did not define the ADC value for each BI-RADS 4 subcategory. In a multicenter study, the ADC value was more useful for BI-RADS category 4 than BI-RADS categories 3 or 5, confirming that many benign lesions have significantly higher ADC values than malignant[5]. In our study, the benign lesions in the three BI-RADS 4 subcategories had an ADC value of 1.3×10^{-3} mm^2/s. In contrast, the malignant lesions had very low values, with the values decreasing in each subcategory: subcategory 4a (0.9×10^{-3} mm^2/s), subcategory 4b (0.8×10^{-3} mm^2/s), and subcategory 4c (0.6×10^{-3} mm^2/s). The ADC value differentiates between benign and malignant BI-RADS 4 breast lesions and may be clinically useful together with non-restricted diffusion in breast DWI to reduce breast biopsy recommendations.

More compressed cells in malignant lesions lead to greater restriction of diffusion of water molecules than in benign lesions. Consequently, malignant lesions have a higher signal intensity with restricted diffusion in DWI and a lower apparent diffusion coefficient (ADC) in breast DWI[6,8]. Cell density is inversely proportional to the ADC value[9,10]. In our study, all 23 (100%) malignant lesions with histopathologic confirmation showed restricted diffusion in breast DWI with a very low ADC value ($\leq 0.9 \times 10^{-3}$ mm^2/s) in all BI-RADS 4 subcategories. Our study of the diagnostic performance of restricted diffusion in breast DWI for predicting a BI-RADS category 4 malignant breast lesion showed a sensitivity of 96.0% and a specificity of 85.4% with a high diagnostic accuracy of 89.0%. The combination of DWI and quantitative ADC analysis is a helpful, non-invasive method for characterizing and identifying malignant breast lesions with high diagnostic accuracy.

Our study has several strengths regarding imaging modality since breast DWI does not require administering an intravenous contrast agent, no preparation is necessary, and the study duration is short (< 5 minutes). In addition, the diagnosis in all cases was confirmed histopathologically as the gold standard. Our study has some limitations related to the small sample size, the retrospective design, and the fact that only one center participated. On the other hand, artifacts and motion may distort the image and thus reduce feature accuracy, the location, and the extent of breast lesions. In addition, small lesions may not be visualized due to the low spatial resolution.

CONCLUSION

Our study demonstrated the high diagnostic performance of non-restricted diffusion in breast DWI for predicting benign BI-RADS category 4 breast. Furthermore, its combination with ADC values improved diagnostic characterization and reduced false-positive results, especially in subcategory 4a, due to the high number of BI-RADS 4 lesions negative for malignancy after biopsy. Multicenter, prospective cohort studies with a larger number of patients are needed to validate the utility of breast DWI in differentiating between benign and malignant lesions.

Acknowledgments

The authors thank Professor Ana M. Contreras-Navarro for her guidance in preparing and writing this scientific paper.

Funding

This research received no external funding.

Conflicts of interest

The authors declare that they have no conflicts of interest.

Ethical considerations

Protection of humans and animals. The authors declare that the procedures followed complied with the ethical standards of the responsible human experimentation committee and adhered to the World Medical Association and the Declaration of Helsinki.

Confidentiality, informed consent, and ethical approval. The authors have obtained approval from the Ethics Committee for the analysis of routinely obtained and anonymized clinical data, so informed consent was not necessary.

Declaration on the use of artificial intelligence. The authors declare that no generative artificial intelligence was used in the writing of this manuscript.

REFERENCES

1. Pan American Health Organization. Breast. Washington: PAHO/WHO. Cancer Program 2022. [cited: 2024 Sep 6]. Available from: https://school-of-radiology.com/kaiser-score/. http://www.paho.org/hq/index.php.
2. D'Orsi C, Sickles EA, Mendelson EB, Morris EA. Breast Imaging Reporting and Data System: ACR BI-RADS breast imaging atlas. 5th Edition. Reston: American College of Radiology. 2013.

3. Baltzer P, Mann RM, Iima M, Sigmund EE, Clauser P, Gilbert FJ, et al. EUSOBI international Breast Diffusion-Weighted Imaging working group. Diffusion-weighted imaging of the breast-a consensus and mission statement from the EUSOBI International Breast Diffusion-Weighted Imaging working group. Eur Radiol. 2020;30(3):1436-1450. doi: 10.1007/s00330-019-06510-3.
4. Honda M, Sigmund EE, Le Bihan D, Pinker K, Clauser P, Karampinos D, et al. EUSOBI International Breast Diffusion-Weighted Imaging working group. Advanced breast diffusion-weighted imaging: what are the next steps? A proposal from the EUSOBI International Breast Diffusion-weighted Imaging working group. Eur Radiol. 2024. doi: 10.1007/s00330-024-11010-0. Epub ahead of print.
5. Rahbar H, Zhang Z, Chenevert T, Romanoff J, Kitsch A, Hanna L, et al. Utility of Diffusion-weighted Imaging to Decrease Unnecessary Biopsies Prompted by Breast MRI: A Trial of the ECOG-ACRIN Cancer Research Group (A6702). Clin Cancer Res. 2019; 25(6):1756-1765. doi: 10.1158/1078-0432.CCR-18-2967.
6. Shi RY, Yao QY, Wu LM, Xu JR. Breast Lesions: Diagnosis Using Diffusion Weighted Imaging at 1.5T and 3.0T-Systematic Review and Meta-analysis. Clin Breast Cancer. 2018;18(3):e305-e320. doi: 10.1016/j.clbc.2017.06.011.
7. Ramirez YA, Cardona S, Ibarra E, Elizondo G. Apparent diffusion coefficient (ADC) value to evaluate BI-RADS 4 breast lesions: correlation with pathological findings. Clin Imaging. 2015; 39(1): 51-55. doi.org/10.1016/j.clinimag.2014.09.015.
8. Lima M, Kataoka M, Honda M, Le Bihan D. Diffusion-Weighted MRI for the Assessment of Molecular Prognostic Biomarkers in Breast Cancer. Korean J Radiol. 2024;25(7):623-633. doi.org/10.3348/kjr.2023.1188.
9. Guo Y, Cai YQ, Cai ZL, Gao YG, An NY, Ma L, et al. Differentiation of clinically benign and malignant breast lesions using diffusion-weighted imaging. J Magn Reson Imaging. 2002;16(2):172-178. doi: 10.1002/jmri.10140.
10. Chen Y, Wang J, Zhang X, Yang W, Chen H, Bao B, et al. Correlation between apparent diffusion coefficient and pathological characteristics of patients with invasive breast cancer. Ann Transl Med. 2021;9(2):143. doi.org/10.21037/atm-20-7746.

JMeXFRI

Journal of the Mexican Federation of Radiology and Imaging

Check for updates

FULL RESEARCH ARTICLE

Intraluminal foreign bodies commonly found in daily practice in a tertiary care hospital: a pictorial essay

Rafael Pimenta-Camilo[1], *Luis R. Marquez-Ferreira de Souza*[1,2*], *Tamires Hortêncio-Alvarenga*[2], *and Felipe Alves-Nazario*[2]

[1]*Department of Radiology;* [2]*Faculty of Medicine. Universidade Federal do Triângulo Mineiro, Uberaba, Minas Gerais, Brazil*

ABSTRACT

Foreign bodies (FBs) are objects that originate from outside the body and can be ingested or introduced voluntarily or involuntarily. Although common in the pediatric population, they are also prevalent in adults, especially in neglected populations. Due to the difficulty in obtaining information, imaging techniques play a key role in etiologic and topographic diagnosis, as certain materials may need to be removed immediately to avoid complications. FBs can be intraluminal, from ingestion or insertion, or extraluminal from other causes. In this pictorial essay, we describe the most common cases of intraluminal abdominal FBs in a tertiary care hospital and suggest investigative approaches in suspected cases. To identify a FB, a standard acute abdominal radiograph is first performed. If no FB is identified in suspected complications, the investigation continues with ultrasound (US) or computed tomography (CT), depending on the suspected material composition. Glass and plastic are usually not visible on X-rays; therefore, CT is the gold standard method. In contrast, metallic materials and animal bones are clearly visible on X-ray images. In such cases, CT is reserved for visualization of suspected perforations or infectious collections outside the intestinal loops. Imaging techniques are essential for diagnosis and management, and the indications and limitations of each method must be considered.

Keywords: *Foreign bodies. Retained surgical objects. Foreign body. Bezoars.*

INTRODUCTION

Foreign bodies (FBs) are objects that originate from outside the body and can be ingested or introduced voluntarily or involuntarily[1]. They are common in the pediatric population and account for 85% of cases of FB ingestion in the United States[2,3]. Their peak incidence is found in patients aged between 6 months to 6 years[2], and they are the leading cause of death in patients younger than 1 year of age[3].In adults, most objects found are related to a previous interventional medical procedure[3], with no reports of deaths[4]. In addition, FB ingestion and insertion are most commonly found in patients with psychiatric disorders, developmental delay, alcohol intoxication, and those who are incarcerated or involved in drug trafficking, which may be neglected due to difficulties in obtaining diagnostic information[3].

Radiologic examination plays a key role in etiologic and topographic diagnosis and in the detection of complications arising from FB in the abdominal cavity. Different methods are available in the imaging departments, depending on the indications and limitations of each case. The aim of this pictorial essay is to show

***Corresponding author:**
Luís R. Marquez-Ferreira de Souza
E-mail: luis.souza@uftm.edu.br

Received for publication: 15-10-2024
Accepted for publication: 05-01-2025
DOI: 10.24875/JMEXFRI.24000044

Available online: 24-04-2025
J Mex Fed Radiol Imaging. 2025;4(1):53-59
www.JMeXFRI.com

the most common cases of intraluminal abdominal FB in a tertiary care hospital, including the routine of radiologists, to describe aspects that should be considered in the imaging assessment, and to suggest the approach to suspected cases.

We analyzed the electronic medical and imaging data from the Department of Radiology and Diagnostic Imaging of the Hospital de Clínicas da Universidade Federal do Triângulo Mineiro in Uberaba, Minas Gerais. Brazil. We included cases referred from the departments of clinical medicine, surgery, pediatrics, gynecology and obstetrics with suspected intraluminal FBs in the abdominal cavity. We selected relevant images of our cases to represent each FB category assessed with different imaging modalities and showed their characteristics and main imaging findings.

Imaging approaches depending on the FB mechanism of injury

- **Ingestion:** frontal and lateral radiographs of the chest, neck and abdomen show the topography of the FB and allow immediate treatment by the treating physician. If the FB is larger than 5 cm, has sharp edges, cannot be characterized or is associated with complications, a computed tomography (CT) scan is performed[2,3,5,6].
- **Manual insertion:** some studies have indicated the usefulness of two radiographs in orthogonal planes for accurate visualization of FB features[7]. In addition, some studies have postulated the use of CT to clearly define the boundaries, the relationship of the object to the mucosa and its integrity, and signs of complications[1,3,4]. This should be arranged by the treating medical team prior to digital exploration to avoid rectal injury from sharp objects[5].

Imaging findings of intraluminal FBs

The FBs are listed in table 1:

- **Glass objects:** these represent up to 30% of ingested FB in children[3] and 9%-24% of all retained FBs[1]. Standard abdominal radiography should be used as the initial imaging modality for diagnosis due to its high accuracy, wide availability and low cost[1]. Most glass objects are radiopaque (Figure 1). However, their identification can be hampered by their small size, which is often a limiting factor in diagnosis[3,8]. Another limiting factor is the positioning of the FB in relation to the X-ray image. If the larger diameter is not parallel to the beam, detection becomes more difficult[8]. Therefore, a negative finding when glass FB ingestion is strongly suspected does not rule out the diagnosis and other methods should be used. Ultrasound (US) shows glass as linear hyperechoic images with dirty posterior acoustic shadowing or reverberation artifacts. In addition, identification becomes difficult with increasing depth of the FB in the body[1,9]. CT is the best imaging modality as it can identify objects as small as 0.1 mm and with a density of 100 Hounsfield units (HU) to 500 HU[1,9-11].
- **Metallic objects:** almost all metallic objects are radiopaque, and their radiopacity value varies depending on the material from 3,000 HU for iron to 30,000 HU for lead[1]; therefore, most of them can be diagnosed on abdominal radiographs. An important exception is aluminium, which has a radiodensity of about 700 HU and is not easily identified by this method[1,12]. On US radiographs, metallic objects can be seen as hyperechoic images with posterior acoustic shadowing and/or reverberation artifacts, while on CT images, various high-density morphologies with radiation hardening artifacts can be seen (Figure 2). Similarly, they generate artifacts on magnetic resonance imaging (MRI), where they are visualized as low-signal objects[1].
- **Batteries:** on radiographs, they appear as radiopaque structures and have a "double-ring" characteristic due to their bilaminar structure[3,4] (Figure 3), whereas on CT they appear as small round FBs with high attenuation[4]. Timely identification of batteries is essential due to the high risk of corrosive lesions, such as esophageal burns and fistula formation[3,4]. They should be removed endoscopically as soon as possible[2].
- **Plastic objects:** X-ray images are sometimes inadequate as plastic objects are predominantly

Table 1. Types of intraluminal FBs

Glass objects
Metallic objects
Batteries
Plastic objects
Bones
Bezoar
Drug packages

FBs: foreign bodies.

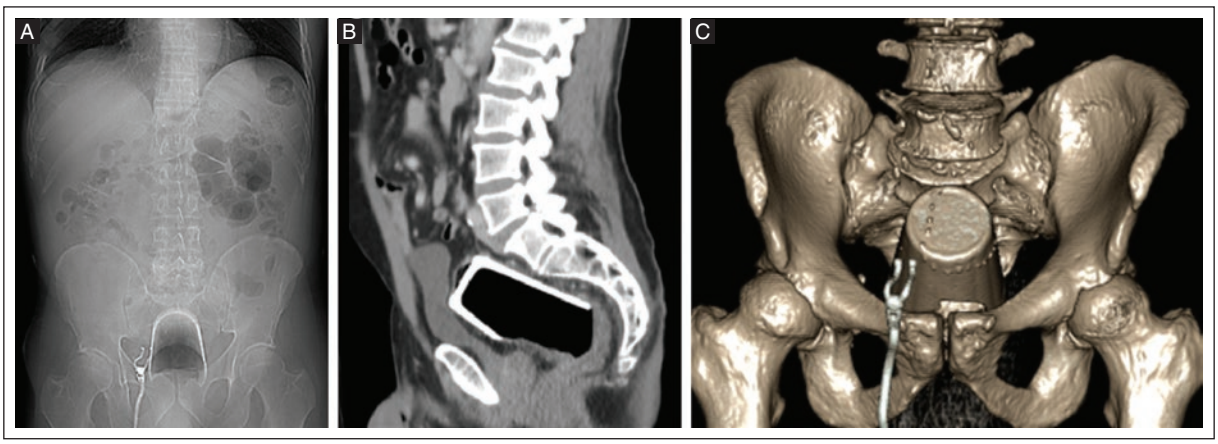

Figure 1. A 65-year-old man was admitted to the emergency room for reportedly getting impaled with a 190-mL glass. **A:** conical radiopaque FB in the rectal topography is visualised on the CT planning image. **B:** sagittal contrast-enhanced CT section of the abdomen confirming the presence of a conical FB with hyperdense margins in the rectal topography image. A content with air density is observed inside the glass. **C:** the anterior three-dimensional CT reconstruction clarifies the anatomical and topographical relationships between structures and is a valuable tool for surgical planning and prognosis.

CT: computed tomography; FB: foreign body.

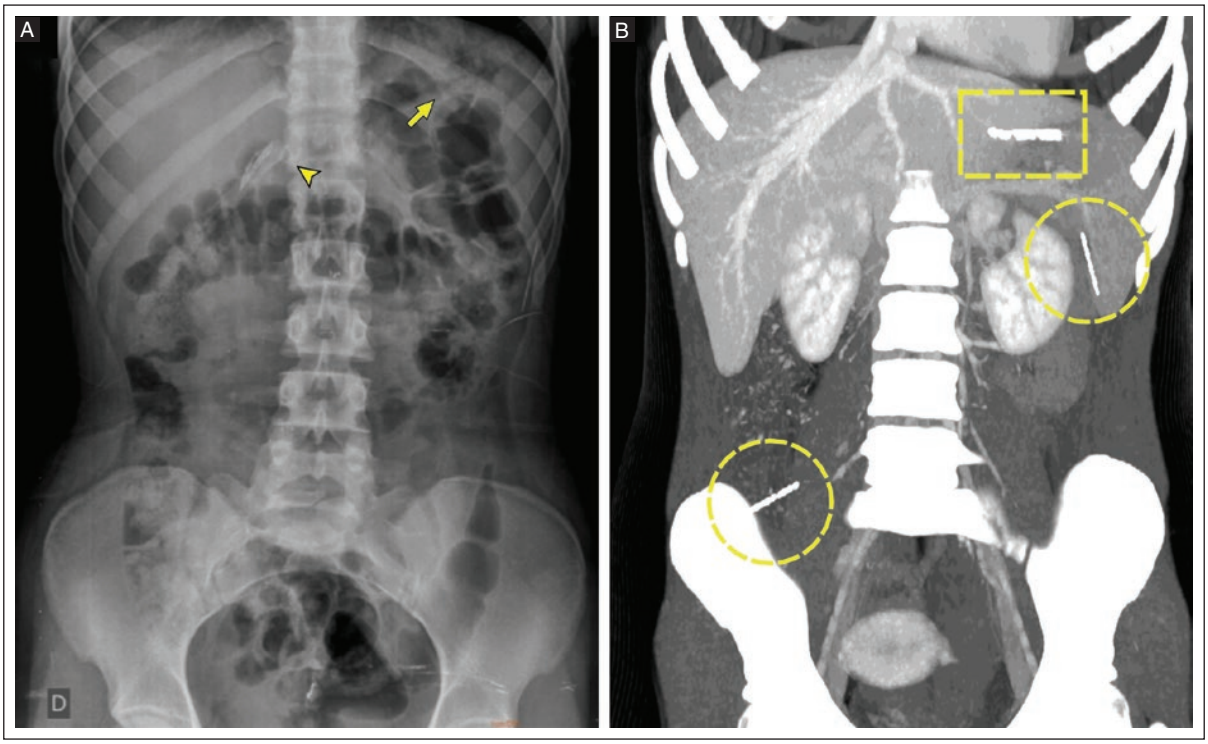

Figure 2. A 15-year-old adolescent with a psychiatric disorder was brought to the emergency room by her mother after ingesting needles and a razor blade in a suicide attempt. **A:** X-ray abdominal view shows the needles in the splenic topography (yellow arrow) apparently in an extraluminal position, and the blade in the gastric antrum projection (arrowhead). No signs of acute perforation were identified. **B:** coronal CT reconstruction with MIP shows needles as hyperdense and sharp FB, in the left supra-mesocolic mesenteric fat, between the spleen and the splenic angle of the colon, and inside the cecum (circles). The blade can be seen in the gastric lumen (square).

CT: computed tomography; MIP: maximum intensity projection.

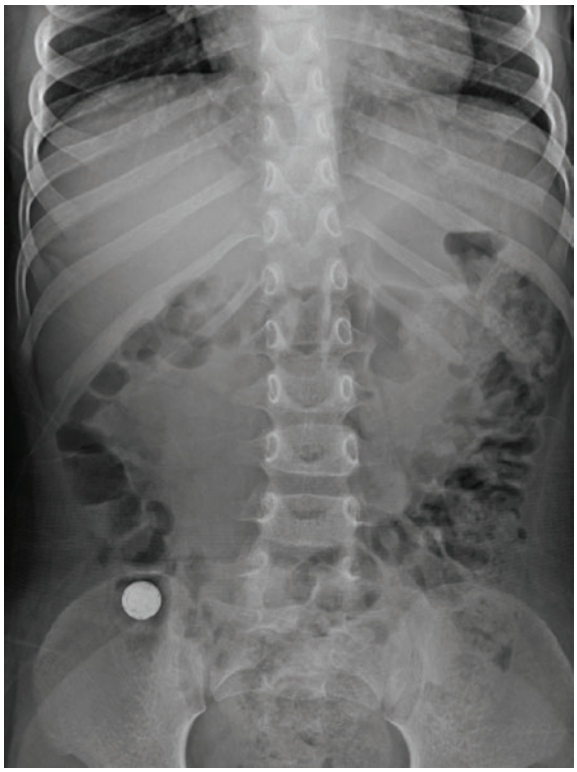

Figure 3. A five-year-old child brought by his father after accidental ingestion of a remote-control battery. X-ray abdominal view shows a rounded radiodense FB can be seen inside the cecum, which appears as a double-ring sign.

FB: foreign body.

radiolucent. Therefore, clinical management is based on the presenting symptoms. However, if complications are suspected, CT is the best method for anatomical examination (Figure 4). It is important to note that plastic has a similar density to blood and a lower density than brain parenchyma; therefore, false positive diagnoses are to be expected[1,3,13].

- **Bones:** fish bones are the most commonly ingested FBs and one of the main causes of perforations6. In general, they can be identified on conventional radiographs due to the characteristic radiopacity of calcified objects. However, their size is an important limitation. Therefore, CT is a fundamental method used for identifying topography and complications. In the presented case, the ingested bones had a similar density to the patient's bones (about 100 HU) and were usually pointed and elongated[5] (Figure 5). Perforation with acute abdomen was the most common complication.
- **Bezoar:** an accumulation of biological material in the lumen of the stomach or small intestine, usually an accumulation of hair, called a trichobezoar (Figure 6). On radiographs it appears as a heterogeneous mass with air trapping and a "bread crumb" aspect, and on a non-contrast CT as a

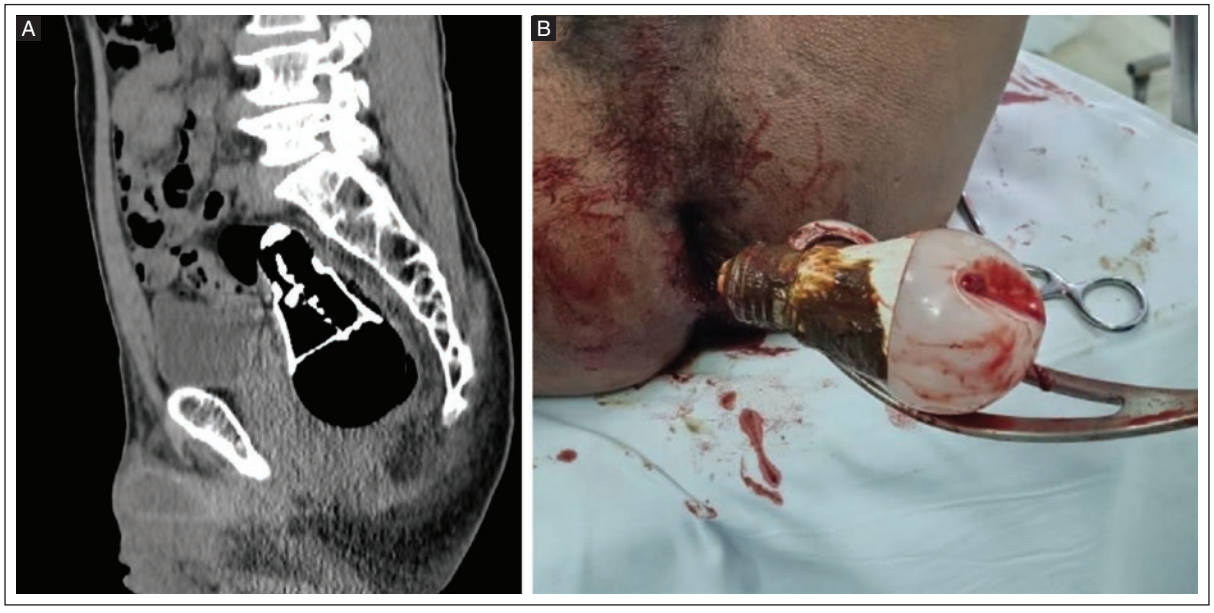

Figure 4. A 56-year-old man impaled with a plastic LED bulb. **A:** sagittal reconstruction of a contrast-enhanced abdominal CT showing the hyperdense FB represented by the metal base, while the plastic bulb is visualised as a hypodense structure on the non-contrast whole abdomen. **B:** surgical excision of the bulb confirms that it is made of plastic, reducing the surgeon's fear of glass fragments perforating the rectum.

CT: computed tomography. FB: foreign body.

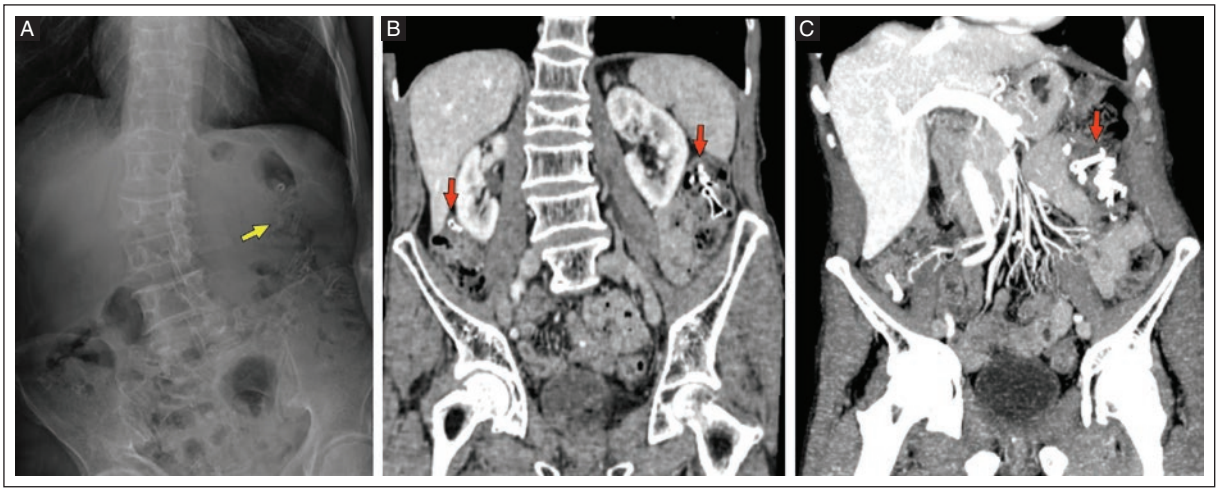

Figure 5. A confused 78-year-old man was admitted to the emergency room with a history of abdominal pain, without other complaints. **A:** plain abdominal radiograph showed an irregular radiopaque FB consistent with that of a fish bone in the topography of the descending colon (yellow arrow), which was confirmed in the clinical anamnesis after radiologic examination. **B:** coronal contrast-enhanced CT in the portal phase and **C:** MIP reconstruction show irregular, multiple, partially sharp FBs (arrows) in the splenic angle and descending colon, resembling bones, but without signs of perforation or bowel obstruction.

CT: computed tomography; FB: foreign body; MIP: maximum intensity projection.

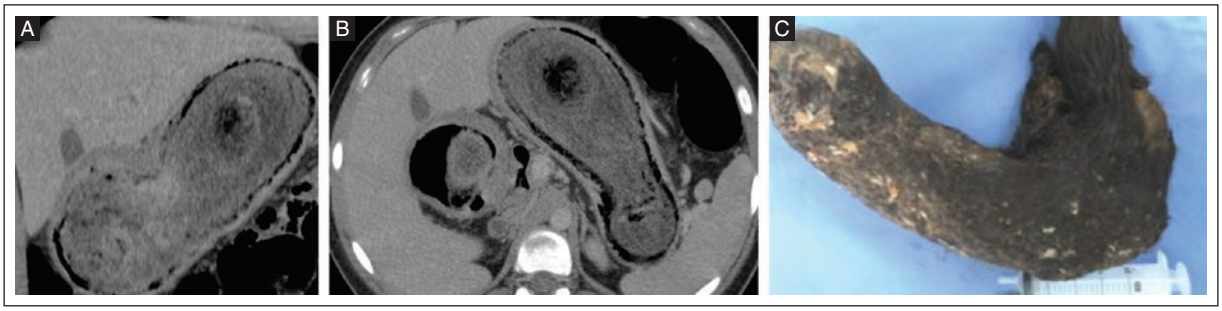

Figure 6. A 14-year-old girl with severe depression presented to the emergency room with nonspecific abdominal pain, heartburn, and bloating. **A:** contrast-enhanced CT scan of the upper abdomen showed a heterogeneous mottled mass and **B:** with an eccentric gaseous focus, without contrast enhancement. **C:** after surgical intervention, a trichobezoar was confirmed; a hair mass in the shape of the gastric lumen was removed.

CT: computed tomography.

well-defined heterogeneous mass with air bubbles. It can cause acute abdominal obstruction if located in the small bowel lumen[4].

- **Drug packages:** these can be potentially fatal in cases of packages rupture and subsequent patient intoxication[14-16]. There is no consensus in the literature on the protocol to be followed; therefore, a multimodality assessment is advocated, with X-ray being considered a screening method[10,17] due to its speed and wide availability, while US and CT are reserved for cases of diagnostic doubt due to their higher sensitivity and specificity[14-19]. CT and MRI provide additional information on the integrity of the package and its relationship to anatomical structures[10].

Packages are often visualized as oval, cylindrical or round objects measuring 2-4 cm[14]. On X-ray, their presence can be suggested by the "double-wrapper sign", formed by a thin halo of gas around the package formed by residual air between it and the substance or between its layers[14,15,18] (Figures 7 and 8), and by the "rosette sign" due to the twisted wrapping end[15,18].

US, which is used to identify radiolucent objects[10], shows hyperechogenic structures with smooth surfaces, curved hyperechoic margin, and clean acoustic

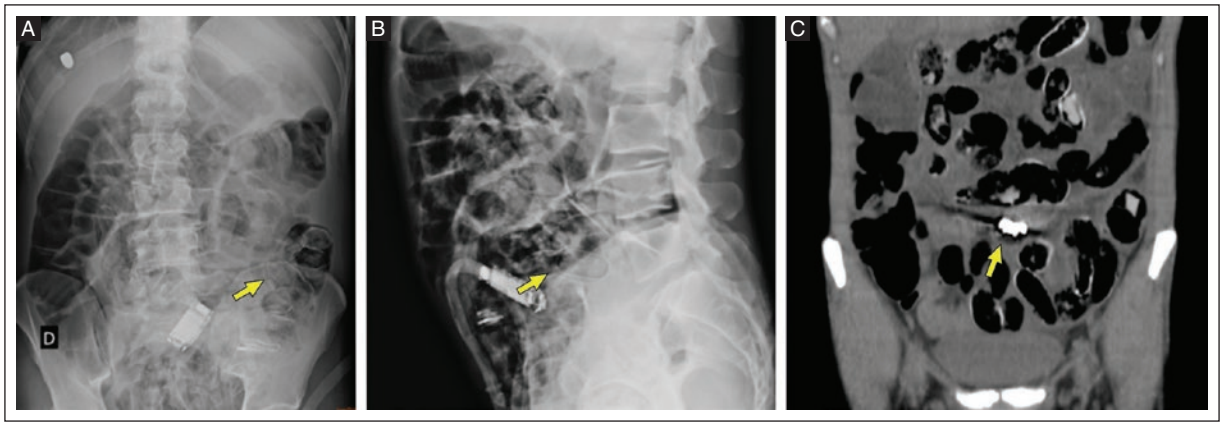

Figure 7. A 27-year-old man brought to the hospital by the police. **A:** abdominal radiograph shows cellular and unspecified images of mottled appearance in the enteric projection (yellow arrow). **B:** lateral view shows radiolucent FBs with the "double-wrapping" sign (yellow arrow). **C:** coronal reconstruction of the non-contrast CT shows hyperdense intermediate-density FBs with hyperdense margin and no signs of rupture of the jejunum lumen (arrow). A hyperdense metallic FBs forming artifacts were also identified.

CT: computed tomography; FBs: foreign bodies.

Figure 8. Multiple handmade packages of marijuana after surgical removal.

shadowing[14,18]. CT and X-ray show similar findings, but CT allows better identification of abscesses and package ruptures when an incomplete hyperdense margin or mixed density is visualised in association with the usual bowel contents[17]. The most common drugs smuggled in body packages are heroin and cocaine[14], which can be distinguished on CT by their radiologic density. Cocaine has a density similar to water or feces, approximately –219 HU; heroin is less dense, –700 HU, and marijuana is dense[14,16].

CONCLUSION

FBs are a common problem in medical practice in tertiary care hospitals, and although complications are not routine, they deserve attention. Imaging techniques are essential for diagnosis and management, and the indications and limitations of each method must be considered.

Funding

This research received no external funding.

Conflicts of interest

The authors declare that they have no conflicts of interest.

Ethical considerations

Protection of humans and animals. The authors declare that no experiments involving humans or animals were conducted for this research.

Confidentiality, informed consent, and ethical approval. The authors have obtained approval from the Ethics Committee for the analysis of routinely obtained and anonymized clinical data, so informed consent was not necessary. Relevant guidelines were followed.

Declaration on the use of artificial intelligence. The authors declare that no generative artificial intelligence was used in the writing of this manuscript.

REFERENCES

1. Carneiro BC, Cruz IAN, Chemin RN, Rizzetto TA, Guimarães JB, Silva FD, et al. Multimodality Imaging of Foreign Bodies: New Insights into Old Challenges. RadioGraphics. 2020;40(7):1965-1986. doi:10.1148/rg.2020200061.
2. ASGE Standards of Practice Committee; Ikenberry SO, Jue TL, Anderson MA, Appalaneni V, Banerjee S, Ben-Menachem T, et al. Management of ingested foreign bodies and food impactions. Gastrointest Endosc. 2011;73(6):1085-1091. doi:10.1016/j.gie.2010.11.010.
3. Pugmire BS, Lim R, Avery LL. Review of Ingested and Aspirated Foreign Bodies in Children and Their Clinical Significance for Radiologists. RadioGraphics. 2015;35(5):1528-1538. doi: 10.1148/rg.2015140287.
4. Gayer G, Petrovitch I, Jeffrey RB. Foreign Objects Encountered in the Abdominal Cavity at CT. RadioGraphics. 2011;31(2):409-428. doi: 10.1148/rg.312105123.
5. Hunter TB, Taljanovic MS. Foreign Bodies. RadioGraphics. 2003;23(3):731-757.
6. Nicolodi GC, Trippia CR, Caboclo MFF, Castro FG, Miller WP, Lima RRD, et al. Perfuração intestinal por ingestão de corpo estranho alimentar. Radiol Bras. 2016;49(5):295-299. doi:10.1590/0100-3984.2015.0127.
7. Akhtar MA, Arora PK. Case of unusual foreign body in the rectum. Saudi J Gastroenterol. 2009;15(2):131-132. doi: 10.4103/1319-3767. 48973.
8. Courter BJ. Radiographic screening for glass foreign bodies — what does a “negative” foreign body series really mean?. Ann Emerg Med. 1990;19(9):997-1000. doi: 10.1016/s0196-0644(05)82562-4.
9. Boyse TD, Fessell DP, Jacobson JA, Lin J, van Holsbeeck MT, Hayes CW. US of Soft-Tissue Foreign Bodies and Associated Complications with Surgical Correlation. RadioGraphics. 2001;21(5):1251-1256. doi: 10.1148/radiographics.21.5.g01se271251.
10. Campbell EA, Wilbert CD. Foreign Body Imaging. [Updated 2023 Jul 30]. In: StatPearls [Internet]. Treasure Island (FL): StatPearls Publishing; 2025 Jan-. Available from: https://www.ncbi.nlm.nih.gov/books/NBK470294/
11. Ingraham CR, Mannelli L, Robinson JD, Linnau KF. Radiology of foreign bodies: how do we image them? Emerg Radiol. 2015;22(4):425-430. doi:10.1007/s10140-015-1294-9.
12. Jarraya M, Hayashi D, de Villiers RV, Roemer FW, Murakami AM, Cossi A, et al. Multimodality Imaging of Foreign Bodies of the Musculoskeletal System. AJR Am J Roentgenol. 2014;203(1):W92-102. doi: 10.2214/AJR.13.11743.
13. Sakamoto N, Fujii S, Masumoto K, Matsuoka A, Toumine S, Hara T, et al. Plastic foreign body in the pharynx can evade detection by computed tomography. J Pediatric Surg Case Reports. 2022; 84:102352. doi: 10.1016/j.epsc.2022.102352.
14. Meijer R, Bots ML. Detection of intestinal drug containers by ultrasound scanning: an airport screening tool? Eur Radiol. 2003;13(6):1312-1315. doi:10.1007/s00330-002-1689-3.
15. Flach PM, Ross SG, Ampanozi G, Ebert L, Germerott T, Hatch GM, et al. “Drug mules” as a radiological challenge: Sensitivity and specificity in identifying internal cocaine in body packers, body pushers and body stuffers by computed tomography, plain radiography and Lodox. Eur J Radiol. 2012;81(10):2518-2526. doi: 10.1016/j.ejrad.2011.11.025.
16. Algra PR, Brogdon BR, Marugg RC. Role of Radiology in a National Initiative to Interdict Drug Smuggling: The Dutch Experience. AJR Am J Roentgenol. 2007;189(2):331-336. doi: 10.2214/AJR.07.2306.
17. Shahnazi M, Sanei Taheri M, Pourghorban R. Body Packing and Its Radiologic Manifestations: A Review Article. Iran J Radiol. 2011;8(4):205-210 doi: 10.5812/iranjradiol.4757.
18. Mehrpour O, Sezavar SV. Diagnostic Imaging in Body Packers. Mayo Clin Proc. 2012;87(7):e53-54. doi: 10.1016/j.mayocp.2012.03.014.
19. Bulakci M, Kalelioglu T, Bulakci BB, Kiris A. Comparison of diagnostic value of multidetector computed tomography and X-ray in the detection of body packing. Eur J Radiol 2013;82(8):1248-1254. doi:10.1016/j.ejrad.2012.12.022.

JMeXFRI

Journal of the Mexican Federation of Radiology and Imaging

Check for updates

CASE REPORT

Contrast-enhanced CT and MRI findings of pancreatic Ewing sarcoma in a pediatric patient: a case report

Heriberto Mendez-Gonzalez[1]* *and Jovanny Zempoalteca-Mendoza*[2]

[1]*Servicio de Radiologia e Imagen, Hospital General de Zona N° 20. Instituto Mexicano del Seguro Social, Puebla;* [2]*Servicio de Radiologia Pediatrica, Hospital para el Niño Poblano, San Andres Cholula. Puebla, Mexico*

ABSTRACT

Pancreatic Ewing sarcoma, a rare tumor in pediatric patients, is a diagnostic challenge from an imaging perspective. We report abdominal contrast-enhanced computed tomography (CT) and magnetic resonance imaging (MRI) findings of a retroperitoneal mass in an 11-year-old girl with abdominal pain, nausea, vomiting, a weight loss of approximately 14 kg, and a palpable epigastric mass on physical examination. A contrast-enhanced CT showed a heterogeneous 7.9 x 6.8 x 10.6 cm mass with necrotic areas in the body of the pancreas displacing adjacent organs and contacting vascular structures with adequate interphase without infiltrating them. Lymph nodes were not observed. The origin of the mass within the circumscribed margin at the level of the pancreatic body was seen on MRI: hypointense in T1, with increased heterogeneous signal intensity in T2 and with hypointense areas in the center, suggesting necrosis, without infiltration of adjacent structures, dilatation of the pancreatic duct or nodal involvement. A biopsy was performed by laparotomy. Immunohistochemical CD99 staining showed intense and diffuse expression of tumor cells in the cytoplasmic membrane, confirming the primitive neuroendocrine tumor. The histopathologic diagnosis was Ewing sarcoma of the pancreas. This is the first case report of imaging findings in Mexico and is published for educational purposes.

Keywords: *Pancreas. Ewing sarcoma. Retroperitoneal mass. Case report.*

INTRODUCTION

Extraosseous Ewing sarcoma, also known as primitive neuroectodermal tumor[1], was first described by Tefft in 1969[2]. It usually affects the lungs and bones, but in rare cases, it originates from the abdominal organs. This tumor occurs in the pancreas in about 0.3% of cases in patients up to 14 years of age[3]. Extraosseous Ewing sarcoma has a chromosomal translocation t(11;22) (q12;q24) associated with a fusion of the Ewing sarcoma breakpoint region 1 protein *(EWSR1)*[1,2,4]. Although there are no specific signs and symptoms, most patients have abdominal pain, nausea, jaundice, and anemia when the retroperitoneum is affected[1,5].

The Ewing sarcoma imaging findings of the pancreas are diverse and non-specific. Contrast-enhanced computed tomography (CT) usually shows a large, calcified cystic mass with enhanced solid components[1,3]. Magnetic resonance imaging (MRI) is the modality of choice for Ewing sarcoma of the pancreas, delineating the pancreatic duct or biliary obstruction. The tumor is iso- or hypointense on T1 MRI and heterogeneous with a high internal signal corresponding to necrosis or cystic areas[1,4]. A T2 MRI shows high signal intensity. We report the contrast-enhanced abdominal CT and MRI findings of a retroperitoneal mass in an 11-year-old girl with a confirmed diagnosis of Ewing sarcoma of the pancreas.

***Corresponding author:**
Heriberto Mendez-Gonzalez
E-mail: heri_94@hotmail.com

Received for publication: 09-06-2024
Accepted for publication: 05-09-2024
DOI: 10.24875/JMEXFRI.M25000093

Available online: 24-04-2025
J Mex Fed Radiol Imaging. 2025;4(1):60-64
www.JMeXFRI.com

CASE DESCRIPTION

An 11-year-old girl with no relevant medical history was admitted to the pediatric department with abdominal pain initially localized in the hypogastrium and later radiating to the mesogastrium, with an intensity of 8/10 on the visual analog scale. The pain was not associated with food intake or defecation. She reported nausea, occasional vomiting, and a weight loss of about 14 kg in six months. A palpable mass in the epigastrium was found on physical examination, and there was moderate pain on deep palpation and decreased peristalsis. A complete blood count, blood chemistry, liver function tests, amylase, lipase, total proteins, serum electrolytes, coagulation times, and carcinoembryonic antigen were normal.

Imaging findings

The diagnosis was made with a contrast-enhanced abdominal CT using a 16-detector BrightSpeed Select™ tomograph (General Electric Co; Cincinnati, OH, USA). A heterogeneous necrotic mass measuring 7.9 x 6.8 x 10.6 cm was seen in the body of the pancreas, displacing adjacent organs without infiltrating vascular structures with adequate interphase (Figure 1). Lymph nodes were not observed.

The abdominal MRI was performed with a Philips 1.5T Multiva™ resonator (General Electric Co; Cincinnati, OH. USA), which showed a 6.7 x 7.9 x 5.4 cm heterogeneous circumscribed mass in T2 (Turbo Spin Eco sequence). A T2 STIR showed hypointense areas in the body of the pancreas, suggesting necrosis (Figure 2).

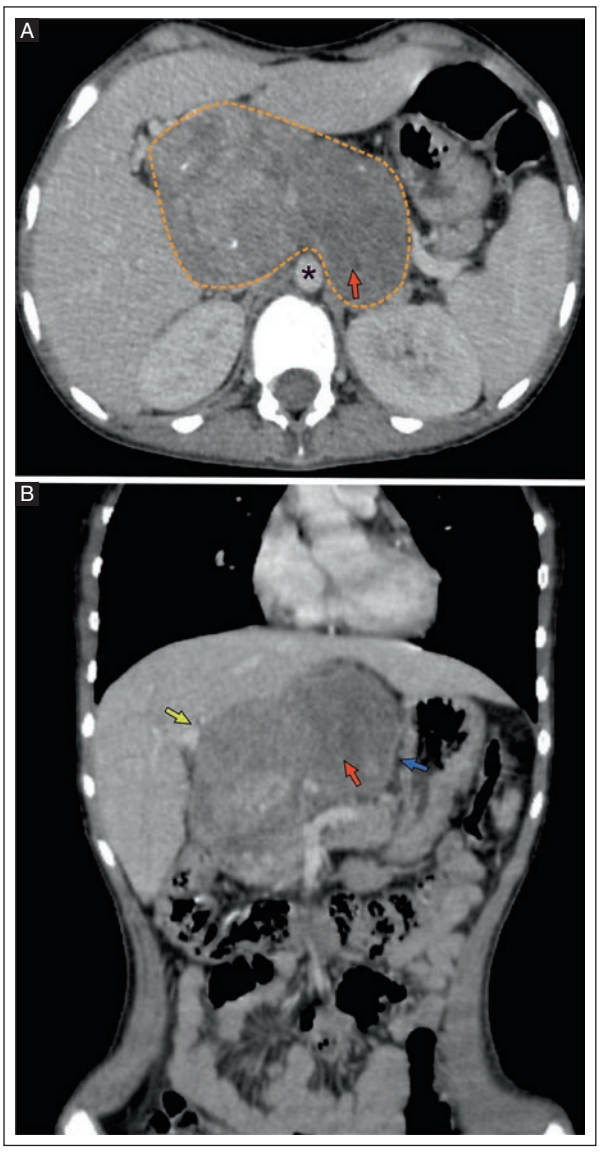

Figure 1. Contrast-enhanced CT in an 11-year-old girl with abdominal pain. **A:** axial view of the arterial phase of the abdomen showing a 7.9 x 6.8 x 10.6 cm mass localized in the pancreatic body with irregular morphology, a circumscribed margin (yellow dashed line), and predominantly hypodense 50 to 72 HU (red arrow), heterogeneous content surrounding other intrabdominal structures without infiltration. The aorta has no evidence of tumor invasion (asterisk). **B:** coronal view of the arterial phase showing the topography of the pancreatic body with an irregular, heterogeneous, predominantly hypodense mass, suggesting areas of necrosis (red arrow) and causing displacement of the right lobe of the liver (yellow arrow) and the lesser curvature of the stomach (blue arrow).

CT: computed tomography; HU: Hounsfield units.

Surgical intervention

A reddish brown, vascularized mass protruding through the greater omentum onto the lesser curvature of the stomach without breaking through the omentum was found on the body of the pancreas during laparotomy. An intraoperative pancreatic biopsy was performed.

Histopathological findings

An invasive, undifferentiated malignant neoplasm was found in the entire biopsy specimen. It consisted of small, round, uniform, "blue" cells arranged in solid nests with some central blood vessels, alternating with areas of "geographic" tumor necrosis suggestive of Ewing sarcoma of the pancreas (Figure 3A). Immunohistochemical CD99 staining was intense, with diffuse expression in the cytoplasmic membrane of the tumor cells, confirming a primitive neuroendocrine extraosseous Ewing sarcoma (Figure 3B). B-catenin, synaptophysin, chromogranin, CK19, and carcinoembryonic antigen were negative (not shown).

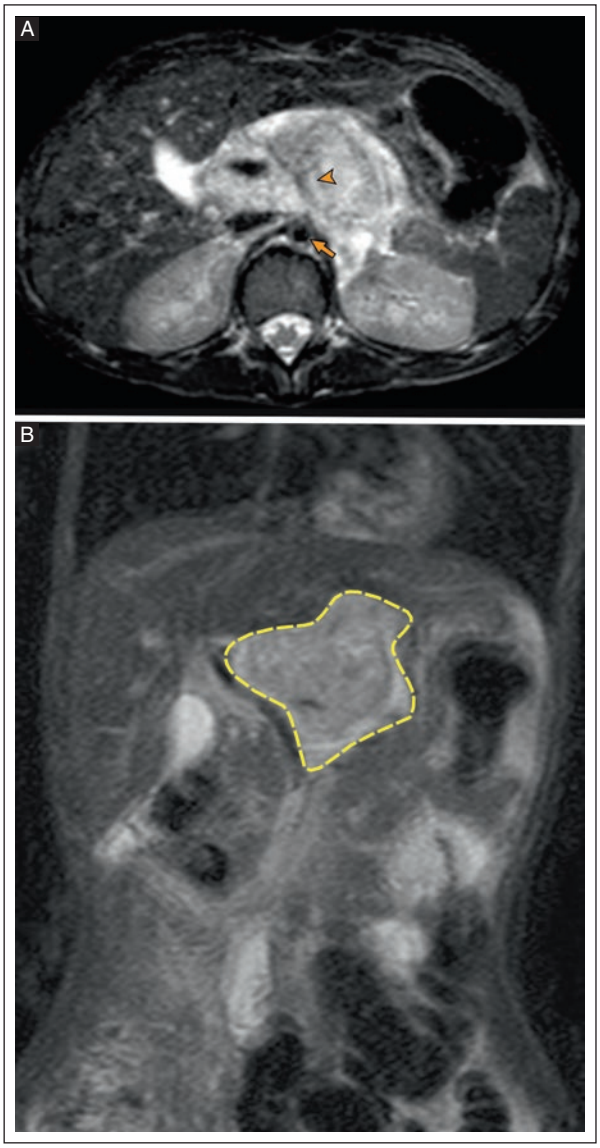

Figure 2. MRI examination of an 11-year-old girl with abdominal pain. **A:** axial T2-weighted turbo spin-echo shows the retroperitoneal 6.7 x 7.9 x 5.4 cm mass in the body of the pancreas. The mass is circumscribed, with a heterogeneous signal intensity (arrowhead), contacting the aorta (arrow) without infiltration. **B:** coronal T2-weighted view confirms stomach and left lobe liver displacement delimiting the adjacent planes (yellow dashed line).

MRI: magnetic resonance image.

DISCUSSION

We present the case of an 11-year-old girl with an irregular, heterogeneous mass in the retroperitoneum displacing adjacent structures, which was examined by contrast-enhanced CT and MRI and histologically diagnosed as Ewing sarcoma of the pancreas. This case report is the first reported in Mexico with imaging findings and is for educational purposes.

There is limited information on imaging findings in retroperitoneal masses in pediatric patients with Ewing sarcoma of the pancreas. Although there are no specific CT findings in evaluating retroperitoneal masses in pediatric patients, the available case reports suggest a large Ewing sarcoma of the pancreas, its behavior with contrast media, and its impact on adjacent structures[1]. Wright et al.[1] reported an expansive growth pattern with predominance in the pancreatic head, large dimensions at the time of diagnosis, and contrast-enhanced CT areas of hypodensity suggestive of necrosis and calcifications in up to 30% of cases. Our patient had a large mass displacing abdominal structures and in contact with the abdominal aorta without infiltrating it. Contrast-enhanced CT showed a large mass without adjacent structure infiltration, suggesting Ewing sarcoma of the pancreas confirmed by histopathology. Bose et al.[6] found a solid lesion in the posterior portion of the junction between the body and tail of the pancreas on a CT scan with adjacent mild ductal dilatation and displacement and compression of the splenic vein[6]. In one case reported by Liu et al.[3], a CT scan showed a well-defined, heterogeneous, calcified mass with enhanced solid components arising from the tail of the pancreas. A biopsy confirmed Ewing sarcoma of the pancreas. In another case reported by Saif et al.[2] a mass was found in an adult patient in the body and tail of the pancreas with hypodense areas suggestive of necrosis or cystic changes. The spectrum of retroperitoneal masses can arise at any site, including the pancreas.

MRI examination of an Ewing sarcoma of the pancreas may show a solid lesion with circumscribed margins and hemorrhage or central necrosis. After administration of a contrast agent, solid component enhancement can be observed[5]. In our case report, MRI showed the origin of the mass within the circumscribed margins at the level of the pancreatic body, hypointense in T1, with increased heterogeneous signal intensity in T2 and hypointense areas in the center suggestive of necrosis, without infiltration of adjacent structures, dilation of the pancreatic duct, or evidence of lymph node involvement. MRI findings are variable depending on the site of origin, and a mass with low to intermediate signal intensity in T1 and high signal intensity in T2 can be observed with heterogeneous enhancement after administration of a contrast agent. MRI is useful for delimiting the origin of the lesion and the involvement of adjacent structures[7].

Ewing sarcoma of the pancreas is rare in adolescents. In this case report, the initial suspected diagnosis

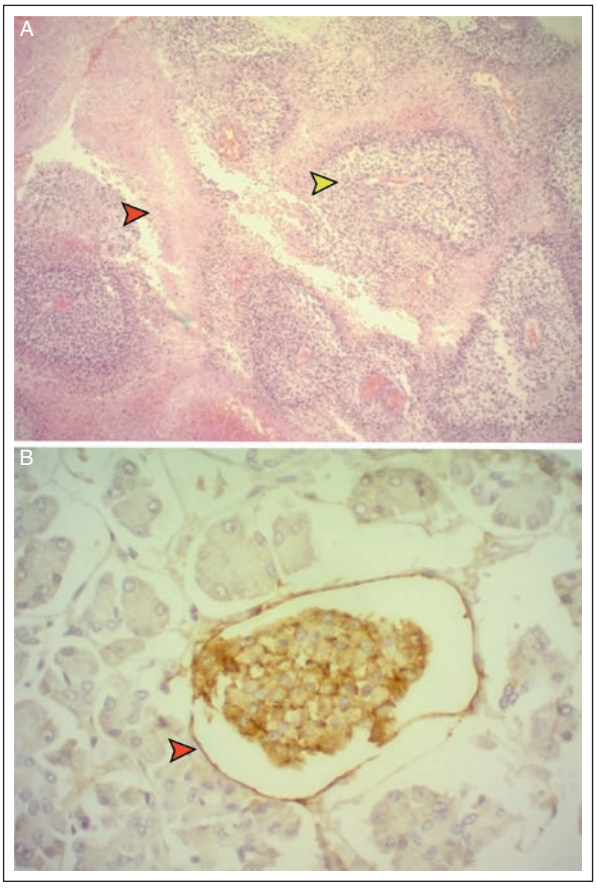

Figure 3. A: biopsy of the retroperitoneal mass shows undifferentiated infiltration of a malignant neoplasm composed of solid areas of small, uniform, round cells alternating with areas of necrosis (red arrowhead) showing a "geographic" pattern (yellow arrowhead) (H&E stain 10x). The diagnosis was Ewing sarcoma of the pancreas. **B:** CD99 immunohistochemistry staining was positive. Vascular lymphatic invasion by the malignant tumor is seen with intense and diffuse CD99 expression (red arrowhead) in the cytoplasmic membrane (H&E stain 100x).

H&E: hematoxylin-eosin.

was pancreatoblastoma, common in young children with non-specific symptoms. Imaging examination showed a retroperitoneal mass, a typical large tumor compressing surrounding structures without invading them,[4] which required evaluation by CT and MRI[1,4]. This case report showed various common imaging findings, such as a large mass with adjacent structure displacement, a heterogeneous component, and areas of hypodensity suggesting necrosis. Contrast-enhanced CT showed a circumscribed mass, and the infiltrating margin is unusual. In some cases, the tumor appears multilocular with enhanced septa. Another differential diagnosis that should be considered depending on age is a pseudopapillary tumor of the pancreas, which is more common in women in the second decade of life and presents with nonspecific symptoms[4]. A pseudopapillary tumor is usually a solitary, well-defined mass surrounded by a thick, fibrous capsule. It shows intense enhancement on contrast CT and ring enhancement on MRI, which is higher than Ewing sarcoma. Other benign pancreatic lesions that should be considered are hemangioendotheliomas, leiomyomas, or lipomas[4].

CONCLUSION

This case report of a girl with a retroperitoneal mass and a histologic diagnosis of pancreatic Ewing sarcoma describes an approach using contrast-enhanced CT and MRI that delimits the origin or extent and rules out other pathologies. Therefore, this case serves as a valuable educational tool.

Acknowledgments

Thanks to Professor Ana M. Contreras-Navarro for her guidance in preparing and writing this scientific paper.

Funding

This research received no external funding.

Conflicts of interest

The authors declare no conflicts of interest.

Ethical considerations

Protection of humans and animals. The authors declare that the procedures followed complied with the ethical standards of the responsible human experimentation committee and adhered to the World Medical Association and the Declaration of Helsinki. The procedures were approved by the institutional Ethics Committee.

Confidentiality, informed consent, and ethical approval. The authors have obtained approval from the Ethics Committee for the analysis of routinely obtained and anonymized clinical data, so informed consent was not necessary. Relevant guidelines were followed.

Declaration on the use of artificial intelligence. The authors declare that no generative artificial intelligence was used in the writing of this manuscript.

REFERENCES

1. Wright A, Desai M, Bolan CW, Badawy M, Guccione J, Rao Korivi B, et al. Extraskeletal Ewing Sarcoma from Head to Toe: Multimodality Imaging Review. Radiographics. 2022;42(4):1145-1160. doi: 10.1148/rg.210226.

2. Saif MW, Kaley K. Extraosseous Ewing's Sarcoma of the Pancreas: An Uncommon but Treatable Disease. Cureus. 2017;9(11):e1882. doi: 10.7759/cureus.1882.
3. Liu YC, Yeh TC, Wu PS, Sheu JC, Lee HC, Yeung CY, et al. Rare presentation in a rare case of pancreatic extraosseous Ewing's sarcoma: A case report. Medicine (Baltimore). 2022;101(47):e31752. doi: 10.1097/MD.0000000000031752.
4. Chung EM, Travis MD, Conran RM. Pancreatic tumors in children: radiologic-pathologic correlation. Radiographics. 2006;26(4):1211-1238. doi: 10.1148/rg.264065012.
5. Qiu L, Trout AT, Ayyala RS, Szabo S, Nathan JD, Geller JI, et al. Pancreatic Masses in Children and Young Adults: Multimodality Review with Pathologic Correlation. Radiographics. 2021;41(6):1766-1784. doi:10.1148/rg.2021210008.
6. Bose P, Murugan P, Gillies E, Holter JL. Extraosseous Ewing's sarcoma of the pancreas. Int J Clin Oncol. 2012;17(4):399-406. doi:10.1007/s10147-011-0311-6.
7. Gurria JP, Dasgupta R. Rhabdomyosarcoma and Extraosseous Ewing Sarcoma. Children. 2018;10(12):1-23. doi:10.3390/children5120165.

JMeXFRI

Journal of the Mexican Federation of Radiology and Imaging

Check for updates

IMAGES IN RADIOLOGY

Pulmonary vein thrombosis as an incidental finding on contrast-enhanced CT

Juan Llovera-Montoya[1]* *and Jesus Cadena-Fragoso*[2]

[1]*Department of Radiology, Unidad Medica de Alta Especialidad Numero 25, Instituto Mexicano del Seguro Social;* [2]*Department of Radiology, Doctors Hospital, Grupo AUNA Monterrey. Monterrey, Nuevo Leon, Mexico*

Case 1 is a 33-year-old man with Ewing sarcoma, pulmonary metastases, and cardiotoxicity due to neoadjuvant chemotherapy. The patient was asymptomatic, and a contrast-enhanced chest computed tomography (CT) scan was performed as a follow-up. The scan showed a filling defect representing a clot in the proximal segment of the right inferior pulmonary vein extending into the left atrium (Figure 1A-B). A diagnosis of pulmonary vein thrombosis (PVT) was made. This finding was not present six months before (Figure 1C).

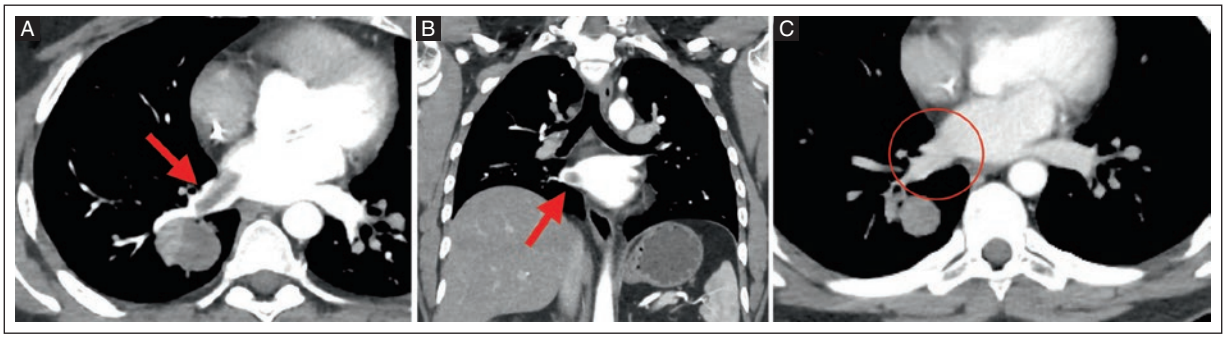

Figure 1. Follow-up contrast-enhanced chest CT of a 33-year-old man with Ewing sarcoma and pulmonary metastases. **A:** axial and **B:** coronal views show a hypodense lineal image in the thickened right inferior pulmonary vein corresponding to a clot causing partial obliteration that spreads to the left atrium (arrows). The diagnosis was PVT. **C:** axial view, this finding was not present six months before (circle).

CT: computed tomography; PVT: pulmonary vein thrombosis.

Case 2 is a 70-year-old woman with clear cell renal carcinoma and pulmonary metastases. The patient was asymptomatic, and a follow-up contrast-enhanced chest CT showed partial occlusion of the right upper pulmonary vein caused by a clot (Figure 2). The diagnosis was PVT.

PVT is a rare condition with potentially catastrophic consequences for the patient[1]. Its incidence is unclear due to the large number of collateral veins draining the lungs. It has a variety of causes, including neoplasms[2,3]. Patients are usually asymptomatic. PVT is discovered incidentally during an imaging examination. A contrast-enhanced chest CT is a useful examination for detecting this condition. However, this finding is often overlooked because the pulmonary veins are rarely examined in detail during oncologic follow-up[4]. Radiologists should assess the systemic and pulmonary vessels in this setting.

***Corresponding author:**
Juan Llovera-Montoya
E-mail: juanllovmont@gmail.com

Received for publication: 06-09-2024
Accepted for publication: 17-12-2024
DOI: 10.24875/JMEXFRI.M25000092

Available online: 24-04-2025
J Mex Fed Radiol Imaging. 2025;4(1):65-66
www.JMeXFRI.com

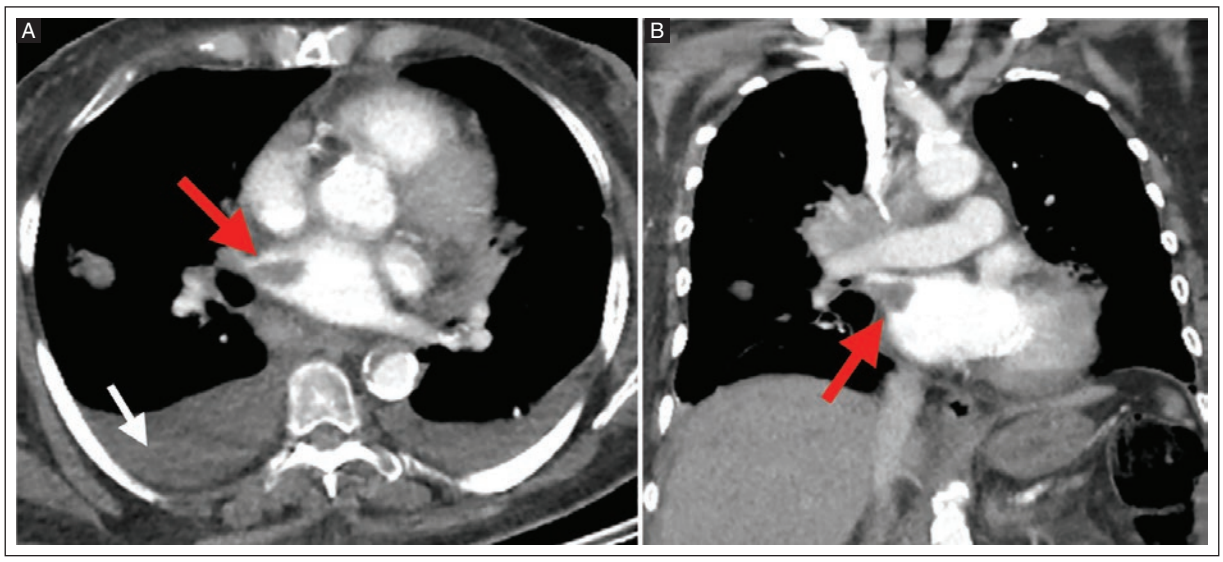

Figure 2. Follow-up contrast-enhanced chest CT of a 70-year-old woman with clear cell renal carcinoma and pulmonary metastases. **A**: axial and **B:** coronal views show an irregular clot image blocking the right superior pulmonary vein (red arrows) and bilateral pleural effusion (white arrow). The diagnosis was PVT.

CT: computed tomography; PVT: pulmonary vein thrombosis.

Acknowledgments

The authors thank Professor Ana M. Contreras-Navarro for her guidance in preparing and writing this scientific paper.

Funding

This paper received no external funding.

Conflicts of interest

The authors declare no conflicts of interest.

Ethical considerations

Protection of humans and animals. The authors declare that the procedures followed complied with the ethical standards of the responsible human experimentation committee and adhered to the World Medical Association and the Declaration of Helsinki. The procedures were approved by the institutional Ethics Committee.

Confidentiality, informed consent, and ethical approval. The authors have followed their institution's confidentiality protocols, obtained informed consent from patients, and received approval from the Ethics Committee.

Declaration on the use of artificial intelligence. The authors declare that no generative artificial intelligence was used in the writing of this manuscript.

REFERENCES

1. Chaaya G, Vishnubhotla P. Pulmonary Vein thrombosis: A Recent Systematic review. Cureus. 2017;9(1):1-13. doi: 10.7759/cureus.993.
2. Hassani C, Saremi F. Comprehensive cross-sectional imaging of the pulmonary veins. Radiographics. 2017;37(7):1928-1954. doi: 10.1148/rg.2017170050.
3. Rana MA, Tilbury N, Kumar Y, Ahmad H, Naser K, Mady AF, et al. Idiopathic Pulmonary Vein Thrombus Extending into Left Atrium: A Case Report and Review of the Literature. J Case Rep Med. 2016;3528393. doi: 10.1155/2016/3528393.
4. Marini TJ, He K, Hobbs SK, Kaproth-Joslin K. Pictorial review of the pulmonary vasculature: from arteries to veins. Insights Imaging. 2018;9(6):971-987. doi: 10.1007/s13244-018-0659-5.

PHILIPS

Ultrasound

Affiniti

Designed for your everyday

Stepping up to today's Philips Affiniti Ultrasound System means stepping up to the next level of performance to help with a confident diagnosis using streamlined workflow.

Upgrade to the latest Affiniti capabilities

Intuitive use

Experience a user interface and workflow that helps increase your productivity.

- Enhances user workflow with **system-guided protocols** that can be easily customized to suit your needs
- **Tablet-like 30.48 cm (12 in) touchscreen** with workflow-related controls for ease of use
- **Next Gen AutoSCAN reduces button pushes by up to 54%** with pixel-by-pixel real-time optimization and reduces the need for user adjustment while also enhancing transducer plunkability.*
- At just 83.5 kg (184 lb), the system is **16% lighter** than its predecessor system**
- **Shared transducer family** across Affiniti and Compact 5000*** series systems helps maximize your investment
- **Wireless networking** aids workflow

* When comparing VM10 performance to VM7.
** HD15.
*** R.S. #1437E2024 SSA.

Battery backup with sleep mode allows the system to **sleep in 2 seconds and return to full functionality in 20 seconds**

Consumes nearly 40% less power compared to our legacy predecessor system*

Intelligent imaging

Flow Viewer

Defines vasculature with a 3D-like appearance using both the velocity and power of the Doppler signal to accurately represent vascular flow topography

MicroFlow Imaging (MFI)

Provides remarkable sensitivity and detail in assessing blood flow

Find out more at
www.philips.com.mx/healthcare/solutions/ultrasound

FUTURA MEDICA

DIAGNÓSTICOS EN RADIOLOGÍA & LABORATORIO

MR

SUPPORTING RADIOLOGY MEDICAL EDUCATION SINCE 1979

www.futuramedicademorelia.com

EI

Diagnóstico Especializado en Imágen

Dr. Gerardo S Navarro Gomez
Radiologist

Dr. Eduardo Sarda Inman
Radiologist

Dra. Beatriz Gonzalez Ulloa
Radiologist

Clinical Laboratory	General Ultrasound
Digital Radiology	Color Doppler Ultrasound
Digital Mammography	4D Structural Obstetric Ultrasound
Tomosynthesis	Musculoskeletal Ultrasound
Contrast-Enhanced Mammography	Peripheral Doppler Ultrasound
Computed Tomography (CT)	Magnetic Resonance Imaging (MRI)

Guadalajara, Jalico. Mexico

Vida®

Women's Imaging Center

"An experience that goes beyond medical care."

OUR SERVICES

ULTRASOUND / X- RAY / MAMMOGRAPHY
DENSITOMETRY / BIOPSY / CT / MRI

+ 52 833 212 0472 + 52 833 658 5800

Tampico, Tamaulipas, México

RADIOLOGY SOLUTIONS

YOUR TRUSTED CABINET

OAXACAN RADIOLOGY OFFICE DEDICATED TO OFFERING IMAGING SERVICES.

Committed to offering image quality and diagnostic certainty to its patients and doctors in Imaging studies.

OUR SERVICES:

Tomography | Ultrasonido

Special X-rays | X-rays

LOCATION:

Calle Álamos #603, Col. Reforma, between Jazmines and Heroico Colegio Militar, Oaxaca de Juárez, Oaxaca.